

Study of Dynamic Interaction and Adhesion between Water Droplets and Gas
Hydrate in Organic Solvents

by
Zihui Chen

A thesis submitted in partial fulfillment of the requirements for the degree of

Doctor of Philosophy

in

Chemical Engineering

Department of Chemical and Materials Engineering
University of Alberta

© Zihui Chen, 2019

Abstract

In the exploration of offshore reservoirs, the hydrate formation and agglomeration in oil and gas pipelines become the major flow assurance challenges, while the interfacial interactions between hydrate particles and water droplets, for which the presence of salt is inevitable in the deepwater flowlines, are critical for hydrate aggregation. Even though the interaction between water droplets and hydrate particles have been studied, the effects of salts on this interaction have rarely been considered.

This study aims at understanding the interaction behaviors including both capillary adhesion forces between brine solution droplets and cyclopentane hydrate particle and the influences of different types of salts on the hydrate growth morphology. Capillary adhesion forces are measured using a new instrument, Integrate Thin Film Drainage Apparatus, in both oil and gas bulk phases, while the hydrate growth morphology is observed visually.

The results showed that the adhesion forces decreased with the increasing of concentrations of NaCl and KCl in water up to 5 wt. %, while the impacts of concentration of either Na₂SO₄ or CaCl₂ on adhesion forces were almost negligible. The adhesion force measured in the gas phase was around twice more than that obtained in the oil phase owing to the wider capillary bridge formation caused by thicker quasi-liquid layer. As observed from the photographic images, the salt solutions with more electronegative ions would delay hydrate growth greatly because these types of salts tended to attract the water molecules more strongly, preventing the formation of hydrate cage and then prohibit the hydrate nucleation more efficiently. Moreover, the longer contact time and the larger solution droplet made critical contributions on the more hydrate formation and higher adhesion force no matter salts present or not, respectively. The hydrate

growth rate was not only dependent on the subcooling but also the amount of guest and host components. Specifically, either the lower subcooling or the lack of guest and host components could slow down the hydrate growth rate.

On the other hand, the surfactants, such as 0.05 g/L asphaltenes and 1 wt. % Span 80, were evaluated as the effective inhibitors to prevent the attachment between water droplets and hydrate particle due to the adsorption layer formed around droplet, resulting in the inhibition of hydrate agglomeration inside pipeline.

The present work is essential to better understanding of the impacts of different salts on the interaction forces between hydrates and water surface, and hydrate agglomeration in the oil and gas pipelines.

Acknowledgements

Firstly, I appreciate Prof. Zhenghe Xu and Prof. Qingxia Liu for supervising and guiding at all time for my research and thesis project. I would like to thank Prof. Hailong Lu for providing me so much help on the fundamental knowledge of my topic. My appreciation also goes to Prof. Nobuo Maeda, who offered some advices on my research. I also feel thankful to suggestions and work done by Bo Liu during my study.

I also would like to thank Mr. Jim Skwarok, Ms. Jie Ru and Ms. Lisa Carriero for their assistance. I appreciate the entire Oil Sands Extraction research group for their timely help and kind suggestions, especially from Zuoli Li, Xurui Zhang and Ye Zhang. I also thank Rogerio Manica for proofreading the thesis.

My appreciation goes NSERC Industrial Research Chair in Oil Sands Engineering for financial support.

Last but not least, I thank my parents who inspired me with love and appreciations. Therefore, this document is dedicated to my beloved parents.

Table of Contents

Chapter 1 Introduction	1
1.1 Clathrate or gas hydrates	1
1.1.1 Phase diagram of clathrate or gas hydrate	1
1.1.2 Characters of clathrate or gas hydrate.....	2
1.1.3 Clathrate or gas hydrate nucleation and growth	7
1.1.4 Thermodynamic and kinetic properties of clathrate or gas hydrate	8
1.1.5 Advantages and disadvantages of clathrate or gas hydrate.....	9
1.1.6 Methods to avoid hydrate plugging in flowlines	11
1.1.7 Thermodynamic & low-dosage gas hydrate inhibitors.....	11
1.2 Gas hydrate-surface interaction mechanisms	12
1.3 Objectives and outline	13
Chapter 2 Literature Review	15
2.1 Cohesion force between CP hydrate particle in oil bulk phase	17
2.1.1 Effects of preload force and contact time	17
2.1.2 Effects of hydrocarbon oils and their modifications.....	18
2.1.3 Effects of different acids with varying concentrations	18
2.1.4 Effects of thermodynamic inhibitors (THIs).....	19
2.1.5 Effects of antiagglomerants (AA)	21

2.2 Adhesion force between CP hydrate particle and other surfaces in oil bulk phase	21
2.2.1 Adhesion force between CP hydrate and water solution droplet	22
2.2.1.1 Interactions between CP hydrate and water solution droplet.....	22
2.2.1.2 Effects of water volumes.....	23
2.2.1.3 Effects of contact time	24
2.2.1.4 Effects of subcooling	24
2.2.1.5 Effects of surfactants.....	25
2.2.1.6 Effects of salts	27
2.2.2 Adhesion force measurement between CP hydrate and solid surface	27
2.2.2.1 Effects of dry solid surface materials and acids	27
2.2.2.2 Effects of presence of water droplet	28
2.2.2.3 Effects of physical and chemical modifications	29
2.2.2.4 Effects of mineral surfaces.....	30
2.3 Mechanism of CP hydrate formation/growth along water-oil interface.....	30
2.3.1 Driving force for crystallization of gas hydrate	31
2.3.2 Macroscopic investigation of gas hydrate film growth	32
2.3.3 Effects of subcooling and amount of gas hydrate former on hydrate formation.....	33
2.3.4 Effects of surfactants on gas hydrate formation	34
2.3.5 Effects of salts on hydrate growth	35
2.4 Sintering mechanism at contact point	36

Chapter 3 Experimental methods.....	38
3.1 Capillary adhesion force measurements	38
3.2 Interfacial tension measurements.....	39
3.3. Crumpling ratio measurements	41
Chapter 4 Experimental materials and setup	42
4.1 Experimental materials	42
4.1.1 Preparation of cyclopentane hydrate	42
4.1.2 Preparation of asphaltenes.....	43
4.2 Experimental Setup	44
4.2.1 Interfacial tension measurement by Theta Optical Tensiometer.....	44
4.2.2 Capillary adhesion force measurements by Integrated Thin Film Drainage Apparatus (ITFDA)	45
Chapter 5 Results and Discussion.....	47
5.1 Interfacial tension measurements with various salts	47
5.2 Capillary adhesion force measurements between CP hydrate and water solution droplet in oil bulk phase	49
5.3 Capillary adhesion force measurements between CP hydrate and electrolyte solution droplet in oil bulk phase	53
5.3.1 Effects of concentrations of electrolyte solution	53
5.3.2 Effects of electrolyte solution droplet size.....	56

5.3.3 Effects of contact time	58
5.4 Hydrate growth morphology in oil bulk phase	60
5.4.1 Morphology of hydrate particle after contact with water solution	60
5.4.2 Morphology of hydrate particle after contact with electrolyte solution	62
5.5 Capillary adhesion force measurements between CP hydrate and electrolyte solution droplet in gas bulk phase	66
5.5.1 Effects of concentration of electrolyte solution	66
5.6 Hydrate growth morphology in gas bulk phase	68
5.6.1 Morphology of hydrate particle after contact with water solution	68
5.6.2 Morphology of hydrate particle after contact with electrolyte solution	71
5.7 Effects of presence of another hydrocarbon	73
5.7.1 Capillary adhesion force measurements between CP hydrate and water solution droplet in 1:1 of cyclopentane and toluene oil phase	73
5.7.2 Hydrate morphology in 1:1 of cyclopentane and toluene oil phase	75
5.7.3 Capillary adhesion force measurements between CP hydrate and water solution droplet in pure decane oil phase	79
5.8 Effects of asphaltenes on interactions between CP hydrate and water solution droplet in 1:1 of cyclopentane and toluene oil phase.....	80
5.8.1 Effect of asphaltenes on water drop – CP hydrate adhesion force	80
5.8.2 Effect of elevated asphaltenes concentration on the adhesion force	82
5.8.3 Effect of salts on water drop - CP hydrate adhesion force	83

5.8.4 Dynamic interfacial tension and crumpling ratio measurements	87
5.9 Effects of Span 80 on interactions between CP hydrate and electrolyte solution droplet in oil bulk phase.....	89
5.9.1 Effects of contact time on adhesion force measurements	90
5.10 Effects of subcooling on interactions between CP hydrate and electrolyte solution droplet	93
Chapter 6 Conclusions and future work	95
6.1 Conclusions.....	95
6.2 Future work.....	100
Bibliography	103

List of Figures

Figure 1-1: Phase diagram for a water/hydrocarbon (HC) system	2
Figure 1-2: Structures of gas hydrates	3
Figure 1-3: Raman spectra of CH ₄ vapor and CH ₄ incorporated into hydrate.....	4
Figure 1-4: Raman spectra of C ₃ H ₈ vapor and C ₃ H ₈ incorporated into hydrate	5
Figure 1-5: CO ₂ molecules (carbon atom, black; oxygen atom, red) in sI large and small cages	6
Figure 1-6: C ₃ H ₈ molecules in sII large cages.....	6
Figure 1-7: Mechanisms of hydrate nucleation	7
Figure 1-8: Distribution of organic carbon in earth reservoirs	10
Figure 1-9: Mechanisms of hydrate plugging in oil-dominated flowlines.....	10
Figure 2-1: Top view of schematic of MMF apparatus	16
Figure 2-2: Schematic procedures of experimental measurements: (a) hydrate particles are placed at the end of cantilevers; (b) the two particles are in contact after applying a preload force with displacement (Δ_P); (c) the upper hydrate moves upwards after a set contact time; (d) the particles break apart with displacement (Δ_D)	17
Figure 2-3: Chemical compounds of four surfactant acids	19
Figure 2-4: Morphological changes of CP hydrate: (A) before pull-off trails; (B) after pull-off trails; (C) explanation of potential mechanism of this change	20

Figure 2-5: Three-phase system of one-component gas, aqueous solution, and gas hydrate....	31
Figure 2-6: Schematic of mechanism of hydrate film formation at the planar water/oil interface	33
Figure 2-7: Schematic of CP hydrate lateral surface growth hypothesis	35
Figure 3-1: Schematic of capillary adhesion for solution-hydrate geometry with relevant parameters.....	39
Figure 3-2: Pendant drop method principle.....	40
Figure 3-3: Skin formation at droplet surfaces	41
Figure 4-1: Schematic diagram of cyclopentane hydrate formation process	43
Figure 4-2: Appearance of electrolyte solution droplet in pure cyclopentane oil phase	45
Figure 4-3: Schematic of the ITFDA configuration (A). An aqueous drop is driven toward a hydrate particle under controlled conditions. The interaction force is measured by the deflection of the bimorph. The typical experiment follows the following protocol (B): approach stage (1); hold stage (2-3) where attachment can occur and retract stage (4)..	46
Figure 5-1: Interfacial tension measured between pure cyclopentane and NaCl solution (A); KCl solution (B); CaCl ₂ solution (C); Na ₂ SO ₄ solution (D).....	48

Figure 5-2 Adhesion force curves obtained from the interactions between CP hydrate probe and water droplet in oil phase 2.0 ± 0.5 °C (A); Corresponding images captured during experimental processes from side camera (B). 51

Figure 5-3: Impacts of Laplace pressure and surface tension on interaction forces measured between CP hydrate particle and water solution droplet..... 52

Figure 5-4: Schematic diagram of capillary interaction (A); Geometric relationship of Equation 3 (B)..... 52

Figure 5-5: Adhesion force curves obtained from the interactions between CP hydrate particle and droplets of NaCl solution (A); KCl solution (B); CaCl₂ solution (C); Na₂SO₄ solution (D) in oil phase at 2.0 ± 0.5 °C 55

Figure 5-6: Corresponding images of three sizes of 2.5 wt. % NaCl solution droplets (A-1): $d = 2.10$ mm; (A-3): $d = 2.20$ mm; (A-5): $d = 2.30$ mm captured at the initial point of capillary bridge formation, coming along with corresponding contact length (A-2): $L = 2.34$ mm; (A-4): $L = 2.80$ mm; (A-6): $L = 3.10$ mm, respectively; (B) Adhesion force curves obtained from the interactions between 2.5 wt. % NaCl solution droplet and CP hydrate with respective to droplet size in oil phase at 2.0 ± 0.5 °C. 57

Figure 5-7: Adhesion force curves obtained from the interactions between 2.5 wt. % NaCl solution droplet and CP hydrate (A); CP hydrate morphologies as a function of contact time: $t = 5$ s (B-1); $t = 25$ s (B-2); $t = 45$ s (B-3). 59

Figure 5-8: Mechanism of hydrate formation. Step 1: formation of thin hydrate film around the water droplet; Step 2: film development; Step 3: complete conversion of hydrate 60

Figure 5-9: Photographic images of hydrate morphology captured from water droplet-CP hydrate interactions in oil bulk phase (A): the point just after detachment of water droplet (point 1); the first point of hydrate shell formation (point 2); final morphology of hydrate after complete conversion from water solution (point 3); (B) Amplification images of initial point of hydrate growth in oil bulk phase..... 62

Figure 5-10: Photographic images of initial point of hydrate shell formation from different solution droplets ($d = 2.10 \pm 0.05$ mm): (A) DI water; (B) 2.5 wt. % NaCl; (C) 2.5 wt.% CaCl₂; (D) 2.5 wt.% Na₂SO₄ at in pure cyclopentane bulk phase 2.0 ± 0.5 °C 65

Figure 5-11: Photographic images of CP hydrate morphology after complete conversion from four solutions with same volume: (A) DI water; (B) 2.5 wt. % NaCl; (C) 2.5 wt.% CaCl₂; (D) 2.5 wt.% Na₂SO₄ in pure cyclopentane bulk phase at 2.0 ± 0.5 °C..... 65

Figure 5-12: Adhesion force curves obtained from the interactions between water droplet and CP hydrate particle in gas and oil phase at 2.0 ± 0.5 °C (A); Corresponding images of hydrate exposed into gas phase (B-1) and oil phase (B-2), respectively..... 67

Figure 5-13: Adhesion force curves obtained from the interactions between electrolyte solution droplet and CP hydrate in gas phase at 2.0 ± 0.5 °C..... 68

Figure 5-14: Corresponding photographic images of conversion process of CP hydrate growth from water solution: before two surfaces contacted (1); at the initial point of capillary bridge formation (2); at the point when water was driven away from CP hydrate particle (3); at the point after some water being left on CP hydrate particle (4) with contact time of 5s (A); 25s (B); 45s (C) 70

Figure 5-15: Corresponding photographic images of conversion process of CP hydrate growth from water solution with respect to three contact time: 5s (A); 25s (B); 45s (C) 70

Figure 5-16: CP hydrate morphologies after contact with 2.5 wt. % NaCl (A); 5 wt. % NaCl (B); 7.5 wt. % NaCl (C), respectively, in gas phase at 2.0 ± 0.5 °C 72

Figure 5-17: CP hydrate morphologies after contact with 2.5 wt. % CaCl₂ (A); 5 wt. % CaCl₂ (B); 7.5 wt. % CaCl₂ (C), respectively, in gas phase at 2.0 ± 0.5 °C 72

Figure 5-18: CP hydrate morphologies after contact with 2.5 wt. % Na₂SO₄ (A); 5 wt. % Na₂SO₄ (B); 7.5 wt. % Na₂SO₄ (C), respectively, in gas phase at 2.0 ± 0.5 °C 73

Figure 5-19: Adhesion forces curves obtained from the interactions between CP hydrate and water droplet in oil bulk phase (black straight line) and in mixture of volume ratio of 1:1 CP and toluene phase (red dashed line) at 2.0 ± 0.5 °C. 75

Figure 5-20: Photographic images of hydrate morphology obtained at initial point of water being left on surface (A-1); the first indication of hydrate shell formation (A-2); final morphology of hydrate after fully conversion from water solution (A-3) in the mixture of cyclopentane and toluene phase (volumetric ratio: 1:1) at 2.0 ± 0.5 °C..... 76

Figure 5-21: Photographic images of hydrate morphologies during the conversion process from 2.5 wt. % NaCl solution droplet in the mixture of cyclopentane and toluene phase (volumetric ratio: 1:1) at 2.0 ± 0.5 °C: t = 0 min (A); t = 5 min (B); t = 10 min (C); t = 15 min (D); t = 20 min (E); t = 25 min (F); t = 30 min (G); t = 50 min (H). 77

Figure 5-22: Photographic images of hydrate morphologies during the conversion process from 2.5 wt. % CaCl₂ solution droplet in the mixture of cyclopentane and toluene phase

(volumetric ratio: 1:1) at 2.0 ± 0.5 °C: t = 0 min (A); t = 5 min (B); t = 10 min (C); t = 20 min (D); t = 30 min (E); t = 50 min (F); t = 60 min (G); t = 75 min (H). 78

Figure 5-23: Photographic images of hydrate morphologies during the conversion process from 2.5 wt. % Na₂SO₄ solution droplet in the mixture of cyclopentane and toluene phase (volumetric ratio: 1:1) at 2.0 ± 0.5 °C: t = 0 min (A); t = 5 min (B); t = 10 min (C); t = 30 min (D); t = 50 min (E); t = 70 min (F); t = 90 min (G); t = 100 min (H). 78

Figure 5-24: Capillary adhesion force measured between water droplet and CP hydrate probe (A); Corresponding pictures of hydrate morphologies captured at the initial contact point of water droplet and after 20 minutes annealing time in pure decane bulk phase (B) at 2.0 ± 0.5 °C. 79

Figure 5-25: Adhesion force curves plotted as a function of time during the interaction between a water droplet and a CP hydrate in the presence of 0.03 g/L asphaltenes in the mixed oil phase at 2.0 ± 0.5 °C (A); Corresponding images of the interactions with the addition of 0.03 g/L asphaltenes (B). 82

Figure 5-26: Effect of concentration of asphaltenes on the interaction force measured between a water droplet and a CP hydrate particle in the mixed oil phase at 2.0 ± 0.5 °C (A); Photographic images captured before contact (stage 1); contact period before droplet ruptured (stage 2); during contact period (stage 3); after detachment process (stage 4) with addition of 0.03 g/L asphaltenes (B) and 0.05 g/L asphaltenes (C), respectively.. 83

Figure 5-27: Effect of 3.5 wt. % NaCl on the interaction force between a water drop and a CP hydrate in the mixed oil phase at 2.0 ± 0.5 °C (A); Images captured at initial contact point (B-

1), first point of droplet rupture (B-2), final point of solution spreading (B-3) and final point of detachment process (B-4).	84
Figure 5-28: Effect of 3.5 wt. % CaCl ₂ on the interaction force between a water drop and a CP hydrate in mixed oil phase (A) at 2.0 ± 0.5 °C; Images captured at initial contact point (B-1), first point of droplet rupture (B-2), final point of droplet spreading (B-3) and final point of detachment process (B-4)	86
Figure 5-29: Dynamic interfacial tension between the aqueous droplet and oil phase with the addition of asphaltenes (A); Schematic diagram of adsorbed asphaltenes around the water drop (B).	87
Figure 5-30: Images of water, 3.5 wt. % NaCl and CaCl ₂ solution drops captured at crumpling point in mixed oil phase with addition of 0.03 g/L asphaltenes (A-1&2&3) and 0.05 g/L asphaltenes (A-4&5&6), respectively; Crumpling ratio measurements for the corresponding cases (B).	89
Figure 5-31: Structure of SPAN 80 (A); Schematic diagram of SPAN 80 adsorbed around droplet and CP hydrate particle (B).	91
Figure 5-32: Comparison of interaction mechanisms between water droplet and CP hydrate in pure liquid cyclopentane bulk phase with and without Span 80, respectively at 2.0 ± 0.5 °C	92
Figure 5-33: Photographic images captured from interactions between CP hydrate and water solution (A); 3.5 wt. % NaCl solution (B); 3.5 wt. % KCl solution (C); and 3.5 wt. % CaCl ₂ solution (D) with respect to contact time	92

Figure 5-34: Corresponding images of hydrate morphologies obtained by the conversion from DI water (A); 2.5 wt. % NaCl (B); 2.5 wt. % CaCl₂ (C); 2.5 wt. % Na₂SO₄ (D) in the pure cyclopentane phase at 5 ± 0.5 °C. 94

List of Tables

Table 1-1: Comparison of various properties between water, ice and gas hydrate	6
Table 5-1: Summary of densities and interfacial tension measurements as a function of concentrations of salt solution	49
Table 5-2: Relevant parameters on capillary adhesion forces measured between hydrate particle and solution droplet	55
Table 5-3: Summary of capillary adhesion forces measured between each electrolyte solution droplet and hydrate particle as a function of droplet size in oil phase	57
Table 5-4: Summary of capillary adhesion forces obtained with respect to contact time when the electrolyte solution bridge ruptures	59

List of Abbreviations

AA	Anti-agglomerants
CMC	Critical micelle concentration
CP	Cyclopentane
CR	Crumpling ratio
DTAB	Dodecyl Trimethyl Ammonium Bromide
ITFDA	Integrated Thin Film Drainage Apparatus
MEG	Mono-ethylene glycol
MMF	Micromechanical force
PVCap	Polyvinylcaprolactam
PVP	Polyvinylpyrrolidone
QLL	Quasi-liquid layer
SDBS	Sodium dodecylbenzenesulfonate
SDS	Sodium Dodecyl Sulfate
SPAN 80	Sorbitan monooleate
THIs	Thermodynamic inhibitors
TPC	Three phase contact
Tween 80	Polysorbate 80

Chapter 1 Introduction

1.1.1 Clathrate or gas hydrates

1.1.1 Phase diagram of clathrate or gas hydrate

The clathrate or gas hydrates, a host-guest compound, are more likely to be formed when hydrogen-bonded water molecules cage gas or hydrocarbon molecules including methane, carbon dioxide and cyclopentane under the preferred conditions. In other words, the low-temperature and high-pressure are considered as thermodynamically stable phase for clathrate hydrates [1] [2]. Figure 1-1 presents the phase diagram for a water/hydrocarbon (HC) system shown by Dutton et al. [3]. This diagram clearly indicates the favorable conditions for hydrate formation: low temperature and high hydrocarbon phase composed of liquid and gas hydrocarbon along with liquid water. Moreover, point Q_1 and Q_2 describe the lower and upper points where the four phases are in equilibrium. Due to the presence of mutual solubility, the phases are not pure. The hydrate formation and dissociation depend on the conditions between segments of Q_1 and Q_2 . Specifically, above the lines between Q_1 and Q_2 , the hydrate formation is stable, while the hydrate starts to dissociate and release water and hydrocarbon gas below this line.

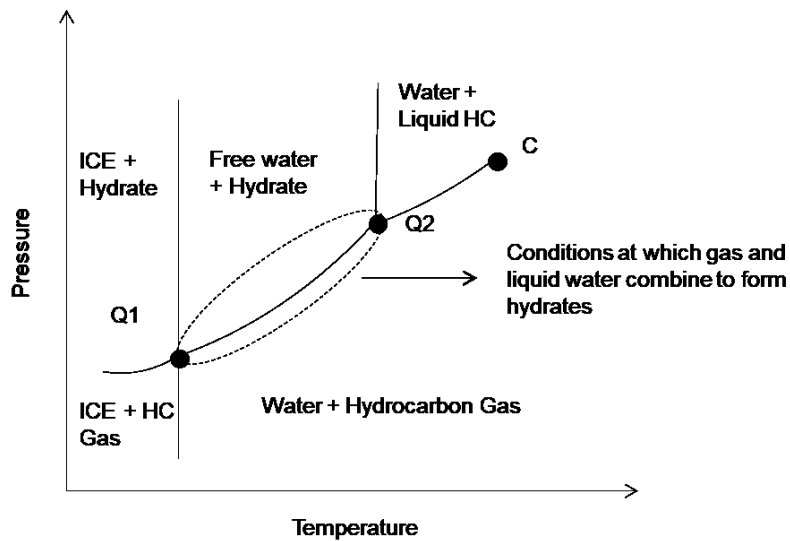


Figure 1-1: Phase diagram for a water/hydrocarbon (HC) system [3].

1.1.2 Characters of clathrate or gas hydrate

The size of guest molecules (i.e. hydrate formers) determines the structures of these crystalline inclusion compounds [4]. Generally, there are three different structures to describe the gas hydrates presented on Figure 1-2 [5]. For each structure, there is a primary building block called hydrate cavity – a pentagonal dodecahedron 5^{12} . This hydrate cavity is complemented by a large cavity. For example, the large cavity of structure I is tetrakaidekahedrons $5^{12}6^2$, containing 12 pentagonal and 2 hexagonal faces on the cage. It means that the structure I is created by 2 small cages (pentagonal dodecahedron) and 6 large cages (tetrakaidekahedrons), and the size of hydrocarbon or gas molecules for this structure is ranging from 0.4 to 0.55 nm. Likewise, 16 small cages and 8 large cages are required to form stable structure II, and the size of gas or hydrocarbon molecules between 0.6 to 0.7 nm can be trapped into the water molecules [5]. In fact, even though there are some vacant cages in the structure, a stable gas hydrate is still achieved by enough occupied cages. Nowadays, some techniques can be used to understand the lattice type and guest occupancy, for instance, powder X-ray diffraction, Raman spectroscopy,

and nuclear magnetic resonance (NMR) spectroscopy [5]. The thermodynamically preferred crystal structure is dictated by a combination of temperature, pressure, and the availability of hydrate-forming guest component. Most natural gas hydrates belong to structures I and II because of the presence of small amounts of larger hydrocarbon molecules in the oil and gas pipeline.

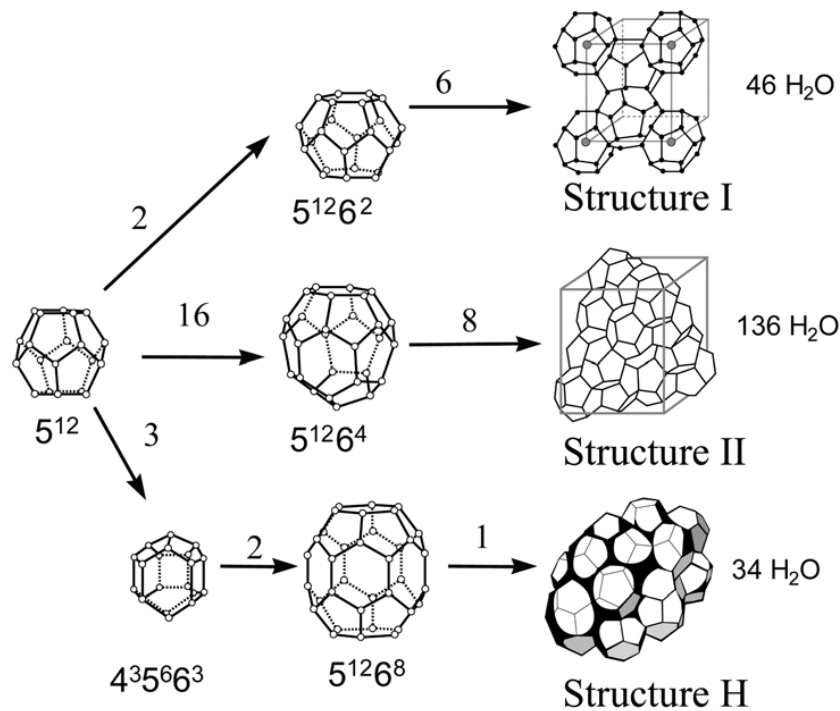


Figure 1-2: Structures of gas hydrates [6].

Figure 1-3 to 1-4 clearly plot Raman spectra for vapor and clathrated species for methane (i.e., CH_4) and propane (i.e., C_3H_8) single hydrates, respectively [7]. More specifically, from Figure 1-3, the splitting of band for CH_4 for the free vapor is distinct from that in the clathrate, indicating CH_4 partitions between the small (5^{12}) and large ($5^{12}6^2$) cavities of sI. Furthermore, the smaller band at high frequency to CH_4 is assigned in the small cavities while the larger band at high frequency to CH_4 is in the large cavities, which is consistent with the two small cavities and six large cavities. On the other hand, Figure 1-4 illustrates the Raman spectra of the C-C stretch for C_3H_8 vapor and C_3H_8 incorporated into hydrate at pressure above the three-phase condition.

Propane as the hydrate former is more likely to form sII hydrate crystals and it only occupies the large cavity ($5^{12}6^2$), therefore there is no split of band.

Figure 1-3 to 1-4 clearly plot Raman spectra for vapor and clathrated species for methane (i.e., CH_4) and propane (i.e., C_3H_8) single hydrates, respectively [7]. More specifically, from Figure 1-3, the splitting of band for CH_4 for the free vapor is distinct from that in the clathrate, indicating CH_4 partitions between the small (5^{12}) and large ($5^{12}6^2$) cavities of sI. Furthermore, the smaller band at high frequency to CH_4 is assigned in the small cavities while the larger band at high frequency to CH_4 is in the large cavities, which is consistent with the two small cavities and six large cavities. On the other hand, Figure 1-4 illustrates the Raman spectra of the C-C stretch for C_3H_8 vapor and C_3H_8 incorporated into hydrate at pressure above the three-phase condition. Propane as the hydrate former is more likely to form sII hydrate crystals and it only occupies the large cavity ($5^{12}6^2$), therefore there is no split of band.

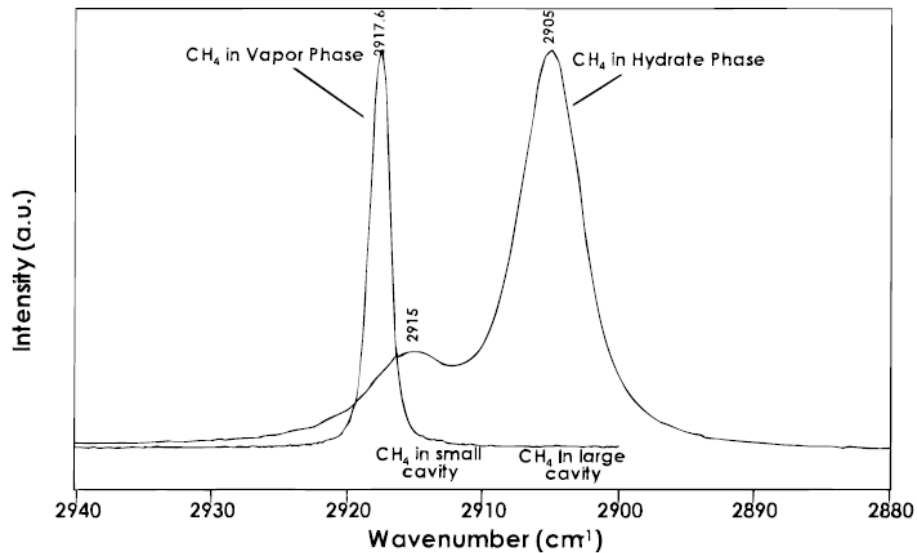


Figure 1-3: Raman spectra of CH_4 vapor and CH_4 incorporated into hydrate [7].

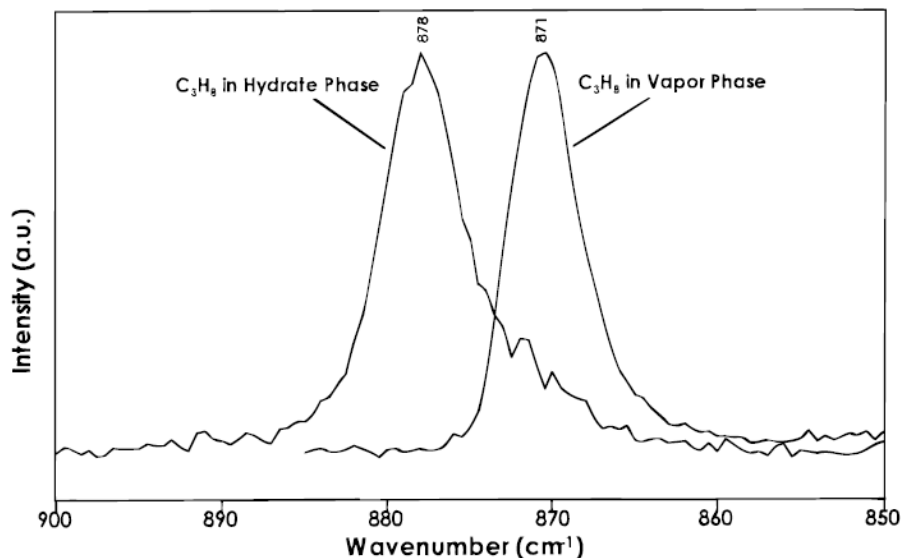


Figure 1-4: Raman spectra of C_3H_8 vapor and C_3H_8 incorporated into hydrate [7].

Rather than Raman spectra analysis, another direct space method to determine the cage occupancies and guest distributions is powder X-ray diffraction. Figure 1-5 shows the CO_2 molecules with full symmetry in small and large cages [8]. In the large cage, the guests lie near to the equatorial plane of the cage, suggesting CO_2 guest in each large cage has its long axis at an angle of 8° to the equatorial plane. In order to allow the carbon in the CO_2 molecules to be located almost at the center of the cage, the best model is to disorder the guest molecules in the small 5^{12} cages. According to Figure 1-6 [8], Takeya stated that C_3H_8 could occupy 92% of the large cages and there is no guest observed in the small cages in his study, whereas all large cages and 0% of the small cages were occupied in the single crystal analysis.

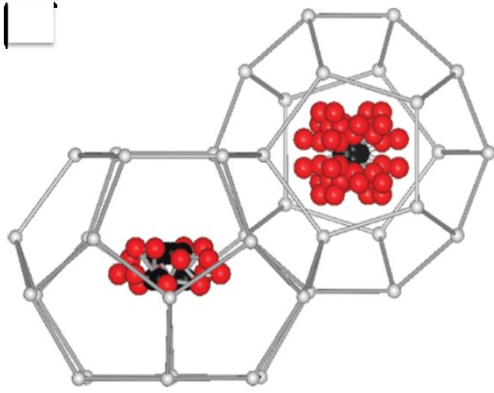


Figure 1-5: CO₂ molecules (carbon atom, black; oxygen atom, red) in sI large and small cages [8]

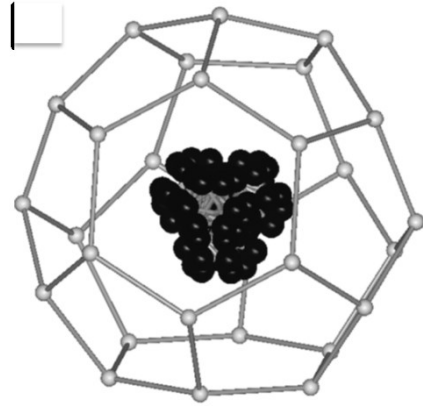


Figure 1-6: C₃H₈ molecules in sII large cages [8]

Actually, over 85 mol % water is found in gas hydrate, which causes many properties of gas hydrate to be similar to those of ice, such as physical appearance, refractive index and density. However, other properties of gas hydrate summarized in Table 1-1 are far different from those of ice, especially thermal diffusivity and thermal conductivity. Besides, the reason for the stronger mechanical strength of hydrate than that of ice is because of the slower rate of diffusion of water in the hydrate.

Property	Ice Ih	Structure I	Structure II
Thermal conductivity λ (W/m*K)	2.21 (283K)	0.57 (263K)	0.51 (261K)
Thermal diffusivity κ (m ² /s)	11.7 * 10 ⁻⁷	3.35 * 10 ⁻⁷	2.60 * 10 ⁻⁷
Heat capacity C _p (J/kg*K)	2052 (270K)	2031 (263K)	2020 (261K)
Compressional wave velocity V _p (km/s)	3.87 (5MPa, 273K)	3.77 (5MPa, 273K)	3.821 (30.4-91.6 MPa, 258-288 K; C ₁ -C ₂)
Bulk modulus K (GPa)	9.09 (5MPa, 273K)	8.41 (5MPa, 273K)	8.482 (30.4-91.6 MPa, 258-288 K; C ₁ -C ₂)
Density ρ (kg/m ³)	917 (273K)	929 (263K)	971 (273K); 940 (C ₁ -C ₂ -C ₃)

Table 1-1: Comparison of various properties between water, ice and gas hydrates.

1.1.3 Clathrate or gas hydrate nucleation and growth

Four requirements to generate the gas hydrate are concluded as followings: (1) low temperature; (2) high pressure; (3) the presence of methane or other hydrocarbon molecules; (4) the availability of water molecules. In nature, the locations for gas hydrates formation are widely observed in small, concentrated permafrost deposit. Generally, the hydrate formation is exothermic process, while the hydrate dissociation is endothermic process. There are two main steps of hydrate formation: hydrate nucleation and hydrate growth, and these two processes mainly occur along the interface, where it is not only with the existence of super-saturation of each component to form hydrate, but also the lower Gibbs free energy of nucleation [5] [6] [9] [10].

Hydrate nucleation: Commonly, the continuous growth and dispersion of small clusters of water and gas molecules until achieving a critical size describes the gas hydrate nucleation process. The relevant mechanisms involved in hydrate nucleation process are illustrated in Figure 1-7 [9]: (A) when pressure and temperature meet the conditions of hydrate formation, the water molecules begin to interact and form the initial partial and complete hydrate cages; (B) the dissolved guest molecules increases the changes of shared planar, and labile clusters form immediately; (C) as guest molecules being adsorbed onto the planar faces of the cages, inducing the local order, these labile clusters can fluctuate via hydrogen bonding; (D) primary crystal growth starts once the cluster reaches a critical value.

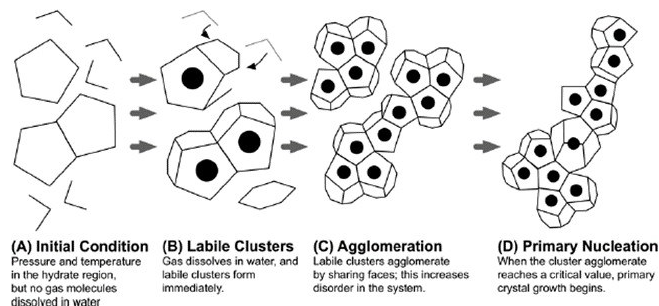


Figure 1-7: Mechanisms of hydrate nucleation [9].

Hydrate crystal growth: Gas hydrate growth occurs at the gas-liquid-solid interfaces when the temperature is below the equilibrium temperature. During this process, both mass and heat transfer play important roles on the hydrate growth rate. After gas hydrate nucleation, a water cluster with guest molecule is driven and attaches to the solid growing hydrate crystal surface by the lower Gibbs free energy and then a hydrate shell grows around the water droplet. It means, initially, a shelled droplet is followed by each successful gas hydrate nucleation, and then the gas hydrate shell grows inwards the droplet interior and converts the water into gas hydrate. A diffusion barrier caused by the hydrate shell formation could affect the growth rate based on the mass transfer limitation, and the thicker hydrate shell results in the longer conversion time owing to the slower mass transfer.

1.1.4 Thermodynamic and kinetic properties of clathrate or gas hydrate

The thermodynamic properties of gas hydrate concern the stability zone of gas hydrate relative with temperature and pressure. As mentioned above, the gas hydrate stability zone is determined by the temperature, pressure, fluid composition and gas composition [5]. In particular, some necessary assumptions are applied to estimate gas hydrate thermodynamic phase boundary: (1) the guest molecules would not distort the water lattice; (2) the cage is occupied by single guest molecules; (3) there are no interactions between guest-guest molecules; (4) there are independent interactions of guest-water molecules from each other. Furthermore, the addition of thermodynamic inhibitors (i.e., methanol or monoethylene glycol) could shift the stable equilibrium hydrate state towards lower temperature or higher pressure. Consequently, the thermodynamic properties of gas hydrate are highly affected by the concentrations of salts and chemical inhibitors.

The kinetic properties of gas hydrate are mainly dependent on time-dependent properties. The rate of gas hydrate nucleation and hydrate growth is controlled by the subcooling and content of each component to form hydrate [5] [11] - [13]. Sloan et al. [5] demonstrated the subcooling of 3.6 ± 0.3 K is essential to initiate the gas hydrate formation. Both the higher subcooling and enough number of guest or host molecules lead to the faster hydrate growth, indicating impacts of both mass and heat transfer rate-limiting make significant contributions on hydrate formation rate. On the other hand, the rate of hydrate growth decreases with the increasing path of transport [5] [14]. If the mass transfer of guest and water molecules across the hydrate shell is very slow, the hydrate formation or growth rate is reduced accordingly.

1.1.5 Advantages and disadvantages of clathrate or gas hydrate

Nowadays, the conventional oil is becoming less accompanying with the fast consumption due to the economic development; therefore, more scientists have focused on some alternative resources to meet this demand. From latest decades, gas hydrates have been treated as a strong candidate because of its largest global hydrocarbon reservoirs [5] [15] [16]. More specifically, Figure 1-8 suggests the amount of energy deposited in gas hydrates is almost twice that of the combination of all other fossil fuels reserves worldwide [17]. In addition, as exploration of offshore reservoirs increases in order to meet the demand for energy, to build a liquefied natural gas plant to transfer the produced gas is a huge challenge. Based on this, the second major advantage to study gas hydrate is because it is considered as a promising storage for natural gas. Based on the literature, once all single cages being occupied by the guest molecules, 1 volume of gas hydrate could store up to 170 volume of gas at standard conditions [4] [5].

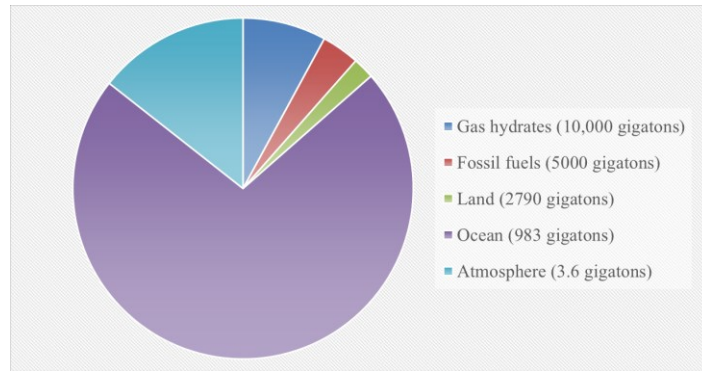


Figure 1-8: Distribution of organic carbon in earth reservoirs [17].

Nevertheless, conventional energy transportation, such as deepwater-oil and gas flowlines, is concluded as the prime location for hydrate formation due to its high operating pressures, and then the hydrate formation and agglomeration causes major flow assurance challenges in the oil and gas pipelines. According to the conceptual hydrate plugging mechanism (Figure 1-9) in oil-dominated line proposed by Turner [2] [6] [18], four steps for hydrate aggregation in pipeline are reported: (1) water is emulsified with oil in the pipeline; (2) a hydrate shell grows around the water droplet; (3) hydrate starts to agglomerate via capillary attraction; (4) the pipeline is plugged by the dramatic pressure drop due to the hydrate agglomeration. Since the temperature on the wall is the lowest; it provides the favorable conditions for the original hydrate formation. Afterwards, the channel becomes narrower as the hydrate deposition increases on the wall, leading to the pipeline pressure drop. The hydrate particles travel downstream once the hydrate wall is unable to bear the stress, and pipeline blockage occurs eventually.

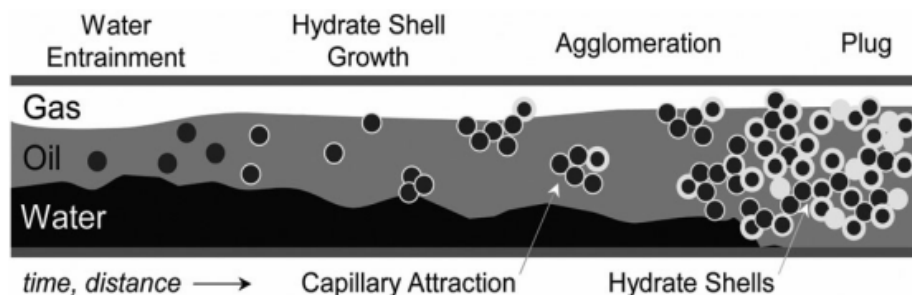


Figure 1-9: Mechanisms of hydrate plugging in oil-dominated flowlines [6].

1.1.6 Methods to avoid gas hydrate plugging in flowlines

As discussed above, the blockage of pipelines would cause the failure of production of oil and gas because the favorable conditions for gas hydrate formation (i.e., low temperature and high pressure) are accomplished by the deepwater transportation pipeline. Attempting to prevent this challenge, there are four main methods reported in the literature [5] [9] [15] [16].

1. Depressurization is one of the economical methods. After applying the depressurization, the gas hydrate equilibrium temperature is lower than that inside the pipeline, resulting in radial dissociation of gas hydrate.
2. Burying or insulating the pipeline is another reasonable method for gas hydrate dissociation. Increasing the environmental temperature prevents the initial gas hydrate formation.
3. The gas hydrate formation is inhibited by heating the gas at the wellhead.
4. Injection of inhibitors into flow lines is widely used. For instance, alcohols and glycols are employed into flow lines to shift the stable hydrate phase conditions towards lower temperature and higher pressure, achieving the goal of hindering hydrate formation.

1.1.7 Thermodynamic & low-dosage gas hydrate inhibitors

In order to prevent pipeline clogging, two main kinds of inhibitors, thermodynamic and low-dosage hydrate inhibitors, have been added into either the aqueous or hydrocarbon phase, respectively. The thermodynamic inhibitors including methanol or salts could inhibit the gas hydrate formation thoroughly via competing with hydrocarbon molecules for free water molecules [1] [5] [19]. Specifically, the addition of thermodynamic inhibitors into the aqueous phase would increase the Gibbs free energy of the interface, which enhances the barrier for gas hydrate formation [5] [20] [21]. On the other hand, all of kinetic inhibitors, such as polyvinylcaprolactam (PVCap) [1] [5], anti-agglomerants (e.g. SPAN 80) [5] [22] [23] and

natural oil surfactant [24] - [29] are classified as low-dosage gas hydrate inhibitors. Those inhibitors are preferred to delay hydrate nucleation or growth instead of total prevention. Hence, the cohesive force between hydrate particles is suppressed by generating hydrophobic hydrate surface and adsorption layers around particles after adding anti-agglomerants, and natural oil surfactant into oil phase, respectively.

1.2 Gas hydrate – surface interaction mechanisms

During the conventional transportation, gas hydrates are more likely to share interfaces with crude oils, liquid water, and hydrocarbon gas [2] [5] [9]. Contact forces are used to identify when the surfaces initially contact, and the contact force measurements between hydrate-hydrate, hydrate-solution droplets, and hydrate-solid surface are critical to reveal the hydrates agglomeration [1] [5]. In general, cohesion forces are determined by interactions between interparticle surfaces, while adhesion forces demonstrate the interaction between two different particles surfaces. Adhesion forces or cohesion forces are defined as the required force to separate two surfaces in contact with each other, at where consisting of multiple forces (e.g. dispersion, interfacial and capillary forces) [1] [5] [9]. The main types of forces acting to hold particles together are dispersion and capillary forces [1] [30]. The dispersion force, known as London Van der Waals forces [31], is the weakest intermolecular force dependent on particle size and distance between particles. Compared to dispersion forces, there are three potential mechanisms to indicate the interactions between two particles above micro length scale [5] [9] [32]. The first mechanism is solid-solid cohesion, and both the particle-fluid interfacial tension and the area measured at cohesive failure point could make contributions [5] [9]. As the second mechanism, the capillary bridge cohesion is governed by the bridge-fluid interfacial tension and bridge-particle contact angle [5] [9] [32]. The last important mechanism is described as the

sintering or hydrate growth mechanism, which is proportional to the product of the solid tensile strength and minimum sintered area [5] [9] [32] [33].

1.3 Objectives and outline

In the offshore oil and gas developments, the existence of salts in the pipeline systems is an essential factor to influence the flow assurance. Even though the salt effect (i.e., Sodium Chloride) on the hydrate formation had been studied and is accepted as a hydrate inhibitor, has been studied, its role on the interfacial dynamic behaviors of hydrates has rarely been investigated. With the increasing amount of salts during the offshore gas production, the impacts of salt should be evaluated for hydrates flow assurance.

In this research, we investigate the effects of salts on the hydrates flow assurance through the analysis of adhesion mechanisms between cyclopentane (CP) hydrate and four types of electrolyte solutions: sodium chloride (i.e., NaCl), calcium chloride (i.e., CaCl₂), potassium chloride (i.e., KCl) and sodium sulfate (i.e., Na₂SO₄) in both gas and liquid cyclopentane bulk phase. During several repeated measurements, variables such as concentration and droplet volume of electrolyte solution, and contact time between solutions droplet and CP hydrate probe would be studied. Thus, the most effective salts for reduction of the adhesion force and delay the hydrate growth and formation could be determined.

Additionally, our main goal is to prevent gas hydrate agglomeration inside the pipeline, and then both anti-agglomerants and natural oil surfactants are introduced into oil phase for better understanding of their influence on slowing the rate of hydrate growth and preventing the particles from adhering together.

Chapter 1 provides a brief introduction of gas hydrate, such as the structures, characters, hydrate

formation process and both the advantage and disadvantages to produce them. Moreover, three potential mechanisms of interactions between gas hydrate and other surfaces are also discussed.

Chapter 2 reviews the published literature on the cohesion interactions between two gas hydrate particles and also the adhesion mechanisms between gas hydrate and other surfaces. The effects of different surfactants are also elaborated.

Chapter 3 talks about the principles of adhesion forces between any solution droplet and cyclopentane hydrate particle. The theoretical background of capillary adhesion force, interfacial tension between water and oil, and the crumpling ratio measurements are also presented.

Chapter 4 gives detailed information of the experimental materials and setup utilized in this study. The preparation of cyclopentane hydrate and asphaltenes are also illustrated in this section.

Chapter 5 presents the experimental results on adhesion force measurements between solution droplet and CP hydrate particle in both oil and gas phase. Moreover, the effects of salts and surfactants on the hydrate growth are also analyzed.

Chapter 6 concludes the research findings of this work and provides suggestions for future studies.

Chapter 2 Literature Review

Significant work has been devoted on clathrate hydrates due to its positive and negative effects on the energy production industries. For decades, the interactions between gas hydrates and other surfaces and also the gas hydrate formation mechanisms had been investigated with relative parameters for better understanding of the gas hydrate. In this section, we will elaborate on these important findings in detail.

As mentioned above, there are three potential mechanisms to illustrate the interactions between gas hydrates and other surfaces: (1) solid-solid cohesion; (2) capillary bridge mechanism; (3) sintering or hydrate growth mechanism. More specifically, the solid-solid cohesion mechanism dominates the interactions between two hydrate particles after longer annealing time, while the interactions between hydrate particle and other surfaces with the presence of aqueous solution are mainly determined by the capillary force mechanism. Sintering mechanism is more likely to be accounted when the contact time is over 30 seconds. Most studies have focused on the interaction forces between hydrate particle and other surfaces in the liquid bulk phase instead of vapor environment because of the likely natural gas formation systems.

The micromechanical force (MMF) apparatus was commonly used in previous research to measure the hydrate-hydrate cohesive forces and hydrate-surface adhesive forces. Figure 2-1 shows the schematic of this experimental cell and Figure 2-2 describes the experimental measurement procedures [9].

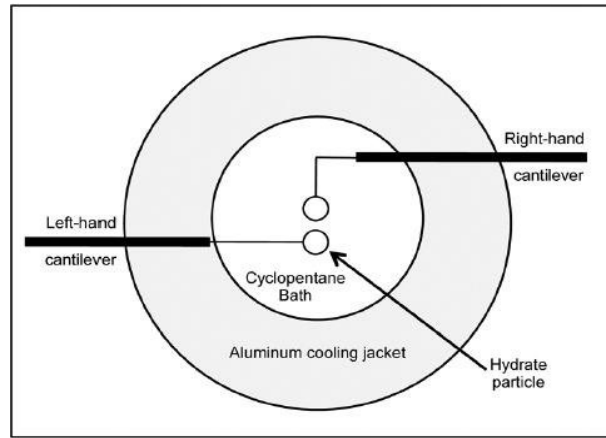


Figure 2-1: Top view of schematic of MMF apparatus [6].

The experimental cell filled with hydrocarbon bulk phase, surrounded by an aluminum cooling jacket, is connected to a water bath for controlling the experimental temperature. The hydrate particle is attached by two glass fiber cantilevers; one cantilever is manually controlled by a micromanipulator, and the other is connected to an automatically operated micromanipulator with a known spring constant (k). The hydrate particle can be prepared based on the following steps: (1) one drop of deionized water is placed at the end of glass cantilever; (2) the water droplet is converted to ice by immersing into liquid nitrogen for 20 seconds; (3) transfer this ice particle into the experimental cell which is filled with pure cyclopentane; (4) wait for 30 minutes to reach equilibrium. After applying a preload force, the upper cantilever starts to approach the lower hydrate particle until it is in contact with displacement (Δ_P in panel b of Figure 2-2), and after a set contact time, the upper hydrate particle is driven upwards to separate the particles (panel c to d of Figure 2-2). Finally, the cohesive force is calculated by the product of the displacement Δ_D and spring constant (k) according to the Hooke's Law [6].

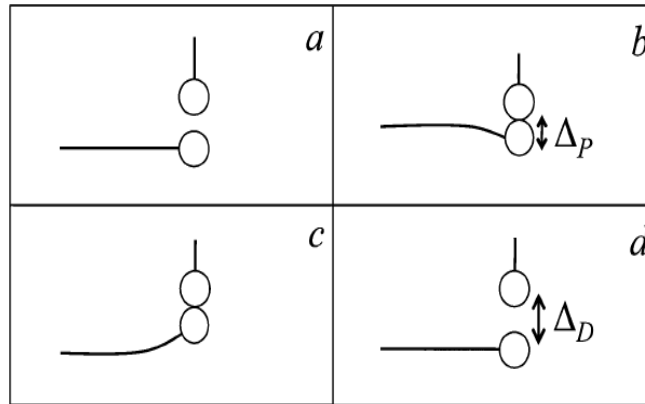


Figure 2-2: Schematic procedures of experimental measurements [6]: (a) hydrate particles are placed at the end of cantilevers; (b) the two particles are in contact after applying a preload force with displacement (Δ_P); (c) the upper hydrate moves upwards after a set contact time; (d) the particles break apart with displacement (Δ_D).

2.1 Cohesion force between CP hydrate particles in oil bulk phase

2.1.1 Effects of preload force and contact time

Based on previous reports [6] [24] [34], the cohesive force measured between CP hydrates in pure cyclopentane bulk phase was about 4.3 ± 1.2 mN/m with the applied preload force of 2 mN/m at 3.2 °C, and this cohesive force was commonly treated as the baseline value.

Typically, the cohesive force presents a direct relationship with the preload force because it relies on the contact area between elastic particles. The higher preload force would result in a larger contact area, and then larger cohesive force between particles [35]. Whereas, according to Aman et al. [9], the impact of preload force on cohesive force measurements between hydrate particles is negligible.

Compared to sintering mechanism, both solid-solid cohesion and capillary adhesion force are time independent. The experimental results found by Aman et al. [9] suggested that the

significant increase of cohesion force was observed until the contact time of up to 30 seconds. In other words, sintering or hydrate growth mechanism made a great contribution on interaction forces when the contact time was above 30 seconds, while capillary adhesion force dominated the interaction force for contact time below 30 seconds. Therefore, the cohesive force measured between hydrate particles is almost unchanged at shorter contact time, and it is continuously increasing with contact time owing to the sintering mechanism.

2.1.2 Effects of hydrocarbon oils and their modifications

Dieker et al. [24] studied the micromechanical cohesion force measurements between two hydrate particles with addition of small amount of crude oil (up to 8 wt. % in CP) and their modifications. The crude oil lowered the cohesive force obtained between two hydrate particles because the surface-active components might be responsible for lowering the interfacial energy and then the surface activity, which was also supported by Sjoblom et al. [25], Buckley et al. [26], Aspenes et al. [27] and Borgund et al. [28]. The existence of asphaltenes and naphthenic acids could not only decrease the interfacial tension between wetting fluid and hydrocarbon but also increase the contact angle between wetting fluids and hydrate particle. Overall, the presence of crude oils (i.e. more amounts of acids and asphaltenes) would prevent the pipeline blockage effectively by reducing the interaction force between two particles. Moreover, the types of acids played more important roles than amounts of acids on hindering hydrate aggregation inside the pipeline [24] [36].

2.1.3 Effects of different acids with varying concentrations

From the work of Aman et al. [2], four kinds of surfactant acids shown in Figure 2-3 with concentrations ranging from 10^{-10} to 10^2 mol/L were mixed manually with mixture of mineral oil and cyclopentane bulk phase to measure the cohesive force between the hydrate particles. It was proposed by Israelachvili [34] and Aman et al. [2] that only the solid-solid cohesion, depending

on the particle-bulk fluid interfacial tension, could be responsible for the measured interaction force. The CP hydrate particle-water interfacial tension and the hydrate-cyclopentane interfacial tension

were estimated at 0.32 ± 0.05 mN/m and 47 ± 5 mN/m, respectively [2]. Under the assumptions of same surfactant adsorption mechanisms, the cohesive force was reduced by applying lower concentrations of all four surfactant acids. The surfactants

were believed to be active along the water-oil interface; however, it was more likely that surfactants with lower concentrations were adsorbed on the hydrate-oil interface instead of on the water-oil interface based on the higher surfactant adsorption density measured at the hydrate-oil interface, which agreed qualitatively with Lo et al. [37].

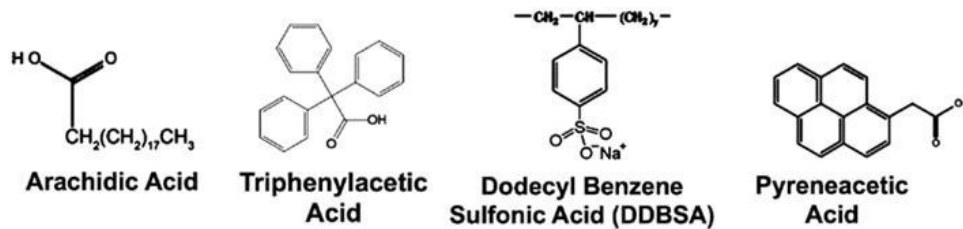


Figure 2-3: Chemical compounds of four surfactant acids [2].

2.1.4 Effects of thermodynamic inhibitors (THIs)

Thermodynamic inhibitors (THIs) were usually injected into flowlines to prevent hydrate formation by shifting the equilibrium state of stable hydrate towards lower temperature and higher pressure. In Lee et al. work [20], the use of thermodynamic inhibitors, such as methanol and ethanol soluble in hydrocarbon phase, mono-ethylene glycol (MEG) and sodium chloride (NaCl) soluble in water phase, were studied to understand their effects on cohesive force between two hydrate particles by using MMF apparatus. From the results evaluated by Lee et al. [20], the cohesive force measured as a function of annealing time decreased gradually from 9 mN/m (without any annealing time) to 4 mN/m (after sufficient annealing time) if there were no

thermodynamic inhibitors. Additionally, the cohesive force with the addition of any THIs was higher than that measured between two hydrate particles in pure oil bulk phase, and this phenomenon could be comprehended by two reasons: (1) the impact of unconverted water inside the hydrate particle; (2) the change in the subcooling due to the presence of THIs. The water conversion rate might be slowed down by these THIs, affecting the cohesive force and the hydrate morphology shown in Figure 2-4. From Figure 2-4 [20], the dendritic morphology of the hydrate on the surface occurred due to the secondary growth generated by the unconverted water with the presence of thermodynamic inhibitors. In other words, a larger amount of unconverted water, as source of capillary liquid bridge, caused by injection of THIs, would significantly enhance the cohesive force between hydrate particles. The panels A and B of Figure 2-4 illustrate the changes of hydrate morphologies before and after pull-off trials based on the mechanism presented in panel C of Figure 2-4. Furthermore, although the lower hydrate dissociation temperature had been found with the THIs injection, there was no temperature dependence on cohesive force only after longer annealing time [19]. Consequently, the annealing time was highly related to the unconverted water in the hydrate particles, and the roughness of the particle was the most important factor contributing to the cohesion force once applying sufficient annealing time.

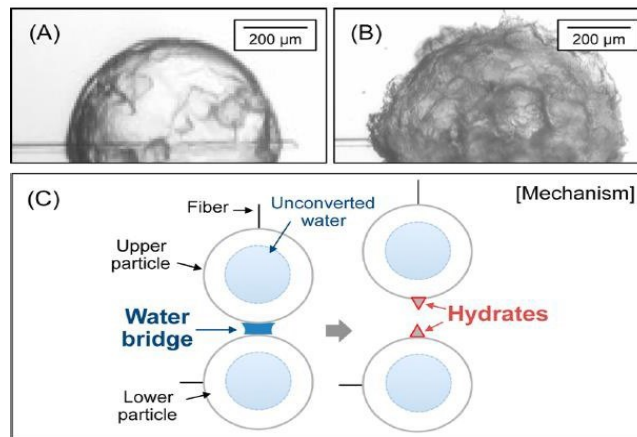


Figure 2-4: Morphological changes of CP hydrate [20]: (A) before pull-off trails; (B) after pull-off trails; (C) explanation of potential mechanism of this change.

2.1.5 Effects of antiagglomerants (AA)

Anklam et al. [38] reported a quantitative model for the interactions between hydrate particles attributed to three kinds of forces: repulsive steric force, attractive dispersion force and attractive capillary force. Moreover, they also studied the shear forces which could separate a pair of particles during flow process. The results suggested that a 2 nm-thick steric barrier was not high enough to prevent aggregation since there was a net attractive force between the particles, and the hydrate aggregation caused by the capillary adhesion could not be overcome by shear force. In addition, the interaction force between hydrate particles was dominated by capillary adhesion, while separating the particles by shear force even with the addition of AA was still difficult. They also observed three possible effects of AA on the capillary adhesion: (1) the increased steric layer because of the adsorption of AA on the hydrate particles; (2) the increased contact angle of water on the hydrate surface due to the adsorption of AA; (3) the reduced interfacial tension because of the adsorbed AA on the liquid-liquid interface. As a result, smaller water droplet formation could lead to smaller hydrate particles, and then the lower adhesion force was measured between two hydrate particles once adding AA into the system.

2.2 Adhesion force between CP hydrate particle and other surfaces in oil bulk phase

In the literature, many studies have evaluated the interactions between hydrate-hydrate, hydrate-solution, and hydrate-solid surfaces. The interactions between hydrate-solution and hydrate-solid surfaces are more critical for better understanding of the mechanisms of gas hydrate formation inside the pipeline. The main strategy to prevent pipeline blockage is the prevention of gas

agglomeration, which means reduction of the adhesive force between hydrate and other surfaces is important.

2.2.1 Adhesion force between CP hydrate and water solution droplet

In most cases, the agglomeration of hydrates presented by hydrate-water droplet interactions contributes to the plugging of pipelines. Unconverted water as a source of the capillary force bridge has attracted many investigations. Not only the solution with surfactants but also the conditions of contact time, contact area and subcooling would greatly affect the interaction mechanisms between hydrate and solution droplets.

2.2.1.1 Interactions between CP hydrate and water solution droplet

Liu et al. [14] studied on the interactions between water droplet and CP hydrate particle by using MMF apparatus. The CP hydrate particle (i.e., $d = 0.68$ mm) was formed at the end of the left-hand cantilever according to methods discussed above, while a water droplet with radius of 0.26 mm was placed onto an aluminum plate which was fixed at the end of the right-hand cantilever. A strong attractive force was observed once the surfaces were in contact because of the formation of the three-phase-contact (TPC) line. Since the CP hydrate was hydrophilic, the spreading of water on the hydrate particle surface was spontaneous. With further preload force applied, the sintered TPC line moved closer to aluminum plate and the new hydrate started to grow along the interface. During the detachment process, the change of the curvature of capillary bridge dominated the interaction forces between water droplet and CP hydrate particle. The linear force curve in this region suggested the droplet behaved as a spring. With the increasing displacement between water droplet and CP hydrate particle, the maximum interaction force was obtained at the point of widest capillary bridge formation. The interaction force was gradually decreasing when the water droplet was further stretched from the hydrate particle along with the presence of the “neck” of the capillary bridge. Finally, some amount of water was left on the hydrate particle

after the bridge was broken. After rupture, the hydrate shell formation was growing around the water droplet placed on the hydrate particle within minutes. Because the faster hydrate formation rate was determined by the higher subcooling, the morphology of new hydrate growth maintained the original spherical shape of the water droplet.

2.1.1.2 Effects of water volumes

Cha et al. [39] determined the effects of aqueous droplet size varying from 100 to 600 μL on the interaction force between CP hydrate probe and water droplet in cyclopentane/n-decane oil mixture. The reason of using CP/n-decane oil mixture instead of pure cyclopentane was to preserve the CP hydrate probe with limited dissociation. During the cycle from contact to detachment, the maximum contact force was observed at the initial contact point due to widest capillary bridge formation and gradually decreased through the retraction process without any aging time when the volume of the water droplet was lower than 100 μL . In contrast, if the volume of water droplet was higher than 100 μL , the capillary bridge was widening during early stage of the detachment process, which indicated that more liquid solution was adsorbed on the surface of the CP hydrate with the displacement of the wetting line. Moreover, the contact force continuously decreased until complete separation of hydrate and water droplet [38]. However, buoyancy was the reason that the contact force did not return to its initial value after retraction.

Nevertheless, the interaction forces were only dependent on the volume of droplet which was smaller than 300 μL . The level-off behavior of interaction force was observed if the droplet volume was larger than 300 μL . The retraction time also increased with the volume of the droplet, then the retraction time and contact force shared the similar trends associated with the volume of the droplet. Consequently, the wider capillary bridge with a large volume of water would result in higher interaction force and more hydrate formation in pipelines.

2.1.1.3 Effects of contact time

In order to understand the effects of contact time on interactions between water droplet and CP hydrate particle, Liu et al. [14] measured the adhesion forces when the surfaces were in contact lasting up to 180 s. The trend of the force curve was similar as the one mentioned in 2.2.1.1 before applying longer contact time. During the extended contact time, the hydrate growth occurred along the interface, resulting in the larger interaction force. However, the maximum interaction force was obtained at the break point of the bridge, which was quite different from the previous case. With shorter contact time, the maximum interaction force was observed at the point of widest capillary bridge formation and the force was decreasing with the width of capillary bridge until ruptured. Furthermore, a larger proportion of the water droplet was covered by the hydrate shell formation under longer contact time, which led to less amount of water being left on the hydrate particle after the surfaces were separated. As a result, the maximum adhesion force measured with extended contact time was greater than the one with shorter contact time, and the interaction force was governed by the tensile strength of the hydrate. In other words, the sintering mechanism dominated the interaction forces after employing a longer contact time.

2.1.1.4 Effects of subcooling

Both subcooling and amount of each component to form hydrate play critical roles on the hydrate formation rate; specifically, either lower subcooling or smaller amount of guest or host species leads to the slower hydrate formation rate [5] [14]. Liu et al. [14] stated that the water-hydrate interaction behaved similarly as water and hydrophilic solid particle. During the experimental process, hydrate formation did not occur due to the lower driving force (i.e., lower subcooling). Eventually, the water left on the hydrate particle required a longer time to convert into hydrate. Therefore, even though hydrate formation started to grow along the interface regardless of

subcooling, the hydrate morphologies were significantly different from each other. At higher subcooling, the hydrate shell was span around the water droplet and the shape was close to the original water droplet, while the irregular basin-like geometry was observed on the hydrate particle at lower driving force. These observations suggested that more water converting to hydrate caused the larger interaction force and huge hydrate agglomeration at higher subcooling, which increased slurry viscosity [14].

2.1.1.5 Effects of surfactants

Surface-active agents, anionic surfactant sodium dodecyl sulfate (SDS), cationic surfactant dodecyl trimethyl ammonium bromide (DTAB), nonionic surfactants of polyvinylcaprolactan (PVCap) and polyvinylpyrrolidone (PVP), were employed onto the smooth AL substrates in the hydrate-solution droplet system surrounded by CP/n-decane oil mixture (65:35 volumetric ratio) at 2.8 ± 0.2 °C with concentrations varying from 100 to 5000 ppm [1]. According to the results obtained by Song et al. [1], for anionic and cationic surfactants, the contact forces decreased with the increasing concentrations because of the decreasing interfacial tension, while the effects of concentrations of nonionic inhibitors were negligible. The adhesion energy showed the same tendency illustrated by Song et al. [1]. As the concentration of cationic and anionic surfactants was increased, the adhesion energy decreased, whereas the adhesion energy was independent of the concentrations of nonionic inhibitors [1].

Sorbian monooleate (Span 80) is a common water-in-oil type surfactant that is treated as an anti-agglomerant on the interactions of hydrate-water droplet. From Liu et al. [14], 1 wt. % Span 80 was added into the hydrate-droplet systems in pure CP bulk phase to investigate its effects on hydrate growth morphology and adhesion forces. In order to keep the droplet on the surface, a brass surface with an epoxy coating was used instead of Al substrate. Since the presence of hydrophilic head and hydrophobic tails in Span 80, the adsorption layer was formed around the

water droplet surface, which prevented the water droplet from breaking when the surfaces contacted [14]. This phenomenon was also found by Li et al. [40]. Once applying larger external force, the droplet ruptured and formed the liquid bridge that spread over the entire hydrate particles due to the reduced interfacial tension between water and cyclopentane by addition of the Span 80. Meanwhile, the volume of the liquid bridge decreased with more water forming hydrate rapidly, which led to significant change on the hydrate morphology [14] [40]. Additionally, the combinations of rapid hydrate formation and an irregular surface growth after internal unconverted water contacted with the bulk phase led to the morphology changing to a hair-like extrusions [14] [41].

Furthermore, Li et al. [40] also studied the effects of concentrations and subcooling on the interactions between CP hydrate probe and water droplet with additives of Span 80. They suggested even with low concentrations of Span 80 (i.e., 0.01 wt. %), the tight packing could ensure the strong mechanical strength of adsorption layer, and then hindered the formation of the capillary bridge and prevented hydrate agglomeration. After droplet attachment, the Span 80 would accelerate the agglomeration because of the decreased w/o interfacial tension. Moreover, the effects of subcooling could influence the interaction behavior greatly once breaking the water droplet. More specifically, the spreading of water droplet on the hydrate particle was spontaneous at the lower temperature, and the water could convert into hydrate rapidly. On the other hand, the lower subcooling caused the mixture of water droplet and water coating film rather than spreading over the whole hydrate particle, therefore, the capillary bridge dominated the interaction behavior after the rupture of the water droplet. Liu et al. [14] and Li et al. [40] concluded that the surfaces of both water droplet and hydrate would be too strong to be broken at contact point if the external force was not large enough with addition of the Span 80; thereby

inhibiting the formation of the liquid bridge and hindering the hydrate agglomeration were expected.

2.1.1.6 Effects of salts

Hydrate risk management, hydrates forming without tendency of plugging, has been expressed in the modern study. The roles of sodium chloride as inhibitors were examined by Lee et al. [21], who stated that NaCl would act as a hydrate inhibitor to hinder the further hydrate crystallization by lowering the subcooling in order to decrease the hydrate formation rate when NaCl solution droplet contacted with hydrate particle. However, the adhesion forces measured were almost unchanged through three consecutive cycles because of the smaller amount of hydrate formation after adding NaCl into the water droplet. Moreover, the concentration of NaCl solution up to 3.5 wt. % was high enough to delay hydrate formation [21]. As mentioned by Song et al. [1], SDS solutions would decrease the interfacial tension and adhesion force, then further decreasing adhesion forces were achieved by adding NaCl to the SDS solutions and the hydrate growth would be inhibited more effectively [22].

2.2.2 Adhesion force between CP hydrate and solid surface

In general, the hydrates forming in the oil/gas pipelines may share interface with solid surface, and the solid surface materials (e.g. carbon steel, stainless steel etc.) with and without naphthenic acids and asphaltenes, and the presence of water cut are related to hydrate formation mechanism. Thus, investigations of mechanism between hydrate and solid surfaces are necessary for better understanding of hydrate agglomeration inside the pipeline.

2.2.2.1 Effects of dry solid surface materials and acids

Following Aspenes et al. [42], the effects of water cut and petroleum acids on adhesion forces between CP hydrate and solid surfaces were studied. Under no free water and acid addition circumstance, the adhesion forces obtained on the interactions between CP hydrate probe and all

of dry solids, such as stainless steel, carbon steel and aluminum, surrounded by liquid cyclopentane bulk phase was almost one order of magnitude smaller than cohesion forces measured between hydrate-hydrate (4.3 ± 1.2 mN/m [6] [42]) owing to the low preference of CP hydrate depositing on the pipeline wall, which confirmed with conclusions found by Nicholes et al. [43]. Another finding has been discovered that adhesion forces measured by the interactions between hydrate and solid surfaces were proportional to surface free energy of these solids, where higher surface free energy led to higher adhesion forces [40]. Nicholes et al. [43] indicated the adhesion forces were increasing with the temperature, which could be explained by the formation of QQL (quasi-liquid layer). The rougher the stainless-steel surface might cause lower adhesion forces. Although the hydrate particles were unlikely to deposit on the pipe wall with the absence of free water, the hydrate nucleation would occur on the pipe wall, the coldest point in the system, via hydrate growth [43]. A water layer was much less likely to be formed between hydrate and solid when the acids were employed into the system since the acids could be adsorbed on the solid surface or hydrate surface or both, then the adhesion forces measured with addition of acids were much lower than cohesion forces between hydrate and hydrate and adhesion forces between hydrate and solids without acid [42]. Nevertheless, the adhesion force on hydrate-solid system without acids (around 0.5 mN/m [42]) was still lower than the cohesion force measured between CP hydrates with acid (around 1.3 mN/m [42]).

2.2.2.2 Effects of presence of water droplet

According to Aspenes et al. [42], the adhesion forces between hydrate and solid surface when a water droplet deposited onto the surface were measured as ten times larger than cohesion forces on hydrate-hydrate system, suggesting that the hydrate might preferentially deposit on water-wetting pipeline wall caused by the larger attractive forces. Furthermore, the addition of acids

could be adsorbed on the surfaces of hydrate and solid to reduce the interfacial tension and enhance the contact angle between water and oil phase, which resulted in less amount of water forming the capillary bridge and almost half value of adhesion forces measured between hydrate and solid lower than those measured from hydrate-solid system without acid [42]. Thus, hydrate particles were unlikely to deposit on the pipeline wall with the absence of free water; in other words, hydrate agglomeration inside pipeline was highly correlated to the existence of water, and the water-wet pipeline was considered as the favorable location for hydrate decomposition [42].

2.2.2.3 Effects of physical and chemical modifications

Impacts of five categories of physical and chemical modification to steel, such as oleamide, graphite, citric acid ester, nonanedithiol and Rain-X anti-wetting agent, on the interaction forces measured between hydrate and steel surfaces under dry and water-wet surface conditions were determined by Aman et al. [32]. For dry conditions, up to 79% reduction of adhesion forces was caused by the graphite coating because of the shifting the surface from hydrophilic to hydrophobic via increasing wetting angle. The chemical nonanedithiol surface coating resulted in the higher adhesion force due to the hydrate growth along the interface, while the presence of stainless-steel surface with citric acid ester coatings reduced the adhesion force because of the lower interfacial tension between water and oil. The citric acid ester also encouraged hydrate growth since this strong surfactant might enable the rapid morphological changes by reducing the interfacial energy barrier to growth. In contrast, the effects of citric acid and graphic coatings on lowering adhesion forces were weakened by the presence of water. These results suggested the challenge of hydrate deposition could not be eliminated by physical or chemical modifications alone when containing a water-wet steel surface.

2.2.2.4 Effects of mineral surfaces

Aman et al. [44] measured the adhesion forces between CP hydrate particle and two mineral surfaces: heterogeneous quartz and calcite substrates. As compared with stainless steel surfaces, these two mineral surfaces could enhance the adhesion forces up to five to ten times, while the rapid hydrate conversion was observed with the employment of raw quartz. Moreover, the adhesion forces as a function of contact time between CP hydrate particle and these two mineral surfaces were increasing with the contact time because the interaction was dominated by sintering mechanism, but there was no visible growth of hydrate on the mineral surfaces. In addition, the influence of contact time was less efficient on the adhesion forces measured on hydrate-steel or -quartz comparing to -calcite. The shorter annealing time resulted in higher adhesion force, which could be understood by the easy migration of unconverted water from the hydrate particle core to the interface due to the presence of more porous hydrate shell [44]. The existing model of capillary adhesion could not well-represent the interaction between hydrate-quartz which was more sensitive to the contact angle than it between hydrate-stainless steel.

2.3 Mechanism of CP hydrate formation/growth along water-oil interface

Both thermodynamic equilibrium and kinetics are two main topics on the hydrate formation, and many researchers have clarified the issues related to nucleation and growth process. It is well known that supersaturation of one-component of gas hydrates is the driving force for the hydrate crystallization. Kashchiev et al. [45] illustrated the expressions of the supersaturation in isothermal and isobaric regime. The nucleation and growth rate depended on subcooling which was investigated by Corak et al. [13]. As mentioned above, the hydrate film growth spans along the water/oil interface. Taylor et al. [11] studied the CP hydrate film growth through the measurements of gas consumption and hydrate film thickness. Moreover, the impacts of salts,

hydrophobic additives and surfactants were determined in last decades as well.

2.3.1 Driving force for crystallization of gas hydrate

Supersaturation ($\Delta\mu$) is defined as the difference between the chemical potentials of a hydrate building in the solution (old phase) and in the hydrate crystal (new phase) [5]. Figure 2-5 showed the three-phase system of a one-component gas, an aqueous solution of gas and a gas hydrate [45]. The supersaturation in hydrate formation could be given in Equation 1 [45].

$$\Delta\mu = \mu_{gs} + n_w\mu_w - \mu_h \quad 1$$

μ_{gs} : chemical potentials of the gas molecules in the aqueous solution
 μ_w : chemical potentials of the water molecules in the aqueous solution
 n_w : number of water molecules in aqueous solution
 μ_h : chemical potential of a building unit (one gas molecules and n_w water molecules)

The nucleation of hydrate occurs only when $\Delta\mu > 0$, which means that the solution is supersaturated. This expression can also be applied to describe the formation of one-component gas hydrate in ice by replacing the aqueous solution with ice [45]. The supersaturation is highly dependent on the concentration of dissolved gas in the aqueous solution, where higher concentration of dissolved gas leads to larger driving force for crystallization. Kashchiev et al. [45] noted the supersaturation shares the inverse relationship with temperature in the isobaric regime when sufficient time is elapsed after the surfaces contact.

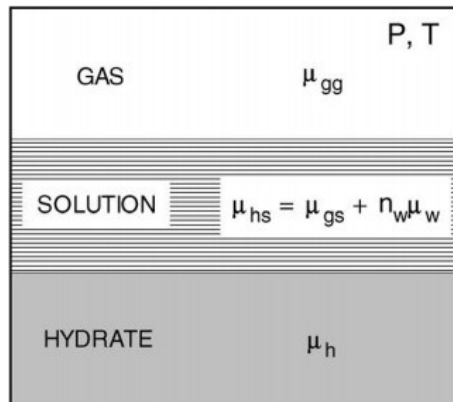


Figure 2-5: Three-phase system of one-component gas, aqueous solution, and gas hydrate [45].

2.3.2 Macroscopic investigation of gas hydrate film growth

Taylor et al. [11] reported the mechanism of hydrate film growth at the water/oil interface via measurements of film thickness, propagation rate and gas consumption. Not only the effects of the amount of water used but also the solubility of the hydrate former in the aqueous solution on hydrate growth was hypothesized in their paper. The initial thickness of 12 μm was observed at a planar water/oil interface as the barrier between water and oil phases. The thickness of the hydrate film was increasing with subcooling and contact time, consistent with previous studies [46] [47]. Moreover, the smaller guest molecular size resulted in a larger diffusion coefficient through the hydrate layer [5] [11]. Even though the addition of other hydrocarbon into the oil bulk phase had limited impacts on the hydrate film thickness, significant longer time was required to achieve the final thickness. The gas consumption was understood by a pressure drop because of aqueous phase dissolution or hydrate formation. After hydrate formation, supersaturation of hydrocarbon in the aqueous phase was found, and the concentration gradient between interface and bulk caused mass transfer of dissolved hydrocarbon consumed by the hydrate film growth [11]. The hydrate growth rate was a function of subcooling and solubility difference, in other words, both higher subcooling and solubility difference could lead to the faster hydrate growth rate. Furthermore, Saito et al. [48] stated that the hydrate-film growth could be better correlated with solubility difference than subcooling by using a power-law function, which suggested both heat (subcooling) and mass (solubility difference) transfer limitations made great contributions on the hydrate film growth rate. Taylor et al. [11] also proposed the mechanism of hydrate film formation at the planar water/oil interface, shown in Figure 2-6. Usually, there were three stages for hydrate film formation: (1) initially, the hydrate film was formed through the propagation of a thin porous hydrate film across the interface; (2) the hydrate film was developed by porous hydrate film being filled with time; (3) within a longer period of

time, the bulk conversion was achieved by all porous hydrate film being filled.

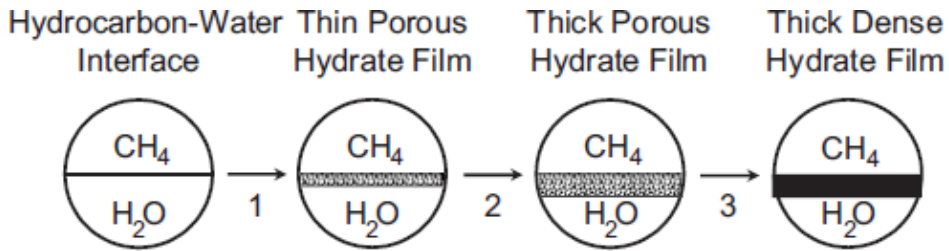


Figure 2-6: Schematic of mechanism of hydrate film formation at the planar water/oil interface [11].

2.3.3 Effects of subcooling and amount of gas hydrate former on hydrate formation

According to Corak et al. [13], the hydrate number, defined as the ratio of the number of water (host) molecules in the hydrate crystals to number of hydrate former (guest) molecules, was depending on the subcooling temperature. Compared with the theoretical hydrate number for CP hydrate as 17 [5], the higher value 19 was measured at subcooling of 3.6 K, which meant less amount of hydrate former were entrapped in the hydrate structure. On the other hand, the lower hydrate number revealed the presence of unconverted cyclopentane at higher subcooling due to the rapid crystallization. Kaskichiev et al. [45] evaluated the positive trend between driving force and subcooling. By increasing the amount of hydrate former, faster growth at higher subcooling was expected because of better mass transport, less diffusion resistance and increased number of nucleation sites. In contrast, the more amount of hydrate formation was measured at lower subcooling, which could be explained by total available mass of cyclopentane. Specifically, the amount of unconverted cyclopentane encapsulated both in hydrate shells and inside pores of the hydrate sample was increasing with subcooling, and these amounts of cyclopentane were unable to form hydrate [13].

2.3.4 Effects of surfactants on gas hydrate formation

To mitigate hydrate agglomeration inside pipeline, the effects of surfactants including dodecylbenzenesulfonic acid and Tween 80 with various concentrations on hydrate growth had been investigated by Brown et al. [49]. The MMF apparatus was used to measure the cohesion force between two CP hydrate particles and the force to break hydrate shell and shell thickness. For hydrate shell strength measurements, the empty top cantilever was pressed into the particle until the shell fractured and the force required to break the shell was calculated by the product of spring constant of cantilever and the maximum displacement of the shell from its resting position [49]. The subcooling was a weaker function than annealing time on the forces which were required to puncture the hydrate shell. Although the puncture force/hydrate shell strength was decreased by the addition of surfactants regardless of concentration, the presence of surfactants showed less dominant impact on the hydrate shell thickness. The use of surfactants could alter the wettability of the hydrate shell and reduce the interfacial tension, causing a more porous hydrate shell. Since there was no significant difference in the macroscopic morphology of hydrate with surfactants, the interactions between hydrate and surfactants could be proposed as the surfactants interacting with the hydrate cages themselves rather than adsorbing on the hydrate surface [49].

Karabjkar et al. [50] reported the effects of Span 80 in the hydrate crystal growth. The hydrate formation occurred along the water/oil interface in a three-step consequence of nucleation, lateral surface growth and radial growth. When a water drop was immersed into surfactant-free cyclopentane phase, a faceted polycrystalline hydrate shell formation was observed around the water droplet. After adding 0.01 vol. % of Span 80, the crystal changed to a unique hollow-conical shape, eventually it formed a mushlike/hairy and porous hydrate morphology after fully conversion of water, being confirmed by Cha et al. [51]. Many researchers also observed similar hydrate morphologies with the presence of surfactants [52] [53] [54], and Aman et al. [53]

believed there was a stronger relationship between hydrate surface morphology and the addition of Span-class surfactants rather than the hydrate former. The hydrate growth was more likely occurring at the cone base (i.e., three phase contact line), and the hydrate crystal could be immersed into the water as the crystal was growing larger. Figure 2-7 presented the proposed mechanism for hydrate growth with the addition of Span 80. The water-oil interfacial area was reduced by the increasing concentration of Span 80, and the surfactant crowding at the interface resulted in an excess surface pressure and the formation of unique hollow conical crystals along the interface [50] [51].

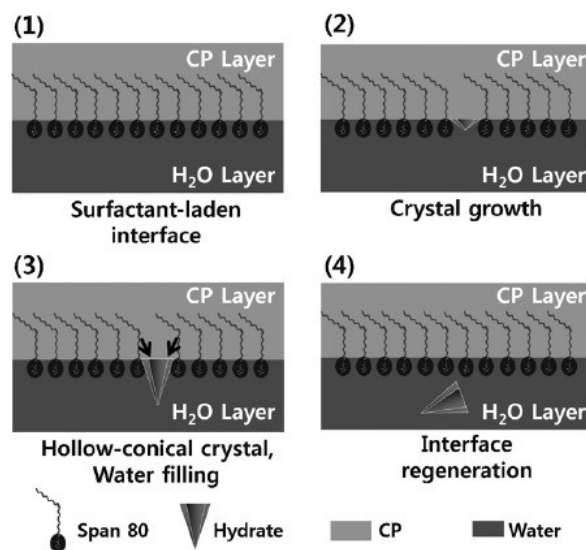


Figure 2-7: Schematic of CP hydrate lateral surface growth hypothesis [51]

2.3.5 Effects of salts on hydrate growth

Based on the literature, the increasing salt concentration weakened the hydrate crystal growth rate [12] [54]. Kishimoto et al. [12] studied the effects of elevated salt concentrations (i.e., higher than 3.5 wt. % NaCl) on the hydrate growth at the interface between seawater and hydrocarbon. The size of hydrate growth was a function of subcooling at atmospheric pressure, and higher subcooling led to the smaller size of hydrate crystals [11]. In addition, the morphology of hydrate

crystal showed limited variation regardless of concentration of NaCl at a specific subcooling, which indicated the subcooling was a more dominant factor on hydrate crystal morphology, and this result agreed with Sakemoto et al. [56] and Zylyftari et al. [57]. Moreover, the concentration of salt could not influence the hydrate growth rate greatly after hydrate nucleation [57] [58]. The increasing of salt concentration inside the water droplet was found accompanying with hydrate formation and consumption of water, which slowed the hydrate growth and limited the water conversion into hydrate due to the less subcooling [57] [59]. At a given subcooling, the hydrate film growth rate was reduced by the increasing NaCl concentration.

2.4 Sintering mechanism at contact point

Sintering is a reactive mechanism, and it probably describes the solidification of liquid solution to bond to a pre-existing solid crystal at longer annealing time [6] [60] [61]. The Equation 2 shown following represents the force required to fracture the hydrate bridge, depending on the tensile strength of cyclopentane hydrate (i.e., $\tau = 0.91$ MPa [6]) and the interfacial area (A_i) at the weakest point (i.e., the neck of the bridge) [6]. This mechanism may explain the “growth” of hydrate along a water-hydrocarbon interface if three criteria are met: (1) Available water bulk phase except QLL is present; (2) Water is in contact with hydrate former; (3) The existence of hydrate seed near the interface is achieved [5] [6]. Uchida et al. [59] estimated the sintering rate based on the observations of sintering process of tetrahydrofuran (THF) hydrate particles, and believed that the rate of sintering was mainly determined by the supplement of each component of hydrate formation (i.e., water and guest molecules) from the bulk phase to the sintering site by mass diffusion. They reported lower sintering rate of hydrate particles than ice particles under normal vapor conditions, but when the bulk phase saturated with guest molecules and the host molecules could diffuse from the inside of gas particle rapidly, faster hydrate growth or sintering

would occur along the interface [5] [6] [60].

$$F_s = \tau * A_i \approx \tau (\pi * 1.5 * t^{0.2498})$$

2

Chapter 3 Experimental methods

3.1 Capillary adhesion force measurements

The work by Aman et al. [6] demonstrated the cohesion or adhesion force in oil bulk phase is dominated by capillary force interactions and sintering mechanism. Capillary force arises from the capillary bridge formation between two surfaces, and Aman et al. [5] proposed three sources of water to form capillary bridge: (1) emulsified water droplets; (2) unconverted water from the hydrates core; (3) a quasi-liquid layer formation under the lower subcooling (i.e., less than 20 K of its melt temperature) [12] [61]-[67]. The former two water sources have been discussed above, while a quasi-liquid layer (QLL) is presented as the product of surface melting when a pure crystal is near its melting temperature with co-existing of a secondary immiscible fluid [5] [6]. The height of QLL is relative with the subcooling; in other words, the higher subcooling would result in the higher capillary force because the thicker QQL reduces the crystal surface roughness. Furthermore, three main contributions are expected to determine the forces of a capillary fluid binding two particles in the presence of a second immiscible fluid, (1) pressure difference between the bridge and bulk phases; (2) the normal component of surface tension; and (3) the energy associated with the three-phase contact line (i.e., contact area and contact angle) [5] [6]. Based on previous studies, the final form of the capillary adhesion force is given as [68].

$$F_c = \Delta P \pi R^2 \sin^2 \alpha + [-2\pi R \gamma \sin \alpha \sin (\theta + \alpha)] \quad 3$$

Where R is the radius of hydrate particle, α is the half-filling angle of the hydrate-capillary bridge contact, γ is the liquid solution - liquid cyclopentane interfacial tension, and θ is the contact angle of the liquid solution on the hydrate particle surface.

The first term of the right hand side of equation is generated by the Laplace pressure, and the second term describes the effects of surface tension and contact angle when solution droplet adheres on the surface of the hydrate probe.

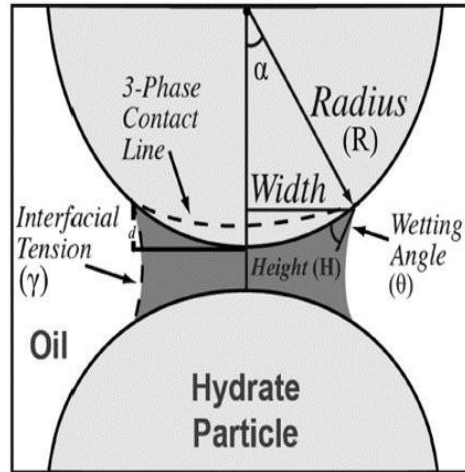


Figure 3-1: Schematic of capillary adhesion for solution-hydrate geometry with relevant parameters [2].

3.2 Interfacial tension measurements

Pendant drop method is used to study the interfacial tension between an aqueous drop and hydrocarbon. Both Equation 4 and Figure 3-2 are applied as the fundamental principles of pendant drop techniques [69]. More specifically, the Young-Laplace equation shows a relationship between the interfacial tension and the drop shape, and it is normally introduced to extract the surface or interfacial tension of the systems by fitting the shape of the droplet to the solution of the equation. Then One Attention software can do the calculations automatically and obtain the results directly according to the different radius of drop curvature [70]. Moreover, in the ideal case, the shape of the drop will not change over time; nevertheless, in the real case, the size of the drop curvature is more likely to shrink with time owing to the poor leakproofness between the syringe and the needle, then the interfacial tension is also expected to decrease

gradually over time.

$$\gamma = \frac{\Delta\rho \times g \times R_0}{\beta}$$

4

γ : surface tension β : shape factor

g : gravitational constant

$\Delta\rho$: density difference

R_0 : radius of drop curvature

$$\begin{aligned} dx/ds &= \cos\Phi \\ dz/ds &= \sin\Phi \\ d\Phi/ds &= 2 + \beta z - \sin\Phi / x \end{aligned}$$

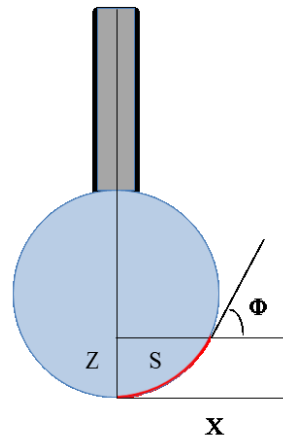


Figure 3-2: Pendant drop method principle [69].

3.3 Crumpling ratio measurements

Generally, there is a phenomena called crumpling observed visually when the droplet surface with rigid layer acts like a steric barrier deflated during withdrawn back process into the micropipette [71], where crumpling ratio is defined as the ratio of the projected area of droplet just when the first observation of crumpling of its initial projected area [72]. To our knowledge of literature, no crumpling takes place with the absence of natural surfactants such as asphaltentic molecules [71], and higher crumpling ratio represents the more irreversible adsorption of asphaltenes on the interface. Furthermore, the crumpling ratio (CR) used to quantify the skin formation is usually described by the following Equation 5 [72].

$$CR = \frac{A_f}{A_i} = \frac{\pi R_f^2}{\pi R_i^2} = \frac{R_f^2}{R_i^2} \quad 5$$

A_f : projected area of droplet just when the first observation of crumpling

A_i : initial projected area of the droplet

Therefore, crumpling ratio can be calculated by Equation 5, and panel I of Figure 3-3 illustrates the initial projected area of the droplet (i.e., A_i), while panel II shows the projected area of droplet right before the point of first observation of crumpling (i.e., A_f).

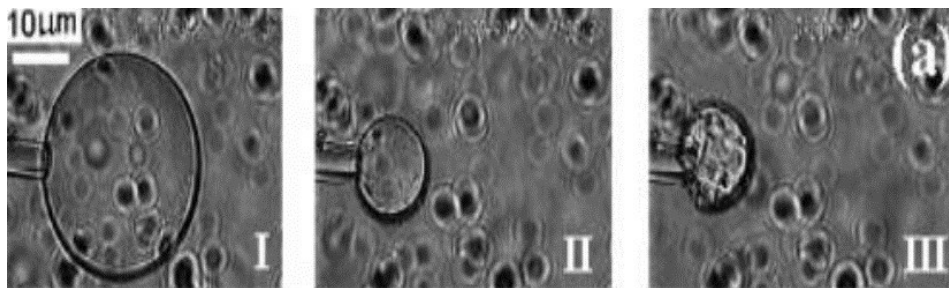


Figure 3-3: Skin formation at droplet surfaces [72].

Chapter 4 Experimental materials and setup

4.1 Experimental materials

4.1.1 Preparation of cyclopentane hydrate

The cyclopentane (Reagent plus grade 98%) used in this study was purchased from Sigma-Aldrich. A platinum probe with 99.995% purity, 1.05 mm in diameter and 45 mm in length, was purchased from KSV Instrument.

In this study, cyclopentane hydrate was chosen for the following reasons:: (i) the equilibrium temperature of CP hydrate is 7.7 °C under ambient pressure, which is suitable for our current available analytic techniques [1] [5] [6]; (ii) CP is a hydrophobic (i.e. immiscible with water) guest molecule [1] [5]; (iii) CP forms the same clathrate structures (sII) as natural gas at atmospheric pressure. [1] [5] [34]. Even though the size methane is preferable for sI, pure methane is stabilized in sI only by the addition stability of the molecule in the large tetrakaidecahedrons cage ($5^{12}6^2$). Therefore, the presence of a small amount of propane encourages the stability of sII, leading to most natural gases form sII because most reservoirs contain small amounts of propane [5]. Hester et al. [73] also suggested that there were two peaks including 2905 cm^{-1} for $5^{12}6^2$ and 2915 cm^{-1} for 5^{12} observed according to Raman studies, and the area for the $5^{12}6^2$ peak is approximately three times that of the 5^{12} , which means natural gas hydrate belongs to sII.

The preparation of the cyclopentane (CP) hydrate followed the method described by Song et al. [30]. The bottle with 10 wt. % of CP in DI water was placed in a freezer at -22 °C for 12 minutes and shaken at room temperature for 3 minutes. This process was repeated around six times until

the appearance of fine white particles. Then the bottle was moved into a refrigerator at 4 °C for a week to form CP hydrate slurry. Using a micropipette, 18 μL of this slurry was transferred to the end of a platinum probe, which was immersed into liquid nitrogen to freeze. The probe was then placed inside a pre-cooled CP bath at 1.0 °C for 2-3 days, after which the CP hydrate slurry was converted into a solid CP hydrate particle. The diameter of the formed CP hydrate was around 4.0 ± 0.1 mm, similar to the size reported in literature [30]. Figure 4-1 demonstrates the schematic diagram for the hydrate formation.

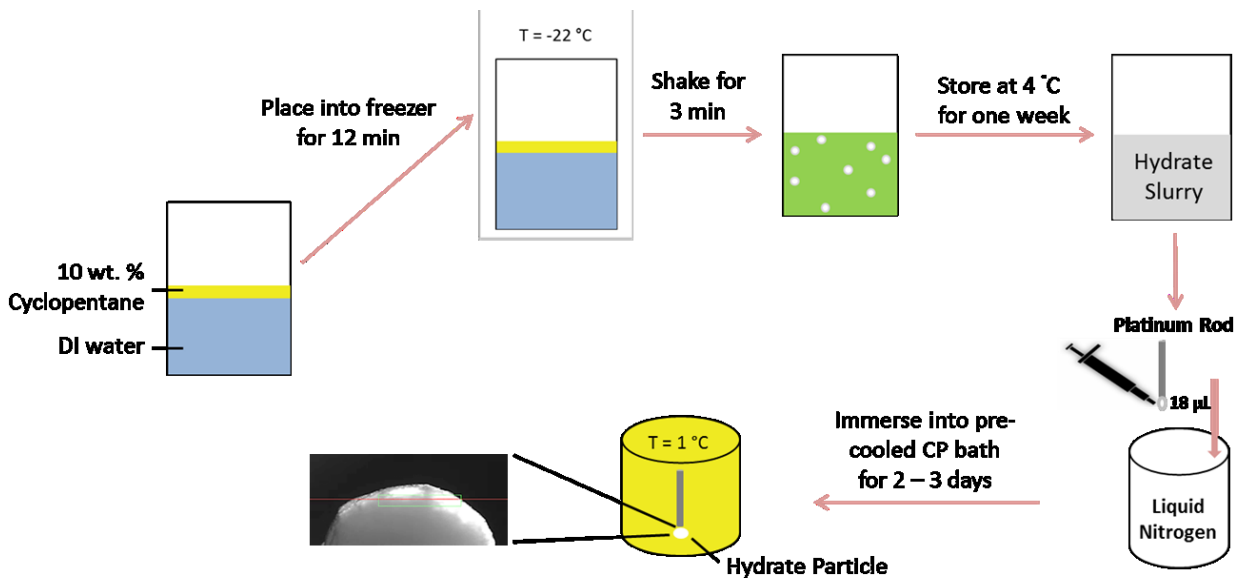


Figure 4-1: Schematic diagram of cyclopentane hydrate formation process.

4.1.2 Preparation of asphaltenes

Asphaltenes were extracted from the Athabasca coker feed bitumen (provided by Syncrude Canada Ltd.).

Following the method given by Wang et al. [74], the asphaltenes preparation was performed in several steps: (1) 1 L glass bottle was used to store the mixture composed of 20 g bitumen and 800 g n-pentane with a mass ratio of 1:40. This bottle was then shaken for 2 hours and left

overnight for asphaltene precipitation and settling. (2) The supernatant was collected before adding another 800 g n-pentane to the settled phase. (3) Steps 1 and 2 were repeated for 15 times until the observation of a colorless supernatant. (4) The settled phase was mixed with n-pentane for 30 minutes to reach equilibrium, and vacuum filtration was introduced to separate this mixture. (5) A Whatman filter paper (grade 50) wetted with n-heptane was placed on the top of the Buchner funnel. (6) Step 5 was repeated until the colorless solvent dripped through the filter paper, meanwhile the filter needed to be replaced after a few rounds for best results. (7) The precipitates were dissolved into toluene with a mass ratio of 1:20 after collecting from the filter paper. (8) To remove solid particles, the mixture was shaken for 20 minutes and divided equally into Teflon tubes before centrifuging it at 20,000 g for 20 minutes. (9) The solutions were transferred from the tubes into a rotary evaporation apparatus. (10) After toluene was removed from the mixture solution by a circulating water bath at 60 °C, the asphaltene could separate out and cling to the glass wall. (11) The asphaltene could be chipped out after drying them in the film hood for 3 days.

4.2 Experimental setup

4.2.1 Interfacial tension measurement by Theta Optical Tensiometer

The interfacial tension between the aqueous drop and oil were measured using the pendant drop method with the Theta Optical Tensiometer at room temperature and atmospheric pressure. A water droplet (~20 μL in volume), generated using a microsyringe, was immersed into the oil phase. The One Attention software was used to calculate the interfacial tension directly based on Young-Laplace equation. The dynamic interfacial tension was measured for 30 min until equilibrium was observed.

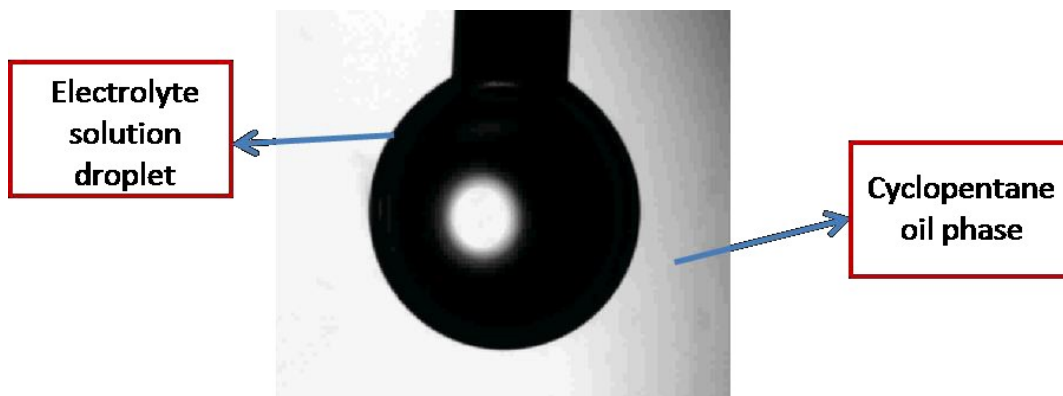


Figure 4-2: Appearance of electrolyte solution droplet in pure cyclopentane oil phase.

4.2.2 Capillary adhesion force measurements by Integrated Thin Film Drainage Apparatus (ITFDA)

Unlike the previous research, an integrated thin film drainage apparatus (ITFDA) is replaced to measure cyclopentane hydrate – electrolyte or water solutions adhesion forces directly.

The integrated thin film drainage apparatus (ITFDA) was used to measure the adhesion force between a water drop and a cyclopentane (CP) hydrate particle directly, using a bimorph as a force sensor [75]. The ITFDA can be used for the measurements of contact force, contact angle, capillary force, and adhesion force between solid particles and liquid droplets in a liquid phase at room temperature [68]. As presented in Figure 4-3 (A), an experimental cell filled with pure cyclopentane liquid surrounded by aluminum jacket was placed atop the stage. The temperature of the continuous phase was controlled by a circulating water bath at around 2.0 ± 0.5 °C. The water drop was created at the end of a capillary tube using a microsyringe, while the CP hydrate particle was clamped at the free end of a bimorph beam. The diaphragm of a high frequency speaker was used to accurately drive the drop toward and away from the hydrate particle, with a possible holding time in between that allows the interfaces to stay in contact. The velocity could be chosen from $\mu\text{m/s}$ to mm/s . As a result, the interaction forces could be plotted based on the charge generated by the deflection of the bimorph. The interaction force measurements

between the CP hydrate and the drop are divided in four steps, as shown in panel B of Figure 4-3. Initially, the drop was placed 280 μm above the CP hydrate particle (Figure 4-3 (B)-1). The approach and retract velocities of the droplet were set at 100 $\mu\text{m/s}$. After the drop contacted the particle for some stipulated time (Figure 4-3 (B)-2), it was lifted up (Figure 4-3 (B)-3) until it finally detached from the particle, leaving residual water behind (Figure 4-3 (B)-4).

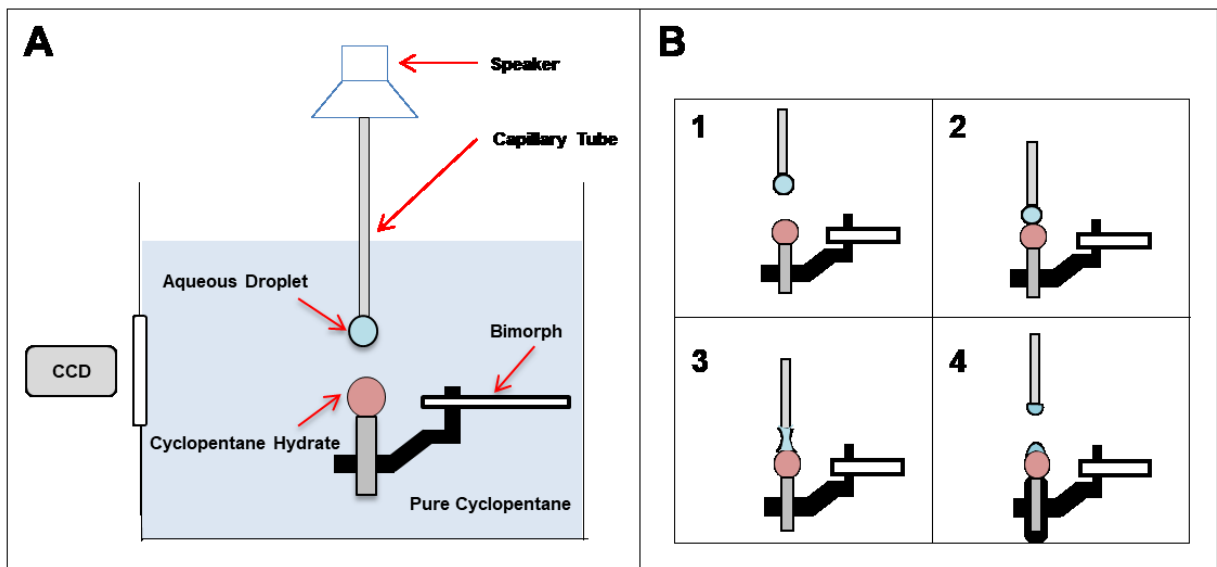


Figure 4-3: Schematic of the ITFDA configuration (A). An aqueous drop is driven toward a hydrate particle under controlled conditions. The interaction force is measured by the deflection of the bimorph. The typical experiment follows the following protocol (B): approach stage (1); hold stage (2-3) where attachment can occur and retract stage (4).

Chapter 5 Results and Discussion

As mentioned above, the hydrates would share interfaces with solid, other hydrate probes, water solution and hydrocarbon, and the presence of water is the main reason to cause hydrate aggregation and block the pipeline. Based on the knowledge of literature, even though the salt, being accepted as a thermodynamic hydrate inhibitor, would shift towards lower hydrate equilibrium temperature [5] [15], its impacts on the interfacial dynamic behaviors of hydrates have rarely been investigated. With the increasing salt amount during the offshore gas production, the effects of salt should be evaluated for hydrates flow assurance. Furthermore, the previous studies were focused on the most common salt: sodium chloride; the work presented herein studies the influences of different salts including NaCl, KCl, CaCl₂ and Na₂SO₄ on the hydrates flow assurance through analysis of adhesion mechanisms and hydrate growth rate.

5.1 Interfacial tension measurements with various salts

Since both interfacial tension of water/oil and Laplace pressure were responsible for the capillary adhesion force, then the interfacial tension of aqueous solutions-cyclopentane interface was measured by Tensiometer with pendant drop method at room temperature and atmospheric pressure. In each experiment, a solution droplet (~10 μ L in volume) generated by microsyringe was immersed in oil bulk phase. Dynamic interfacial tension was measured lasting up to 5 min after reaching equilibrium state. Additionally, the water solution droplet would be replaced by the different electrolyte solutions once obtaining the density of each brine solution. The interfacial tension measurements between different solution droplets and cyclopentane bulk phase were plotted as a function of time shown in Figure 5-1. Moreover, Table 5-1 listed both densities of each aqueous solution with various concentrations and the corresponding interfacial tension

measured between solution and cyclopentane, which agreed with literature [76]. As shown, the interfacial tension of oil-water interface was increased with the concentration of salts. Additional, other than the brine solutions with monovalent ions, the higher IFT was measured when the salt solutions with divalent ions presented. It was well known that the interfacial tension between salt solutions and oil was larger than that between pure water and oil because the surface charge induced by the ions repelled itself from the interface when approaching a dielectric interface, resulting in the negative surface excess concentration of salt, while ionic depletion from the interfacial region caused the increase of interfacial tension [77].

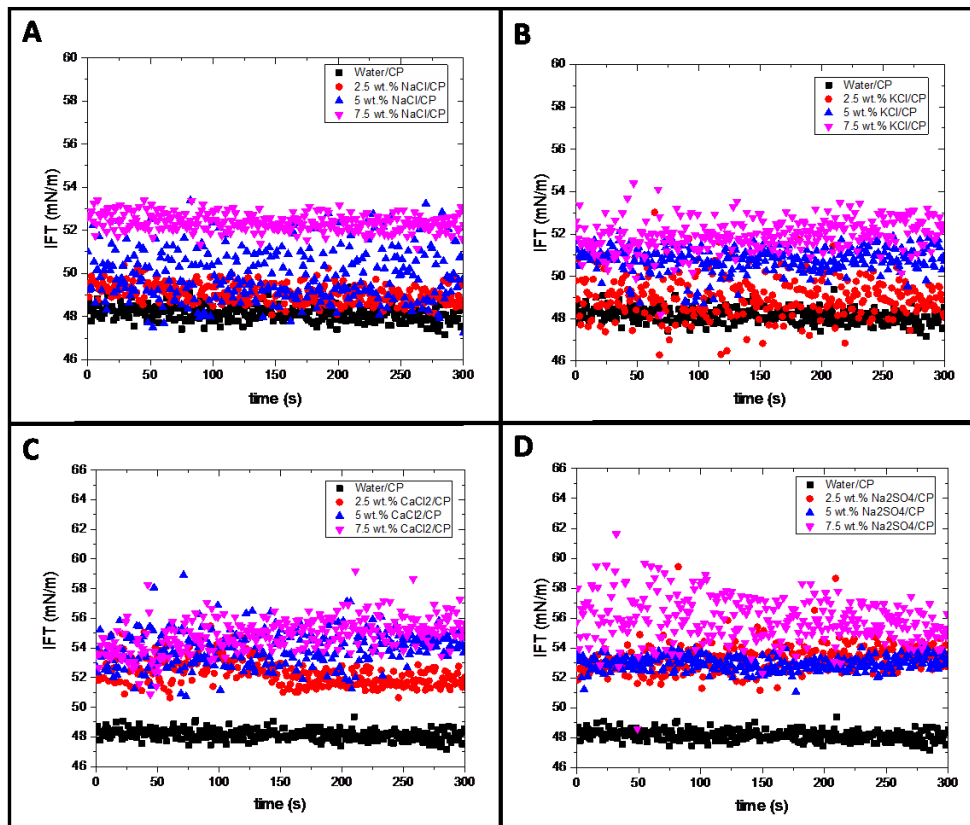


Figure 5-1: Interfacial tension measured between pure cyclopentane and NaCl solution (A); KCl solution (B); CaCl₂ solution (C); Na₂SO₄ solution (D).

Solution droplet – Oil Phase	Density (g/cm ³)	Interfacial Tension (mN/m)
Water - Cyclopentane	1	48.7 [5]
2.5 wt.% NaCl - Cyclopentane	1.017	49.3 ± 0.02
5 wt.% NaCl - Cyclopentane	1.034	50.5 ± 0.02
7.5 wt.% NaCl - Cyclopentane	1.053	51.2 ± 0.02
2.5 wt.% KCl - Cyclopentane	1.014	49.5 ± 0.02
5 wt.% KCl - Cyclopentane	1.030	51.8 ± 0.02
7.5 wt.% KCl - Cyclopentane	1.047	52.9 ± 0.02
2.5 wt.% CaCl ₂ - Cyclopentane	1.019	52.5 ± 0.02
5 wt.% CaCl ₂ - Cyclopentane	1.040	53.6 ± 0.02
7.5 wt.% CaCl ₂ - Cyclopentane	1.062	54.7 ± 0.02
2.5 wt.% Na ₂ SO ₄ - Cyclopentane	1.018	52.8 ± 0.02
5 wt.% Na ₂ SO ₄ - Cyclopentane	1.044	53.3 ± 0.02
7.5 wt.% Na ₂ SO ₄ - Cyclopentane	1.067	54.1 ± 0.02

Table 5-1: Summary of densities and interfacial tension measurements as a function of concentrations of salt solution.

5.2 Capillary adhesion force measurements between CP hydrate and water solution droplet in oil bulk phase

In order to study the reliability of our home designed instrument, Integrated Thin Film Drainage Apparatus, the force curves plotted to describe the hydrate particle-water droplet interactions was shown in Figure 5-2 (A). More specific, according to the analysis of corresponding images given in Figure 5-2 (B), the “theoretical results” being considered as reference data was calculated based on Eqn. (3) with the required parameters. Figure 5-2 (A) presented the two capillary force

curves obtained from the experimental data and theoretical calculation for a CP hydrate particle ($d = 4.00 \pm 0.1$ mm) and a water droplet ($d = 2.05 \pm 0.05$ mm) in CP liquid bulk phase (i.e., oil phase) at 2.0 ± 0.5 ° C. During the force measurement process, both approaching time and holding time were 5 seconds, and the detachment time was 5 seconds. Since there was no contact from point 1 to 2, the capillary force curve kept almost constant during this process. The two surfaces were upon in contact after 5 seconds, resulting in a significant increase of the attraction on both curves because of the formation of hydrate-liquid CP-water three phase contact (TPC) line (point 3). Once water solution droplet got contacted with CP hydrate, a new hydrate-water interface was formed with a very low interfacial tension (i.e., $\gamma = 0.32 \pm 0.05$ mN/m). In order to reach an equilibrium state with minimum interfacial Gibbs free energy, the water droplet spread on the surface spontaneously. The attractive force corresponding to this spreading process which was around 0.23 mN was defined as the initial contact force between CP hydrate particle and water solution droplet. The three-phase-contact line formed after initial contact would slide a little bit on the hydrate particle to reach the final pinned point, and then sintered without any spreading of water solution. During this short contact period, the interaction force was almost same because the bridge volume was treated at a constant value (point 3-4). As the capillary bridge becoming “thinner” along with the detachment process, the attractive force kept decreasing until the bridge broke at neck (point 5-7), and eventually some amount of water was left on the hydrate particle (point 8), leading to a repulsive force at equilibrium due to the higher density of water compared to the continuous phase. The residual water that resulted in a repulsive force of around 0.13 mN was also the reason for the obvious deviation of the measured force from the theoretical force after capillary bridge ruptured. Other than that, the experimental data (red line) agrees well with the forces calculated from Equation 3 (black line), indicating that ITFDA was a reliable instrument to measure the interaction force between a water droplet and CP

hydrate even at a low temperature of 2 °C.

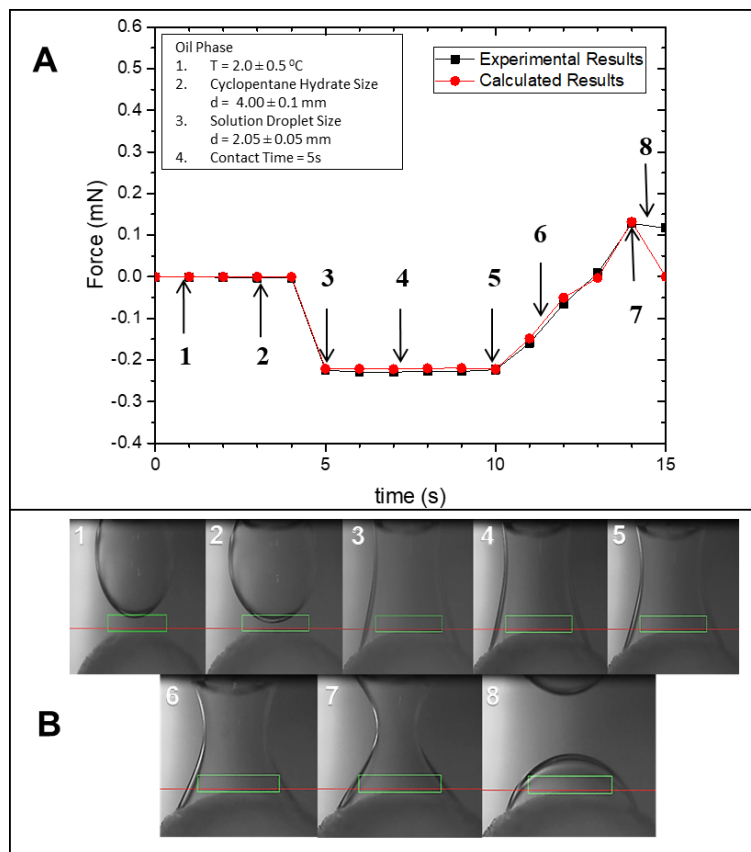


Figure 5-2: Adhesion force curves obtained from the interactions between CP hydrate probe and water droplet in oil phase 2.0 ± 0.5 °C (A); Corresponding images captured during experimental processes from side camera (B).

As discussed above, both surface tension and Laplace pressure played important roles on capillary force which was the major contribution to the interaction force between hydrate and solutions. Generally, the attractive force is dominantly attributed to the surface tension during the approaching process, while the interaction force measured through detachment process is caused by the effect of Laplace pressure. For clear understanding, we described the force curve based on these two effects. According to Figure 5-3, the attractive force generated by the TPC line was determined by both interfacial surface tension of water-oil interface and the contact angle

measured between water solution and hydrate particle, which reached the maximum value at the point of widest capillary bridge. In contrast, as the capillary bridge became thinner along with the retraction process, the Laplace pressure was more responsible for the interaction force based on the change on bridge curvature. The schematic of spreading of water solution droplet on the hydrate surface was also shown in Figure 5-4 (A), while Figure 5-4 (B) illustrated the corresponding geometric relationship of Eqn. 3.

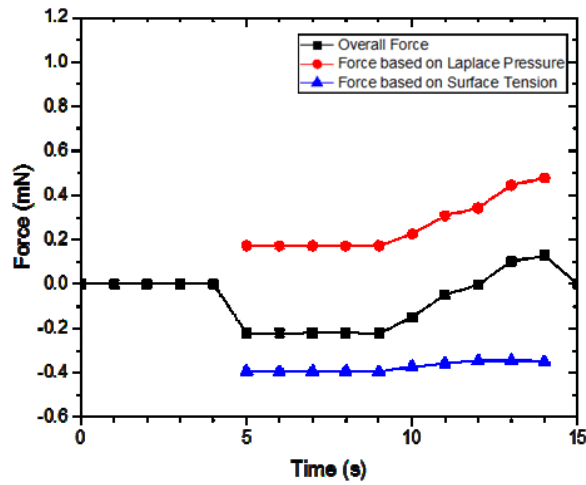


Figure 5-3: Impacts of Laplace pressure and surface tension on interaction forces measured between CP hydrate particle and water solution droplet.

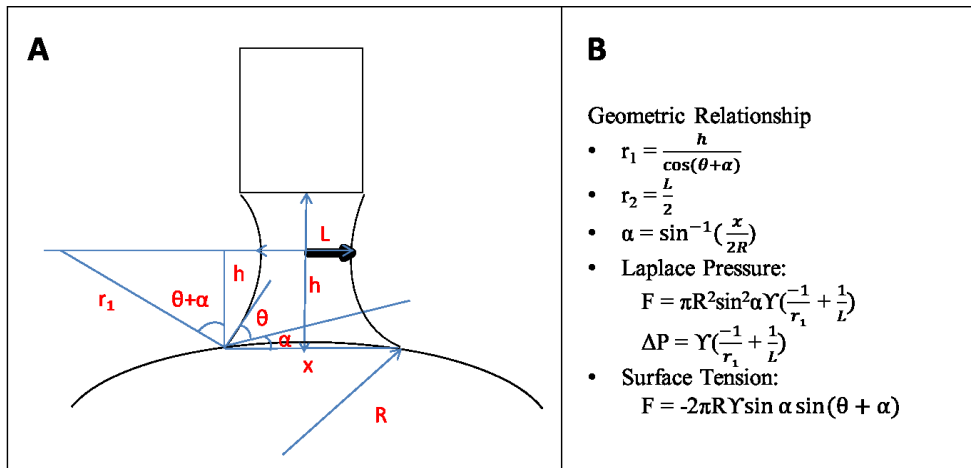


Figure 5-4: Schematic diagram of capillary interaction (A); Geometric relationship of Equation 3 (B).

5.3 Capillary adhesion force measurements between CP hydrate and electrolyte solutions in oil bulk phase

5.3.1 Effects of concentrations of electrolyte solution

Following the previous experimental procedures, the water solutions were replaced by the different brine solutions.

Table 5-2 summarized some relevant variables associated with capillary forces between CP hydrate particle and different solution droplets. Obviously, the longer three-phase contact line associated with lower contact angle could lead to the higher adhesion force obtained from the interactions between water solution droplet and CP hydrate particle. With increase of salts content with monovalent ions, the wetting angle was slightly enhanced because of the higher interfacial tension between brine solution droplet and pure cyclopentane bulk phase. However, when the pure water solution droplet was replaced by brine solutions with divalent ions, the even larger wetting angle was observed, and this finding could be explained by followings: (1) according to Young's Equation, the resulted interfacial tension played positive roles on contact angle [66]; (2) the salts with divalent ions perhaps decreased three-phases-contact line velocity [67]; (3) the hydrate surface charge was reversal due to the formation of a layer of strongly adsorbed divalent ions, leading to larger contact angle [78].

Figure 5-5 showed the capillary forces measured between CP hydrate particle and different brine solution droplet in pure cyclopentane bulk phase in 2.0 ± 0.5 °C. From this figure, we could tell the maximum attractive force was reduced by the presence of salts, and it was probably because the available water molecules were more likely to interact with the ions, leading to less water molecules being interact with external cyclopentane to form hydrate. While a decrease of the adhesion force was observed along with the increasing salt concentration up to 5 wt. % for both of NaCl and KCl solutions (Figures 5-5 (A)&(B)), while the capillary adhesion forces were

almost constant for either CaCl_2 or Na_2SO_4 solutions (Figure 5-5 (C)&(D)) regardless of concentrations. Therefore, 5 wt. % and 2.5 wt. % were the critical concentrations for reducing adhesion forces for NaCl & KCl, and CaCl_2 & Na_2SO_4 solutions, respectively. Furthermore, there was no significant difference of adhesion forces between NaCl and KCl solutions, which could be explained by the similar salt solution-oil interfacial tension and wetting angle when these two solutions contacted with hydrate particle. On the other hand, the much lower critical concentration of the divalent salts than the monovalent salt might be attributed to the inhibiting effects of salts, depending on both valence and the surface tension gradient with respect to salt concentration [63]. Craig et al. [63] demonstrated the inhibition of bubble coalescence can be achieved by the combination of $\alpha\alpha$ or $\beta\beta$ salts. Not only because the anions (SO_4^-) and cations (Ca^{2+}) were with higher charge density, but also that both CaCl_2 and Na_2SO_4 show stronger hydrated ability than NaCl and KCl to prevent the hydrate crystallization more effectively. In other words, the amount of water available to form hydrate was lowered by addition of salts, which was consistent with the report of Zylyftari et al [65].

Combining with Figure 5-5 and Table 5-2, even though the interfacial tension was increasing with addition of salts, the capillary adhesion force represented the inverse relationship with salts. Since both interfacial tension and contact angle significantly affected the volume of capillary bridge, the decreasing capillary adhesion force caused by presence of salts was perhaps owing to the increasing contact angle and shorter TPC line. Thus, by contrast, both the contact angle and length of TPC line were more important factors on the capillary adhesion force than interfacial tension measured between solution and oil.

	Droplet Diameter (mm)	Contact Length (mm)	Bridge width (mm)	Contact Angle	Capillary Force (mN)
Water	2.05 ± 0.05	2.34 ± 0.05	1.58 ± 0.05	29° ± 1°	0.23 ± 0.1
2.5 wt.% NaCl	2.05 ± 0.05	2.30 ± 0.05	1.60 ± 0.05	32° ± 1°	0.21 ± 0.1
2.5 wt.% KCl	2.05 ± 0.05	2.27 ± 0.05	1.63 ± 0.05	34° ± 1°	0.20 ± 0.1
2.5 wt.% CaCl ₂	2.05 ± 0.05	2.18 ± 0.05	1.68 ± 0.05	43° ± 1°	0.15 ± 0.1
2.5 wt.% Na ₂ SO ₄	2.05 ± 0.05	2.13 ± 0.05	1.72 ± 0.05	46° ± 1°	0.13 ± 0.1

Table 5-2: Relevant parameters on capillary adhesion forces measured between hydrate particle and solution droplet.

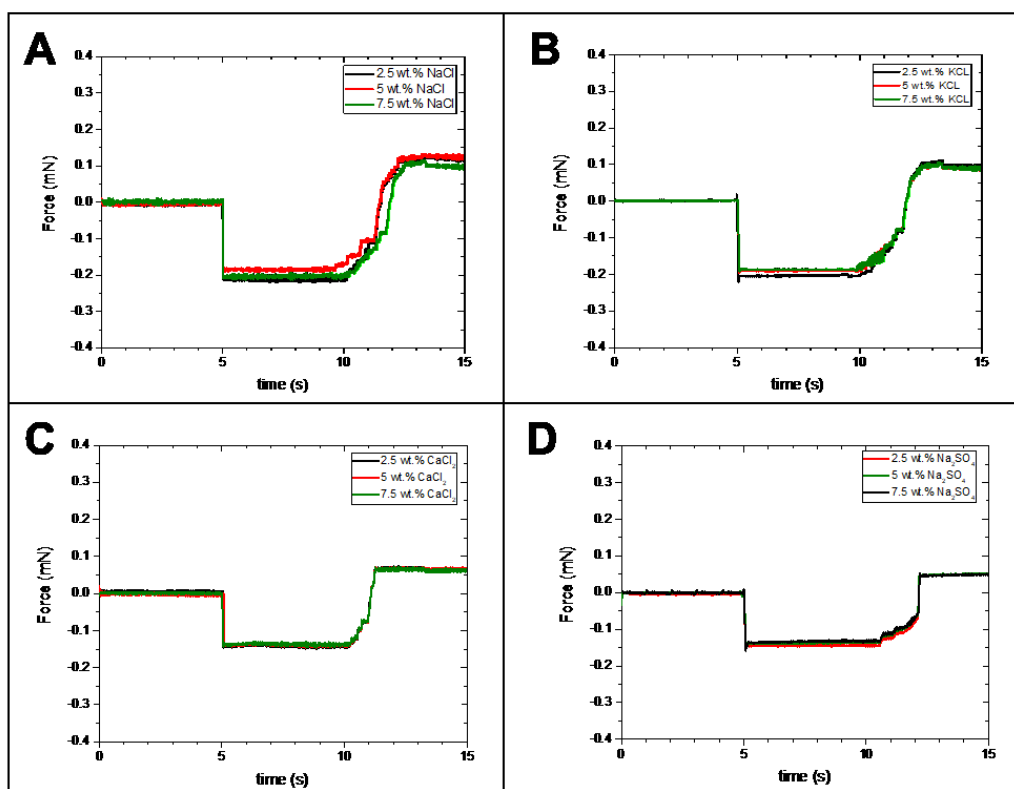


Figure 5-5: Adhesion force curves obtained from the interactions between CP hydrate particle and droplets of NaCl solution (A); KCl solution (B); CaCl₂ solution (C); Na₂SO₄ solution (D) in oil phase at 2.0 ± 0.5 °C.

5.3.2 Effects of electrolyte solution droplet size

According to many studies, the surface tension has been determined as the more dominated factor on capillary force compared to Laplace pressure, which was also in consistent with our analysis. According to Equation 3, the contact area, referring as the circular area of the initial three phases contact line, would be noted to greatly affect the interaction force between the solution droplets and CP hydrate particle. In other words, understanding the impacts of the contact area determined by the droplet volume was very important for investigation of the hydrate agglomeration. For convenience, the length of initial three phases contact line was analyzed instead of contact area to understand the effects of droplet volume. Then three different solution droplet diameters were chosen varying from 2.10 mm to 2.30 mm with 0.05 mm deviation. For instance, Figure 5-6 (A) showed the corresponding images of initial contact line formation with three sizes of 2.5 wt. % NaCl solution droplets (i.e., $d = 2.10, 2.20, 2.30 \pm 0.05$ mm) at 2.0 ± 0.5 °C in pure CP bulk phase. From panels 1 & 2 to panels 3 & 4 to panels 5 & 6 of Figure 5-6 (A), it clearly represented the larger solution droplet would cause the longer three phases contact line formation on the hydrate particle, and then the larger capillary force (i.e., shown in Figure 5-6 (B)), which was in consistent with Equation 3.

The summary of capillary adhesion forces as a function of droplet sizes measured from the interactions between the electrolyte solution droplets and CP hydrate particle was listed in Table 5-3. Although the addition of higher concentration of salts showed the negative impacts on capillary adhesion force, the interaction forces were still increased by the larger solution droplet regardless of concentration and type of salts. Therefore, the solution volume was the more essential factor on affecting capillary adhesion force than either type or concentration of salts.

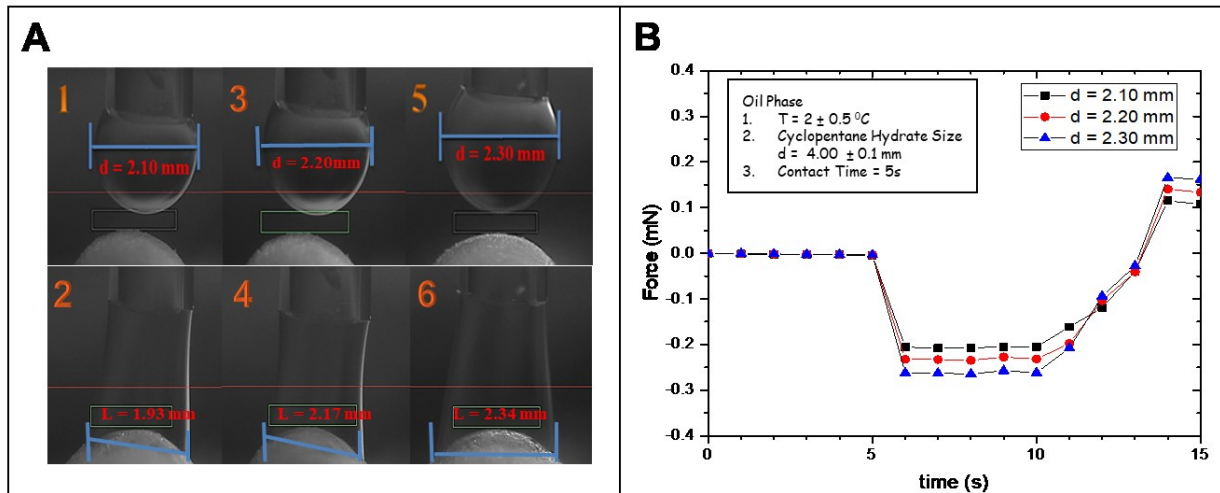


Figure 5-6: Corresponding images of three sizes of 2.5 wt. % NaCl solution droplets (A-1): $d = 2.10$ mm; (A-3): $d = 2.20$ mm; (A-5): $d = 2.30$ mm captured at the initial point of capillary bridge formation, coming along with corresponding contact length (A-2): $L = 2.34$ mm; (A-4): $L = 2.80$ mm; (A-6): $L = 3.10$ mm, respectively; (B) Adhesion force curves obtained from the interactions between 2.5 wt. % NaCl solution droplet and CP hydrate with respective to droplet size in oil phase at 2.0 ± 0.5 °C.

	NaCl			KCl			CaCl ₂			Na ₂ SO ₄		
	2.5 wt.%	5 wt.%	7.5 wt.%	2.5 wt.%	5 wt.%	7.5 wt.%	2.5 wt.%	5 wt.%	7.5 wt.%	2.5 wt.%	5 wt.%	7.5 wt.%
Droplet Size $d = 2.10 \pm 0.05$ mm	0.215 ± 0.1 mN	0.194 ± 0.1 mN	0.188 ± 0.1 mN	0.207 ± 0.1 mN	0.196 ± 0.1 mN	0.193 ± 0.1 mN	0.148 ± 0.1 mN	0.146 ± 0.1 mN	0.143 ± 0.1 mN	0.133 ± 0.1 mN	0.131 ± 0.1 mN	0.130 ± 0.1 mN
Droplet Size $d = 2.20 \pm 0.05$ mm	0.234 ± 0.1 mN	0.226 ± 0.1 mN	0.225 ± 0.1 mN	0.228 ± 0.1 mN	0.215 ± 0.1 mN	0.212 ± 0.1 mN	0.162 ± 0.1 mN	0.160 ± 0.1 mN	0.157 ± 0.1 mN	0.147 ± 0.1 mN	0.148 ± 0.1 mN	0.147 ± 0.1 mN
Droplet Size $d = 2.30 \pm 0.05$ mm	0.258 ± 0.1 mN	0.247 ± 0.1 mN	0.241 ± 0.1 mN	0.246 ± 0.1 mN	0.234 ± 0.1 mN	0.230 ± 0.1 mN	0.188 ± 0.1 mN	0.185 ± 0.1 mN	0.181 ± 0.1 mN	0.166 ± 0.1 mN	0.165 ± 0.1 mN	0.166 ± 0.1 mN

Table 5-3: Summary of capillary adhesion forces measured between each electrolyte solution droplet and hydrate particle as a function of droplet size in oil phase.

5.3.3. Effects of contact time

The reactive sintering mechanism was strongly dependent on the contact time. In other words, the longer contact time led to the larger amount of new hydrate formation. Figure 5-7 plotted the force curves as a function of contact time measured from the interactions between electrolyte solution droplet and CP hydrate particle in oil phase. In order to understand the influences of contact time, there different contact time was chosen from 5 to 45 seconds with deviation of 20 seconds. The black solid line was the capillary force curve described the interactions between 2.5 wt. % NaCl solution droplets and CP hydrate particle after 5 seconds contact time, and the constant adhesion force accompanying with no hydrate growth during this short contact time was confirmed with previous results. However, there was a slightly increasing of interaction force with the increasing contact time up to 25 seconds, and the obvious “new” hydrate growth was also found, which was shown in the panel II of Figure 5-7. When the contact time were up to 45 seconds, the trend of continuous increase of interaction force was clearly observed after 30 seconds due to the rapid formation of hydrate shell and then the new hydrate growth (i.e., blue solid line). Eventually, the capillary force obtained at break point of bridge was enhanced by the contact time as well. The longer contact time resulted in the larger amount of hydrate formation and then the higher capillary force at rupture point, agreed by Liu et al. [14]. Moreover, panel II (A-C) of Figure 5-7 illustrated the corresponding hydrate morphologies as a function of contact time. Table 5-4 reported the capillary forces measured with respect to contact time when the electrolyte solution bridge ruptured.

The results indicated that the presence of small amount of salts with divalent ions could prevent the hydrate formation than those with monovalent ions, and then the lower capillary forces at rupture point were also measured. Although the interaction force obtained at the rupture point of

bridge was enhanced by the contact time, the introduction of salts with divalent ions still depressed this increasing trend. In other words, the addition of salts with divalent ions into aqueous solution could delay the hydrate growth greatly. As the concentration of salts increased, the prohibition of hydrate growth was significantly enhanced; consequently, the capillary forces measured at rapture point were also decreasing.

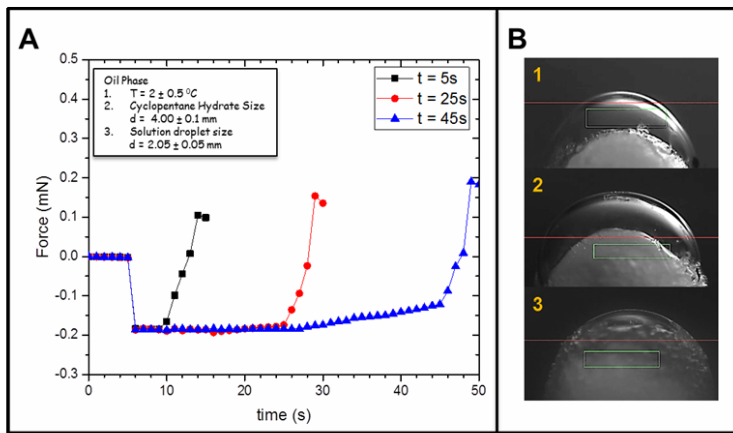


Figure 5-7: Adhesion force curves obtained from the interactions between 2.5 wt. % NaCl solution droplet and CP hydrate (A); CP hydrate morphologies as a function of contact time: $t = 5s$ (B-1); $t = 25s$ (B-2); $t = 45s$ (B-3).

	NaCl			KCl			CaCl ₂			Na ₂ SO ₄		
	2.5 wt. %	5 wt. %	7.5 wt. %	2.5 wt. %	5 wt. %	7.5 wt. %	2.5 wt. %	5 wt. %	7.5 wt. %	2.5 wt. %	5 wt. %	7.5 wt. %
Contact time $t = 5s$	0.107 ± 0.1 mN	0.096 ± 0.1 mN	0.092 ± 0.1 mN	0.101 ± 0.1 mN	0.094 ± 0.1 mN	0.092 ± 0.1 mN	0.058 ± 0.1 mN	0.053 ± 0.1 mN	0.051 ± 0.1 mN	0.048 ± 0.1 mN	0.045 ± 0.1 mN	0.041 ± 0.1 mN
Contact time $t = 25s$	0.135 ± 0.1 mN	0.127 ± 0.1 mN	0.123 ± 0.1 mN	0.126 ± 0.1 mN	0.118 ± 0.1 mN	0.115 ± 0.1 mN	0.065 ± 0.1 mN	0.063 ± 0.1 mN	0.060 ± 0.1 mN	0.053 ± 0.1 mN	0.049 ± 0.1 mN	0.047 ± 0.1 mN
Contact time $t = 45s$	0.188 ± 0.1 mN	0.176 ± 0.1 mN	0.171 ± 0.1 mN	0.180 ± 0.1 mN	0.173 ± 0.1 mN	0.170 ± 0.1 mN	0.071 ± 0.1 mN	0.068 ± 0.1 mN	0.065 ± 0.1 mN	0.059 ± 0.1 mN	0.055 ± 0.1 mN	0.053 ± 0.1 mN

Table 5-4: Summary of capillary adhesion forces obtained with respect to contact time when the electrolyte solution bridge ruptures.

5.4 Hydrate growth morphology in oil bulk phase

5.4.1 Morphology of hydrate particle after contact with water solution

Besides the interaction force measurements, the rate of CP hydrated shell growth has also been determined. The impact of sintering, described as the hydrate growth along the interface, is essential for understanding the hydrate agglomeration inside pipelines. Aman et al. [6] and Taylor et al. [11] investigated the presence of super-saturation along the interface was the main reason of the hydrate shell formation around water surface, which was believed as the first step for hydrate nucleation. Since contact time is the critical factor on sintering mechanism; therefore, the reactive sintering mechanism is to account for fracture between hydrate bridges that form over time [3]. According to Eqn. (4), sintering adhesion force is governed by both the size or growing hydrates bridge and hydrate tensile strength. Sloan et al. [5] suggested the hydrate conversion was via the feature of “inward-growth hydrate shell”. That was to say, the conversion process from water to hydrate was generated by the hydrate shell growth from water surface towards water core.

Figure 5-8 described the mechanism of hydrate formation from a water droplet. In fact, the formation of hydrate shell was the first indication of hydrate nucleation, and it continuously grew until the presence of a thin hydrate film formation around the water surface. Afterwards, the water could convert to hydrate via hydrate film development.

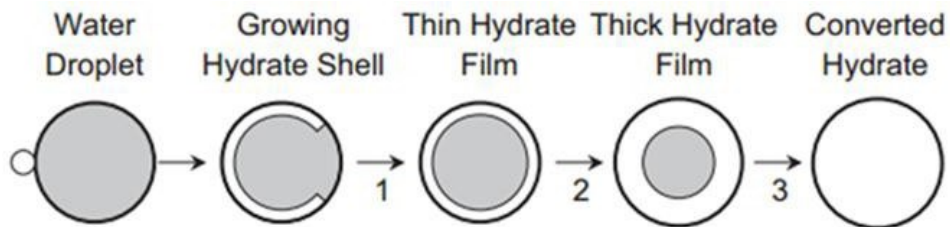


Figure 5-8: Mechanism of hydrate formation. Step 1: formation of thin hydrate film around the water droplet; Step 2: film development; Step 3: complete conversion of hydrate [11].

For better understanding of the sintering mechanism, not only the time required for the first point of hydrate shell formation but also for the completion of hydrate conversion was evaluated via visually observation. Panel I of Figure 5-9 presented the corresponding images of CP hydrate morphologies captured at the first point of water being left on surface (Figure 5-9 (A)-1), the first indication of hydrate shell formation (Figure 5-9 (A)-2), and final morphology of hydrate after fully conversion from water solution (Figure 5-9 (A)-3) in pure cyclopentane bulk phase. Moreover, the amplifications of first point of hydrate shell formation were also given in panel B of Figure 5-9. Aman et al. [8] established that the sintering adhesion force became more dominated compared to capillary adhesion force when the contact time was over 30 seconds, and then the larger amount of “new” hydrate growth was visually observed with contact time. As contact time increasing, new hydrate would start to grow along the interface, where the region full of supersaturated components for hydrate formation. For shorter contact time (Figure 5-9 (A)-1), only water solution was left on the hydrate particle surface, indicating no hydrate growth along the solution-hydrate interface due to the absence of sintering mechanism. As the contact time was up to 2 minutes (Figure 5-9 (A)-2), the “new” hydrate formation was initially visible, and it was more likely a “growth” of pre-existing hydrate along the interface and then the liquid capillary bridge slightly converted to hydrate capillary bridge. The complete cycle of hydrate growth was obtained after 11 minutes (Figure 5-9 (A)-3). Therefore, as contact time up over 2 minutes, the hydrate capillary bridge was generated from the conversion of solution capillary bridge. Furthermore, the amount of each component to form hydrate was consumed by the hydrate formation, suggesting the density gradient from interface to the bulk phase was decreasing accompanying with the hydrate formation.

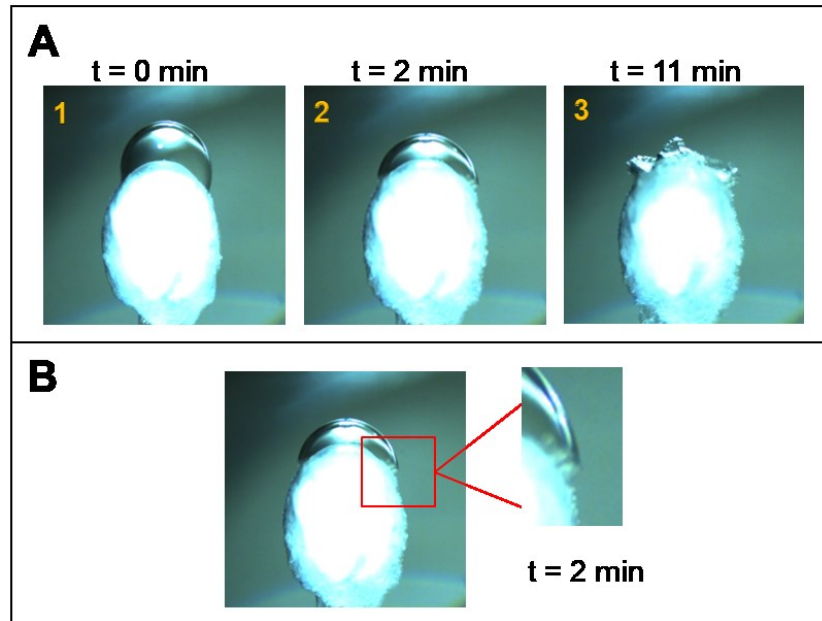


Figure 5-9: Photographic images of hydrate morphology captured from water droplet-CP hydrate interactions in oil bulk phase (A): the point just after detachment of water droplet (point 1); the first point of hydrate shell formation (point 2); final morphology of hydrate after complete conversion from water solution (point 3); (B) Amplification images of initial point of hydrate growth in oil bulk phase.

5.4.2 Morphology of hydrate particle after contact with electrolyte solution

Salts not only prevent the hydrate agglomeration via decreasing the liquid bridge volume, but also reduce the rate of gas hydrate growth. Even though the effects of salts on hydrate agglomeration via adhesion force measurements have been determined, its impacts on the rate of gas hydrate growth were rarely studied. Zylyftari et al. [57] revealed that the larger amount of NaCl was responsible for lower hydrate equilibrium temperature. Moreover, Kishimoto et al. [12] focused on the influences of various concentrations of NaCl on hydrate growth, and found that the hydrate film growth rate was increased while the size of hydrate crystals was reduced at higher subcooling (the larger difference between experimental temperature and equilibrium

temperature). The new hydrate growth or sintering was more likely to occur along the interface, where existed high amount of each component (i.e., guest and host molecules) to form hydrate. Sloan et al. [5] demonstrated three common conditions for hydrate growth along the water/hydrocarbon interface: (i) Existence of hydrate seed near the interface; (ii) Presence of water as bulk phase; (iii) Region of co-existence of water and hydrate former. As a result, both the subcooling and the presence of surfactants in either phase were considered as driving force for hydrate growth [5].

Based on the results shown above, since the effects of KCl and NaCl on capillary forces were almost same, and then only NaCl solution was analyzed accompanying with other three solutions (i.e., DI water, CaCl₂ and Na₂SO₄). Figure 5-10 showed the images of first point of hydrate shell formation with respect of four different solutions. The hydrate shell formation taking place along the interface initially was confirmed in our studies. Moreover, as compared with other three salts, the time required for pure water to form hydrate shell was shortest although most amount of water solution was left on the hydrate particle, and the delay of hydrate growth caused by the addition of salts was also agreed with previous research. The salts with higher valence could affect hydrate formation more significantly, which could be comprehended from two concepts: (i) the solutions with higher interfacial tension after adding salts with divalent ions would shift towards much lower equilibrium temperature for hydrate stability [30]; (ii) the much lower subcooling could slow down the hydrate growth greatly [5].

As mentioned above, the hydrogen bonding between water molecules to form cage was critical for hydrate formation [15]. Figure 5-11 gave the photographic images of final cyclopentane hydrate morphology after fully conversion of four solution droplets with same volume size (i.e., $d = 2.10 \pm 0.05$ mm): (A) DI water; (B) 2.5 wt. % NaCl solutions; (C) 2.5 wt. % CaCl₂ solutions

and (D) 2.5 wt. % Na₂SO₄ solutions in pure cyclopentane bulk phase at 2.0 ± 0.5 °C. Most water (Figure 5-11 (A)) was left on the CP hydrate particle caused by the strong attractive hydrogen bonding force between water molecules in water solution and CP hydrate particle, leading to more hydrate formation. Furthermore, there was a surprising observation about the hydrate morphologies after complete hydrate conversion from pure water solution. The dendritic morphology of the hydrate shown in panel A of Figure 5-11 was because some part of the solution droplet would collapse if the water converted to hydrate with a fast speed, resulting in the continuous decreasing of internal droplet volume [5].

When the water solution was replaced by the brine solution, the less hydrate growth along the interface could be explained by salts being considered as hydrate inhibitors [21]. This was to say the salts could compete with hydrates for available free water to prevent the formation of hydrate cage. Additionally, the lower adhesion force measured between salt solutions with divalent ions and CP hydrate particle were because of the less capillary bridge volume [6]. Figure 5-11 indicated that the largest amount of “new” hydrate was generated by pure water solutions within shortest conversion time. On the other hand, the time required to complete the hydrate conversion from Na₂SO₄ solutions was longest not only because of the latest observation of beginning of hydrate shell formation but also due to lack of large amount of component for hydrate nucleation (i.e., less amount of available water solution). The evidences shown in Figure 5-10 and 5-11 conclude that, the highly electronegative ions in the aqueous solution (such as Cl⁻ or SO₄²⁻) could be hydrogen-bonded with water molecules, inhibiting the hydrate crystallization. In addition, the solutions with higher valence would lead to less hydrate formation, and these phenomena could be comprehended by the stronger hydrogen bonding between higher electronegative ions and water molecules. Consequently, both CaCl₂ and Na₂SO₄ might be considered as the more

effective inhibitors of hydrate formation than the salts with monovalent ions: such as NaCl and KCl.

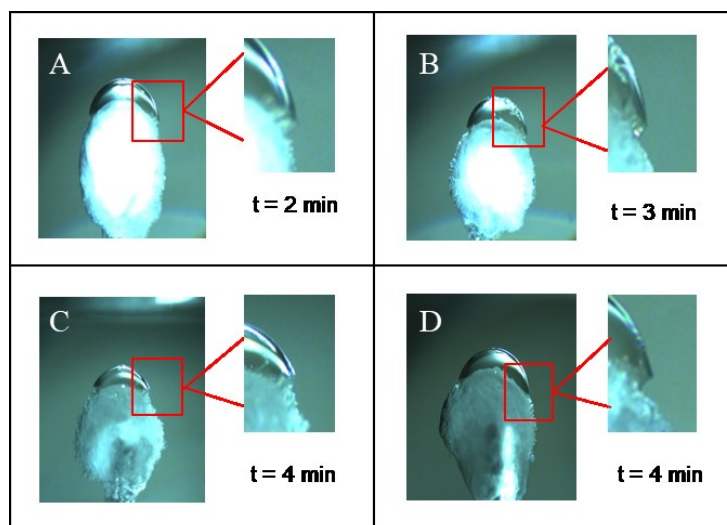


Figure 5-10: Photographic images of initial point of hydrate shell formation from different solution droplets ($d = 2.10 \pm 0.05$ mm): (A) DI water; (B) 2.5 wt. % NaCl; (C) 2.5 wt.% CaCl_2 ; (D) 2.5 wt.% Na_2SO_4 at in pure cyclopentane bulk phase at 2.0 ± 0.5 °C.

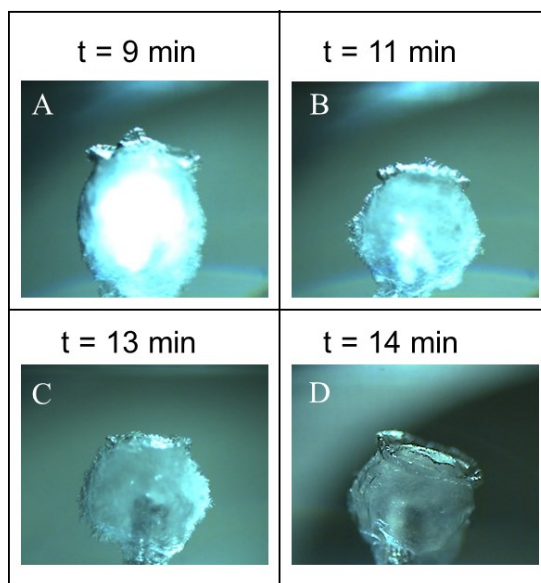


Figure 5-11: Photographic images of CP hydrate morphology after complete conversion from four solutions with same volume: (A) DI water; (B) 2.5 wt. % NaCl; (C) 2.5 wt. % CaCl_2 ; (D) 2.5 wt. % Na_2SO_4 in pure cyclopentane bulk phase at 2.0 ± 0.5 °C.

5.5 Capillary adhesion force measurements between CP hydrate and electrolyte solution droplet in gas bulk phase

5.5.1 Effects of concentration of electrolyte solution

In order to study the interactions between brine solution droplets and CP hydrate probe in gas phase, the hydrate particle was initially annealed in the pure CP bulk phase, and then the liquid CP was slowly drawn out by using a syringe so that the hydrate particle could be exposed to the gas phase.

To our knowledge of literature, higher capillary force could be achieved by either decreased contact angle or increased interfacial tension. From Figure 5-12 (A), it clearly stated the capillary adhesion force measured in the gas phase was approximately twice more than the force measured in the oil phase when the water solution droplet contacted to CP hydrate probe. This behavior could be explained in two possible reasons: 1) A decreased contact angle was observed when droplet attached to CP hydrate particle; 2) An increased Quasi-liquid-layer size when the CP hydrate was exposed to the gas phase. In other words, higher adhesion force in gas phase was not only because of formation of a larger quasi-liquid layer, but also the changing wettability of hydrate surface. Wider liquid bridge was arising from the more unconverted water released from hydrate core, caused by fracture of hydrate shell when the hydrate particle was exposed into gas phase, leading to a larger bridge-hydrate contact angle. Furthermore, the other reason for higher adhesion force obtained in gas phase was the resulted higher interfacial tension between water and air than that between water and oil (i.e., $\gamma_w (= 72 \text{ mN/m}) > \gamma_{wo} (= 48.7 \text{ mN/m})$). Thus, once the hydrate particle was exposed into gas phase, its surface could become more wettable due to the unconverted water being drawn out from hydrate core, and then the rapid hydrate formation was observed visually. Once two surfaces contacted each other, the continuous increasing force suggested the rapid hydrate growth along the interface during this holding period. Additionally,

the higher interaction force required to separate CP hydrate particle and water solution droplet was expected due to the presence of larger amount of “new” hydrate growth. There was an interesting observation of different CP hydrate morphology after being exposed into gas and oil phase, respectively. Compared to the relative smooth hydrate surface exposed into oil phase, some small dendrites grew on the surface of CP hydrate particle if presented in the gas phase (Figure 5-12 (B)-1) due to heat transfer limitations from the surroundings. These observations were also found when the salts were added into aqueous solution, and the adhesion force curves measured between electrolyte solution droplets and CP hydrate were plotted in Figure 5-13.

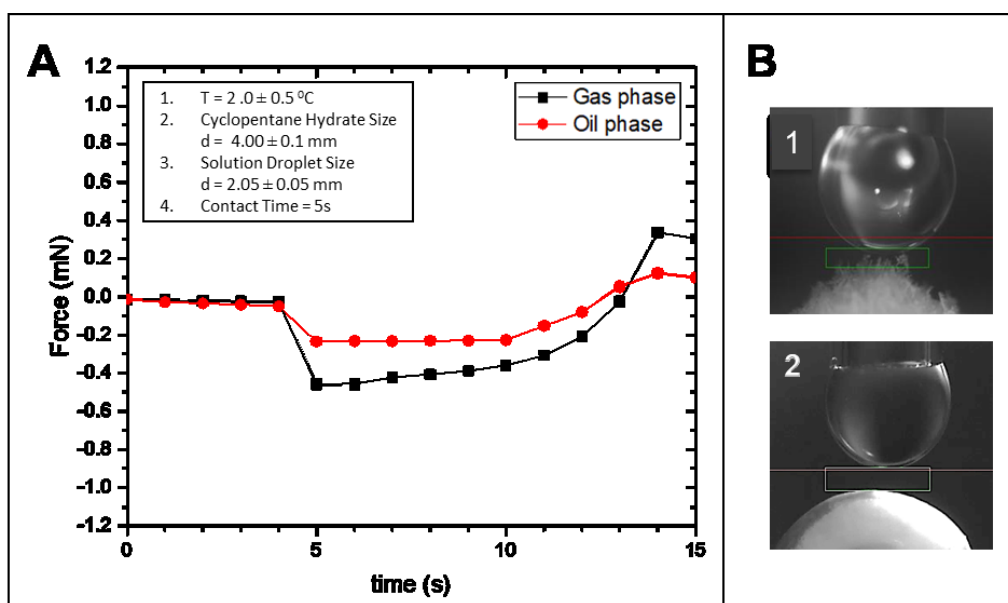


Figure 5-12: Adhesion force curves obtained from the interactions between water droplet and CP hydrate particle in gas and oil phase at 2.0 ± 0.5 °C (A); Corresponding images of hydrate exposed into gas phase (B-1) and oil phase (B-2), respectively.

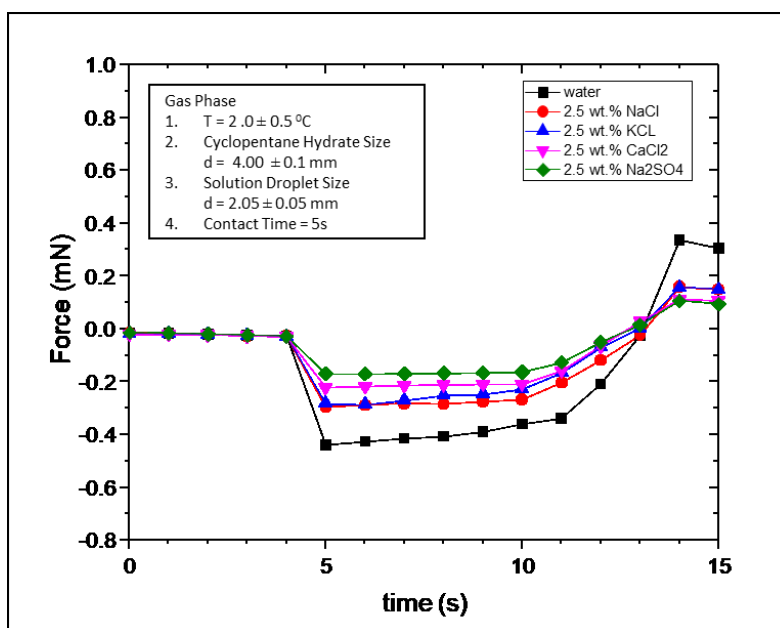


Figure 5-13: Adhesion force curves obtained from the interactions between electrolyte solution droplet and CP hydrate in gas phase at $2.0 \pm 0.5 \text{ } ^\circ\text{C}$.

5.6 Hydrate growth morphology in gas bulk phase

5.6.1 Morphology of hydrate particle after contact with water solution

As mentioned in the previous section, the reason for hydrate morphologies exposed in gas phase being far away from that exposed in the oil phase could be explained by the heat transfer limitation. As illustrated by Sloan et al. [5], both heat transfer limitations and mass transfer limitations made significant contributions on the hydrate growth rate. When gas hydrate was drawn into the gas phase, the hydrate surface was easily cracked in pieces so that the surface could become more wettable owing to the diffusion of unconverted water from hydrate core, resulting in thicker QLL layer and rapid hydrate formation. The images shown in Figure 5-14 supported this hypothesis. The panels A (1-2) and A (3-4) of Figure 5-14 described the corresponding images to describe this processes that a water droplet approached to and retracted

from CP hydrate particle after 5 seconds contact time in the gas phase at 2.0 ± 0.5 °C, respectively. Specifically, before two surfaces contacting, the equilibrium state of CP hydrate and water droplet was shown in the panel A-1 of Figure 5-14; afterwards, the images shown in panel A-2 indicated the point of initial contact, while panel A-3 presented the water droplet being separated apart from CP hydrate particle. Finally, the hydrate morphology after separation of droplet was told in panel A-4. Likely, panel B (1-4) and C (1-4) of Figure 5-14 illustrated the corresponding pictures captured during the experimental processes when contact time increased to 25 seconds and 45 seconds, respectively, while the red boxes highlighted the change of hydrate morphologies as a function of contact time. It was clear to speak that the rate of hydrate formation along the interface was much faster if the CP hydrate particle was exposed in the gas phase than that exposed in the oil phase due to the existence of lager amount of QLL layer. The amount of liquid water was inversely proportional to the contact time. The faster hydrate formation reduced the amount of liquid water after the solution bridge ruptured at neck because more water have started to convert to hydrate. The crystal pieces observed inside the capillary bridge provided the insight that the hydrate shell around the hydrate particle was cracked when exposed into gas phase, and those amounts was increasing with contact time. In other words, the longer contact time led to the more hydrate to grow along the interface since the larger amount of water was supplied by both the unconverted water diffusing from hydrate core and external water droplet. As a result, the time for complete hydrate conversion from water in the gas phase was greatly shortened to less than 3 minutes, according to observations reported in Figure 5-15. The shorter time required to ignite hydrate growth was confirmed with longer contact time.

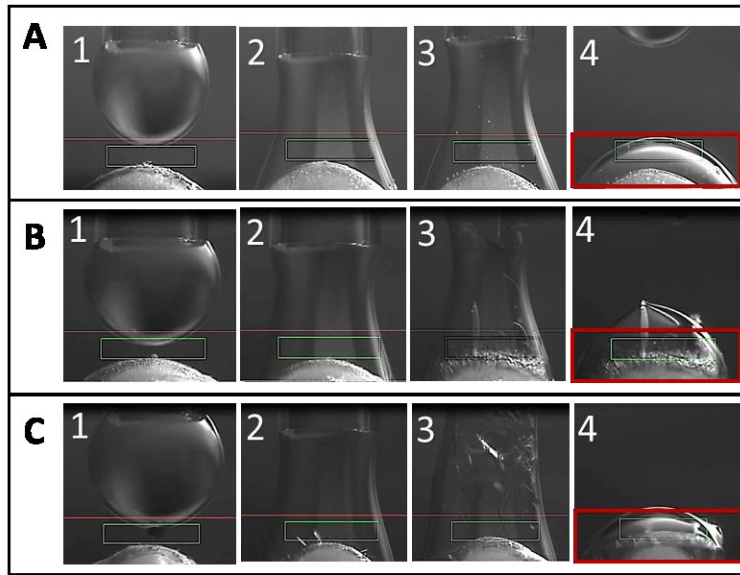


Figure 5-14: Corresponding photographic images of conversion process of CP hydrate growth from water solution: before two surfaces contacted (1); at the initial point of capillary bridge formation (2); at the point when water was driven away from CP hydrate particle (3); at the point after some water being left on CP hydrate particle (4) with contact time of 5s (A); 25s (B); 45s (C).

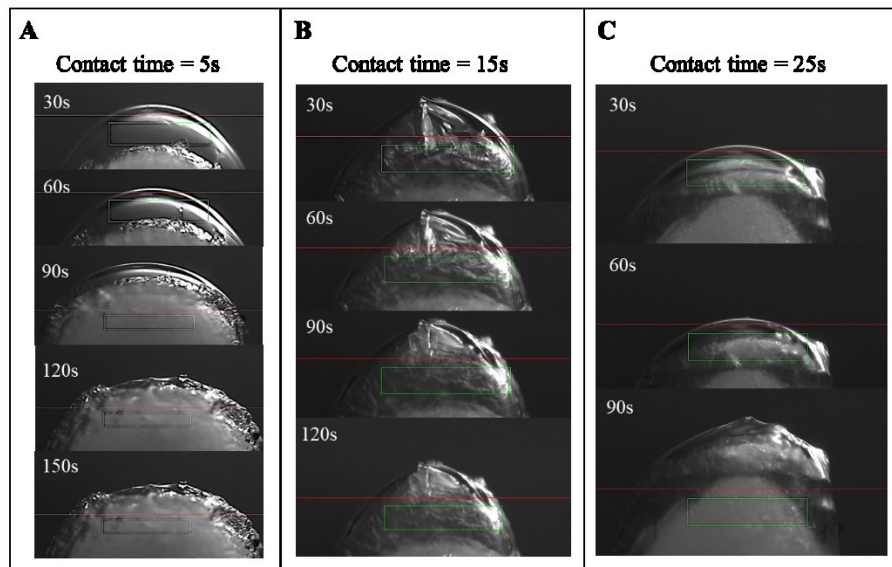


Figure 5-15: Corresponding photographic images of conversion process of CP hydrate growth from water solution with respect to three contact time: 5s (A); 25s (B); 45s (C).

5.6.2 Morphology of hydrate particle after contact with electrolyte solution

Under same subcooling circumstance (i.e., around 5K), the water was replaced by three electrolyte solutions with varying concentrations, and the corresponding images of hydrate morphologies were also captured at the contact point of two surfaces. Figure 5-16, 5-17, 5-18 presented the hydrate morphologies once the droplets of NaCl, CaCl₂ and Na₂SO₄ solution attached on the particle in the gas phase, respectively. Additionally, the effects of concentration of each salt were understood by the hydrate growth rate shown in panels A, B and C of Figure 5-16, 5-17, 5-18, respectively. From Figure 5-16, the relative faster hydrate grow rate was caused by addition of lower concentration of NaCl solution. Whereas, the start point of hydrate shell formation was delayed by the existence of salts due to their inhibiting impacts on hydrate formation. The more salts (i.e., higher concentration) were added into the aqueous solution, the less amount of solution droplet was left on the hydrate particle because the attractive force between ions and water molecules was stronger than the hydrogen bonding formed between two water molecules; therefore, the strong binding enhanced the competition with the hydrate former for water. The activity of water was decreasing with concentration of salts, resulting in less available water to form hydrate interacting with the guest molecules [78]. As compared to the pure water solution, not only the delayed hydrate growth but also the less amount of hydrate formation was found when the salts were introduced into the aqueous solution. Even though the concentration of salts did not make huge contribution on the adhesion force, it played an essential factor on the hydrate morphology. It was well known that the hydrate rate was controlled by the mass transfer limitation (i.e., amount of component for hydrate formation), heat transfer limitation (i.e., subcooling) and the presence of surfactants (e.g., thermodynamic or kinetic inhibitors). In our system, neither mass nor heat transfer limitation was variable; therefore, the change of hydrate growth rate and morphology was only dependent on the presence of salts. In

other words, the hydrate growth rate was lowered by the salts, and the much rougher “new” hydrate surface was eventually observed [5]. Furthermore, the hydrate growth rate showed limited variations regardless of concentration of CaCl_2 and Na_2SO_4 solution, being in consistent with adhesion force measurements. Thus, even with lower content, the influence of salts with divalent ions (i.e., CaCl_2 and Na_2SO_4) on hydrate prevention was more effective than the salts with monovalent ions (i.e., NaCl or KCl). These observations were agreed with the case in the oil phase as well.

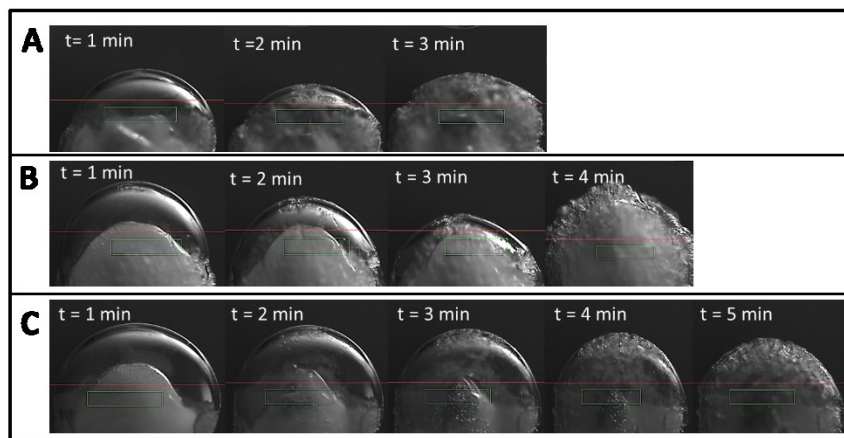


Figure 5-16: CP hydrate morphologies after contact with 2.5 wt. % NaCl (A); 5 wt. % NaCl (B); 7.5 wt. % NaCl (C), respectively, in gas phase at 2.0 ± 0.5 °C.

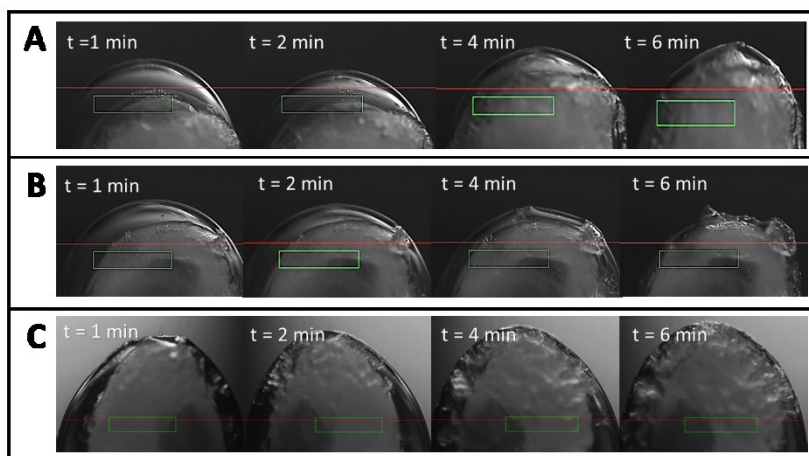


Figure 5-17: CP hydrate morphologies after contact with 2.5 wt. % CaCl_2 (A); 5 wt. % CaCl_2 (B);

7.5 wt. % CaCl_2 (C), respectively, in gas phase at 2.0 ± 0.5 °C.

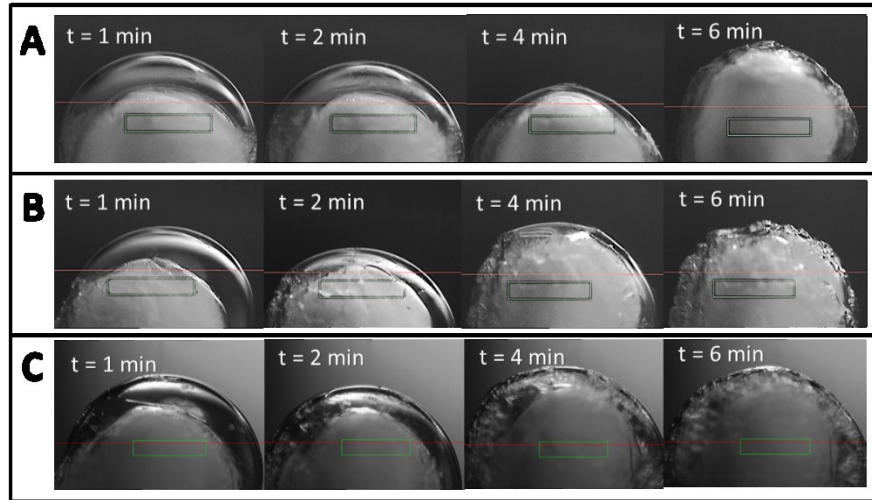


Figure 5-18: CP hydrate morphologies after contact with 2.5 wt. % Na_2SO_4 (A); 5 wt. % Na_2SO_4 (B); 7.5 wt. % Na_2SO_4 (C), respectively, in gas phase at 2.0 ± 0.5 °C.

5.7 Effects of presence of another hydrocarbon

5.7.1 Capillary adhesion force measurements between CP hydrate and water solution droplet in 1:1 of cyclopentane and toluene oil phase

Many studies have reported the mechanism of interactions between CP hydrate particle and water bulk solution in pure cyclopentane oil phase, and Liu et al. [17] demonstrated the maximum interaction forces measured between hydrate particle and water droplet were around 0.33 mN, and the extended contact time would result in larger interaction forces because of new hydrate growth. Lee et al. [21] discussed the gradually increasing adhesion forces between CP hydrate particle and pure water solution based on studies of three consecutive cycles of adhesion force measurements due to the sintering mechanism as well.

Figure 5-19 clearly showed interaction forces measured between CP hydrate ($d = 4.00 \pm 0.1$ mm) and water droplet ($d = 2.05 \pm 0.05$ mm) both in pure cyclopentane oil phase (black

straight line) and in the mixture of cyclopentane and toluene in volume ratio of 1:1 (red dashed line) at 2.0 ± 0.5 °C. In this experiment, it took 5 seconds to drive water droplet towards CP hydrate particle until being contact. The interaction force was almost unchanged before the water drop attached to CP hydrate particle. In both cases, accompanying with a dramatic drop of force at initial contact point, the water solution could spread on the hydrate particle spontaneously, leading to the initial formation of three-phase-contact (TPC) line. The water was more likely to slide a little bit along the hydrate particle until reaching the final equilibrium state with minimum interfacial Gibbs free energy, and the TPC line could sinter at that point afterwards. Generally, this attractive force (i.e., capillary force) was defined as the initial contact force. As compared to pure cyclopentane liquid phase, the force measured in mixed oil phase was lower. According to previous studies, the occurrence of this phenomenon was due to the lower interfacial tension between water and mixture of cyclopentane and toluene ($\gamma = 40.2$ mN/m) than that between water and pure water ($\gamma = 48.7$ mN/m) [5] [14]. During the contact period lasting to 5 seconds, without any further preload force, the interaction forces were almost unchanged regardless of the surrounding bulk phase because there was no change of bridge curvature. When the water droplet started to detach from hydrate particle, the capillary bridge was continuously becoming “thinner”, leading to the increased interaction forces along with the detachment process. Once the capillary bridge reunited, some amount of water being left on the hydrate particle was the reason for that the interaction forces would not go back to value “0”.

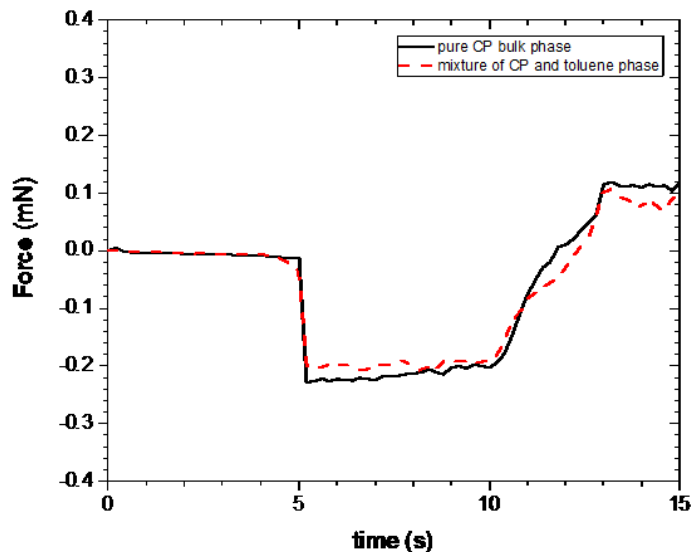


Figure 5-19: Adhesion forces curves obtained from the interactions between CP hydrate and water droplet in oil bulk phase (black straight line) and in mixture of volume ratio of 1:1 CP and toluene phase (red dashed line) at 2.0 ± 0.5 °C.

5.7.2 CP hydrate morphology in 1:1 of cyclopentane and toluene oil phase

Likely the previous measurements, the rate of CP hydrated shell growth had also been determined. Panel A of Figure 5-20 presented the images of CP hydrate morphologies captured at initial point of water being left on surface (Figure 5-20 (A)-1), the first indication of hydrate shell formation (Figure 5-20 (A)-2), and final morphology of hydrate after fully conversion from water solution (Figure 5-20 (A)-3) in the mixed oil bulk phase. Also, panel B of Figure 5-20 provided the amplifications of the first observations of CP hydrate shell formation around water surface in the mixture of cyclopentane and toluene with a volumetric ratio of 1: 1. From experimental results, the CP hydrate growth rate was higher with presence of more content of cyclopentane, and the time required for the fully conversion was longer as expected compared to that in pure cyclopentane bulk phase, illustrated in Figure 5-11. Therefore, the lower concentration of hydrate former would slow hydrate shell formation and hydrate growth. Two proposals given followings

could explain this observation: (1) The growth of hydrate was limited by both subcooling (i.e., the difference between experimental temperature and hydrate equilibrium temperature) and the driving force which was generated by the super-saturation of hydrocarbon or water in the bulk phase [11] [12]. Without changing of subcooling, the greater number of required components (i.e., water and hydrocarbon) would decrease the concentration gradient from interface to the bulk phase. (2) The hydrate shell growth depended on mass transfer limitations, and then the less concentration of required hydrocarbon could slow down the diffusion through the hydrate shell. Furthermore, there was a surprising observation about the hydrate morphologies after water conversion in two bulk phases. As mentioned above, the collapse of solution droplet was found in the pure cyclopentane phase due to the fast formation of hydrate conversion. However, the less content of cyclopentane resulted in the lower hydrate growth and formation, and then the whole hydrate shell around water solution was present instead.

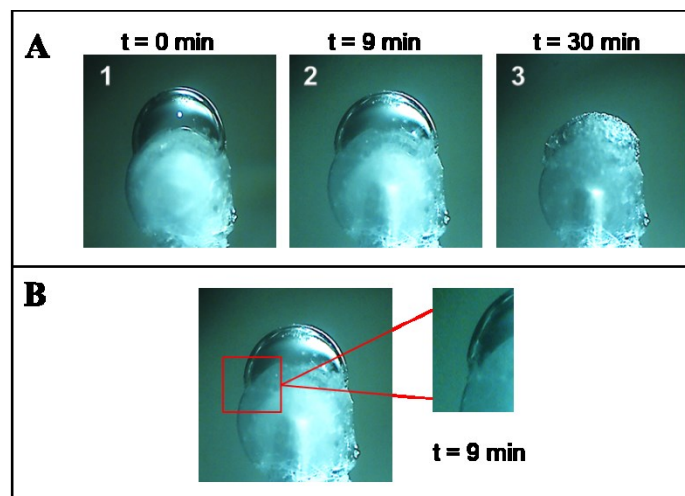


Figure 5-20: Photographic images of hydrate morphology obtained at initial point of water being left on surface (A-1); the first indication of hydrate shell formation (A-2); final morphology of hydrate after fully conversion from water solution (A-3) in the mixture of cyclopentane and toluene phase (volumetric ratio: 1:1) at 2.0 ± 0.5 °C.

On the other hand, the hydrate formation rate was further lowered by the presence of salts, confirmed by the Figure 5-21 to 5-23, clearly representing the process of hydrate morphology changing with addition of 2.5 wt. % NaCl, 2.5 wt. % CaCl₂ and 2.5 wt. % Na₂SO₄, respectively. When electrolyte solution droplet adhered on the CP hydrate probe, the time required to complete the hydrate conversion was increasing as expected. The impact of NaCl on the hydrate morphology was less significant than other two salts with divalent ions. Specifically, it could take about 50 minutes to complete the hydrate conversion from solution droplet with 2.5 wt. % NaCl, while even longer annealing time, up to 75 minutes, was observed for fully hydrate conversion if the NaCl solution was replaced by CaCl₂ solution. Nevertheless, fully conversion was absent even after 100 minutes holding time when 2.5 wt. % Na₂SO₄ solution droplet attached to the CP hydrate, indicating that the salt Na₂SO₄ was the more effective inhibitor to delay the hydrate growth. It might be explained by this reason: the ions with divalent ions could reduce the solubility of hydrocarbon in the aqueous phase, resulting in the lower hydrate growth rate [79].

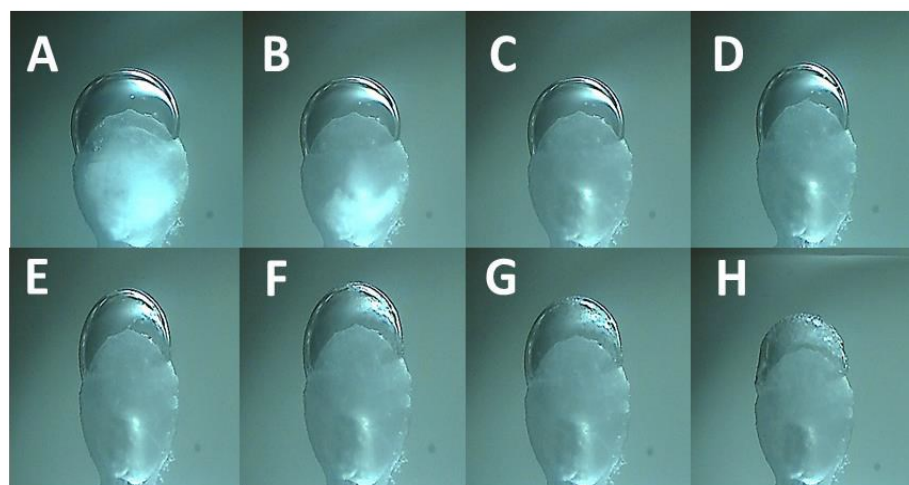


Figure 5-21: Photographic images of hydrate morphologies during the conversion process from 2.5 wt. % NaCl solution droplet in the mixture of cyclopentane and toluene phase (volumetric ratio: 1:1) at 2.0 ± 0.5 °C: t = 0 min (A); t = 5 min (B); t = 10 min (C); t = 15 min (D); t = 20 min (E); t = 25 min (F); t = 30 min (G); t = 50 min (H).

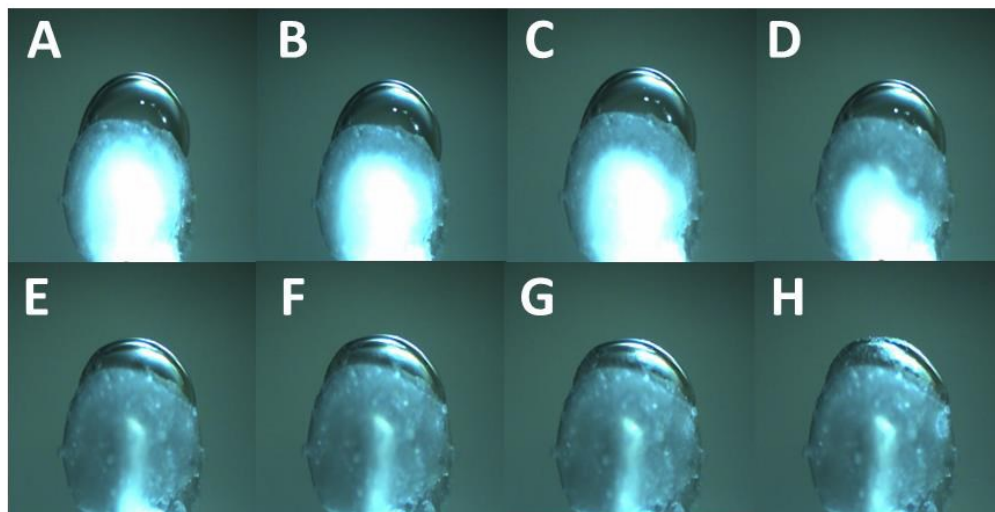


Figure 5-22: Photographic images of hydrate morphologies during the conversion process from 2.5 wt. % CaCl_2 solution droplet in the mixture of cyclopentane and toluene phase (volumetric ratio: 1:1) at 2.0 ± 0.5 °C: t = 0 min (A); t = 5 min (B); t = 10 min (C); t = 20 min (D); t = 30 min (E); t = 50 min (F); t = 60 min (G); t = 75 min (H).

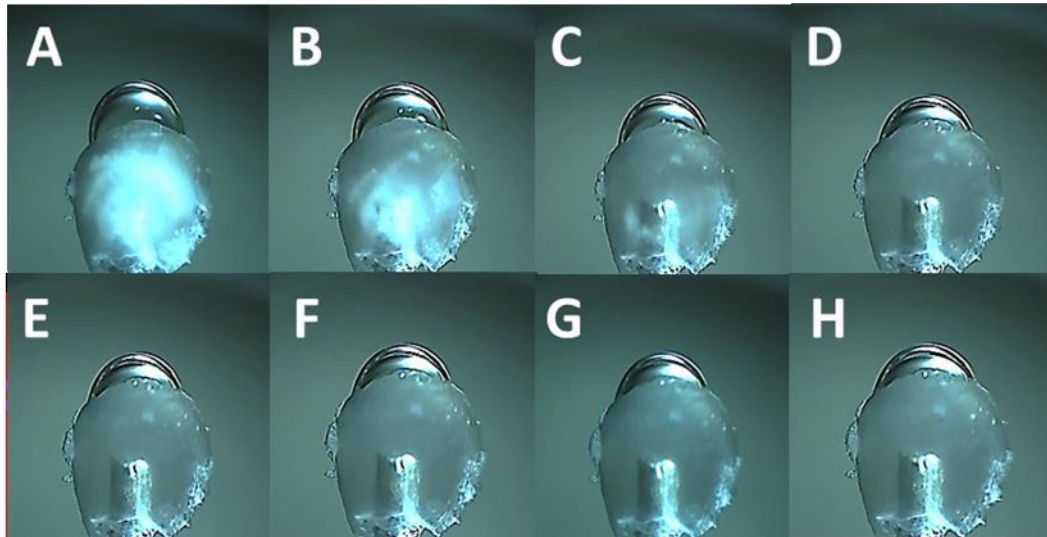


Figure 5-23: Photographic images of hydrate morphologies during the conversion process from 2.5 wt. % Na_2SO_4 solution droplet in the mixture of cyclopentane and toluene phase (volumetric ratio: 1:1) at 2.0 ± 0.5 °C: t = 0 min (A); t = 5 min (B); t = 10 min (C); t = 30 min (D); t = 50 min (E); t = 70 min (F); t = 90 min (G); t = 100 min (H).

5.7.3 Capillary adhesion force measurements between CP hydrate and water solution droplet in pure decane oil phase

For better understanding the effects of hydrocarbon on hydrate growth rate, the pure decane was also employed as the oil phase instead of pure cyclopentane. From panel A of Figure 5-24, the capillary force curve plotted from interactions between water droplet and CP hydrate probe in the pure decane bulk phase at 2.0 ± 0.5 °C. The similar mechanism of capillary bridge formation in the pure decane bulk phase was found, but the higher interfacial tension between decane and water phase (i.e., $\gamma = 51.96$ mN/m [80]) led to the higher initial contact force. However, absence of hydrate growth was observed as expected because of the lack of component to form “new” hydrate (i.e., cyclopentane in this case). The images of hydrate morphologies captured at the initial point of contact (i.e., $t = 0$ min) with water droplet and after 20 minutes of contact were shown in panel B of Figure 5-24, respectively. It was obvious there was no new hydrate growth even under the equilibrium CP hydrate stable zone (i.e., atmospheric pressure and experimental temperature) after 20 minutes annealing time.

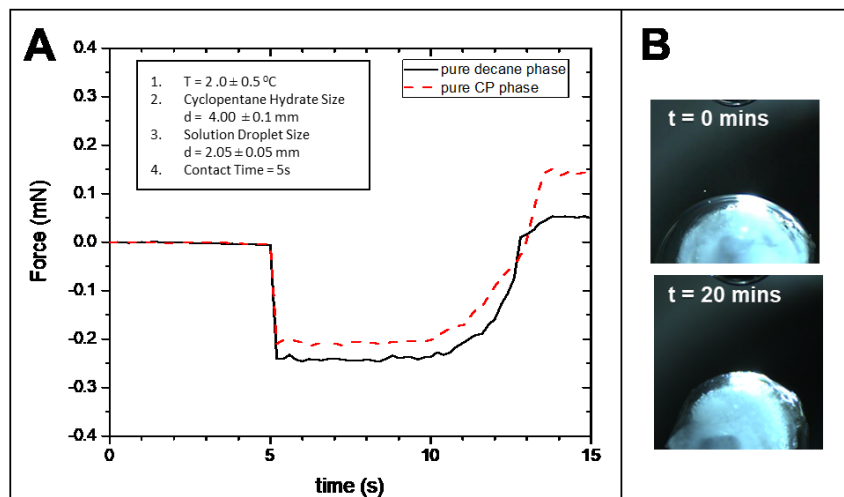


Figure 5-24: Capillary adhesion force measured between water droplet and CP hydrate probe (A); Corresponding pictures of hydrate morphologies captured at the initial contact point of water

droplet and after 20 minutes annealing time in pure decane bulk phase (B) at 2.0 ± 0.5 °C.

5.8 Effects of asphaltenes on interactions between CP hydrate and water solution droplet in 1:1 of cyclopentane and toluene oil phase

5.8.1 Effect of asphaltenes on water drop – CP hydrate adhesion force

Since asphaltenes are insoluble in n-pentane but soluble in toluene, the pure cyclopentane (referred as “pure oil phase”) was replaced by a mixture of toluene-cyclopentane with a volumetric ratio of 1:1 (referred as “mixed oil phase”). In order to determine the effect of asphaltenes, the interaction force between a CP hydrate ($D_h = 4.00 \pm 0.1$ mm) and a water drop ($D_d = 2.00 \pm 0.05$ mm) were investigated in both pure and mixed oil phases. Additionally, because the colorless mixture changed to yellow after adding asphaltenes into the bottle filled with the mixed oil phase, the bottle was then sonicated for 1 hour to reach complete dissolution of asphaltenes.

In Figure 5-25 (A), we plotted the force curves as a function of time in mixed oil phase at 2.0 ± 0.5 °C with presence of 0.03 g/L asphaltenes. The measurement process consisted of an approach time of 3 seconds, followed by a hold time of 7 seconds, and finally a retract time of 3 seconds. Moreover, the approach and retraction velocities were set as 100 $\mu\text{m/s}$. The time “ $t=0$ ” was defined as the point when the force started changing [81].

Figure 5-25 (A) showed the force curve obtained with the addition of 0.03 g/L asphaltenes in the mixed oil phase. Unlike the cases in Figure 5-19, the rupture of the oil film did not occur at the initial contact under the same experimental conditions. Therefore, the approach velocity was increased to 200 $\mu\text{m/s}$ while still driving the drop for 3 seconds to enlarge the contact area between the drop and the hydrate for increasing the chance of attachment. Looking at Figure 5-25

(A), the force curve was once again explained in different labelled stages: (1) The drop was driven towards the hydrate particle for the first 1.5 seconds. (2) As drop and hydrate overlapped, the repulsive force increased from 0 to 0.045 mN when the approach was stopped at 3 seconds. This repulsive force was a consequence of the hydrodynamic pressure build up in the thin oil film between the drop and the hydrate. (3) Film rupture eventually took place after another 0.7 seconds of holding time. This film rupture delay could be explained by the adsorption of asphaltenes around the water droplet. The strong polar asphaltenes were shown to adsorb on the oil-water and oil-air interface [82]-[87], and it was suggested that the adsorption of asphaltenes was irreversible [88]. (4) Once the water spread on the surface of the hydrate particle, the attractive force was weaker at 0.18 mN due to the further reduced interfacial tension (i.e., 35 mN/m) caused by the addition of asphaltenes which acted as surface-active components into the system. After contact, the formation of hydrate-oil-water three phase contact line resulted in a significant increase of the attraction force. The force remained unchanged during the contact period; (5) During the retract stage, the interaction force was dominated by the increasing curvature of the liquid bridge until the neck broke; (6) Some water was left on the hydrate particle and the weight of that water resulted in a positive force at the end. In addition, the less amount of new hydrate growth was observed after water contacting with CP hydrate maybe because the presence of asphaltenes could reduce the gas diffusion and then exhibit the stronger inhibition of hydrate nucleation and growth [18] [89] [90].

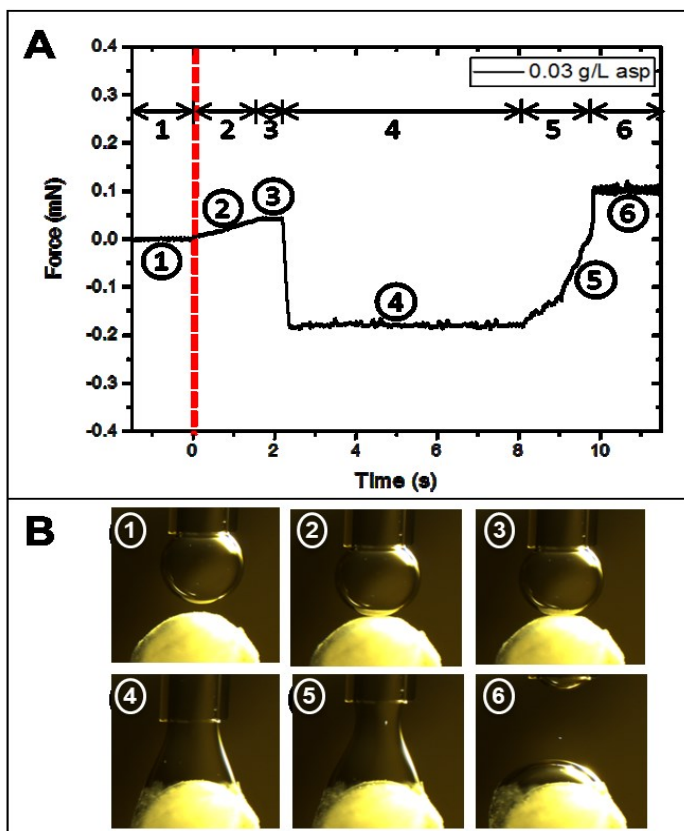


Figure 5-25: Adhesion force curves plotted as a function of time during the interaction between a water droplet and a CP hydrate in the presence of 0.03 g/L asphaltenes in the mixed oil phase at 2.0 ± 0.5 °C (A); Corresponding images of the interactions with the addition of 0.03 g/L asphaltenes (B).

5.8.2 Effect of elevated asphaltenes concentration on the adhesion force

When the concentration of asphaltenes added into mixed oil phase was increased to 0.05 g/L, the interaction force showed very different features when compared with 0.03 g/L (Figure 5-26 (A)). The force remained repulsive for the entire experimental procedure for 0.05 g/L, indicating that the thin oil film between the water drop and the CP hydrate did not rupture. Figures 5-26 (B) and 5-26 (C) showed the corresponding images, where it is clear that with 0.05 g/L asphaltenes, the drop was retracted without leaving behind any water. The contact

time was then increased, but still no rupture of the film happened even as the interaction lasted for up to 25 seconds for the same external force. Consequently, these experimental results provided strong evidence that the concentration of 0.05 g/L asphaltenes could efficiently prevent the capillary bridge formation due to the thicker adsorption layer around the droplet.

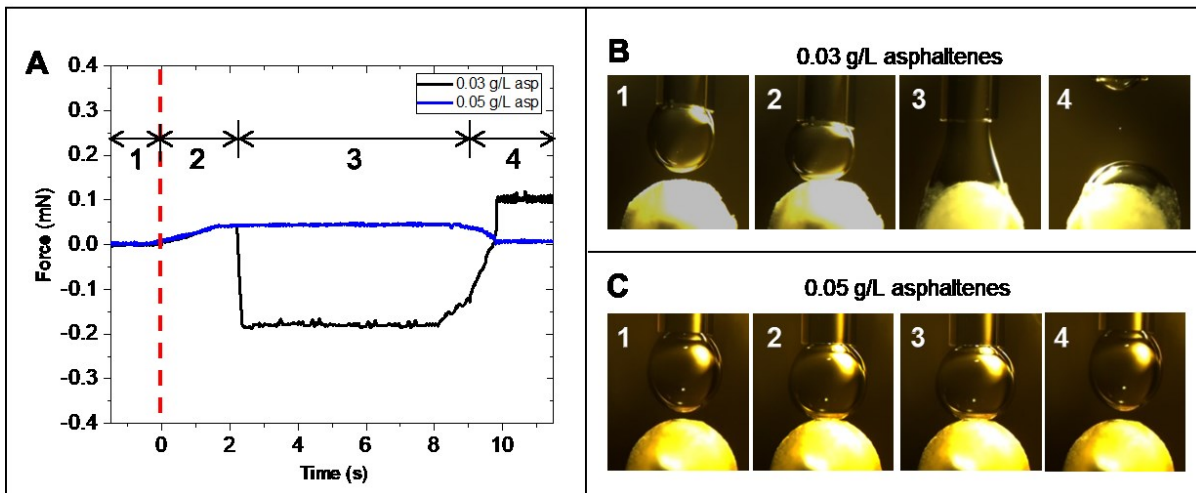


Figure 5-26: Effect of concentration of asphaltenes on the interaction force measured between a water droplet and a CP hydrate particle in the mixed oil phase at 2.0 ± 0.5 °C (A); Photographic images captured before contact (stage 1); contact period before droplet ruptured (stage 2); during contact period (stage 3); after detachment process (stage 4) with addition of 0.03 g/L asphaltenes (B) and 0.05 g/L asphaltenes (C), respectively.

5.8.3 Effect of salts on water drop - CP hydrate adhesion force

In the previous section, we showed that asphaltenes are effective anti-agglomeration surfactants that could prevent hydrate agglomeration. However, during oil production and transportation, the emulsified water always contains salts. According to previous studies [1] [79] [80], salts are believed to operate as thermodynamic inhibitors that can lower the melting temperature of hydrate and decrease the solubility of guest species (hydrocarbon) in the host phase (water). Therefore, it is essential to understand the combined influence of asphaltenes and salts. After

adding 0.03 g/L asphaltenes into the oil phase, the water solution was replaced by both 3.5 wt. % NaCl (i.e., 0.6 mol/L NaCl) and CaCl₂ (i.e., 0.3 mol/L CaCl₂) because 3.5 wt. % is the bulk concentration of seawater.

When 3.5 wt. % NaCl with monovalent ions were present in the water drop (see Figure 5-27 (A)), the rupture of the film did not take place at the initial contact (point 1) once again. After applying an external force of 0.045 mN, the spreading of the salt solution droplet was observed for 0.6 seconds longer than pure water (point 2). Rather than fast spontaneous spreading, only a small amount of aqueous solution propagated very slowly on the hydrate, leading to a much weaker attractive force once equilibrium was reached (point 3). As the drop was driven away from the hydrate particle, a further adhesion force was measured due to the decreasing contact angle. Eventually, most amount of brine solution was left on the hydrate once the bridge ruptured at the neck (point 4). Figure 5-27 (B) presented the corresponding side-view photographs as time progresses. These interesting findings could be explained as follows: (1) the polarized aqueous phase could enhance the asphaltenes adsorption at the interface, confirmed by the delay of thin film rupture; (2) the aqueous solution caused a larger advancing contact angle on the hydrate particle due to the surface charge reversal caused by a layer of highly charged cations [91].

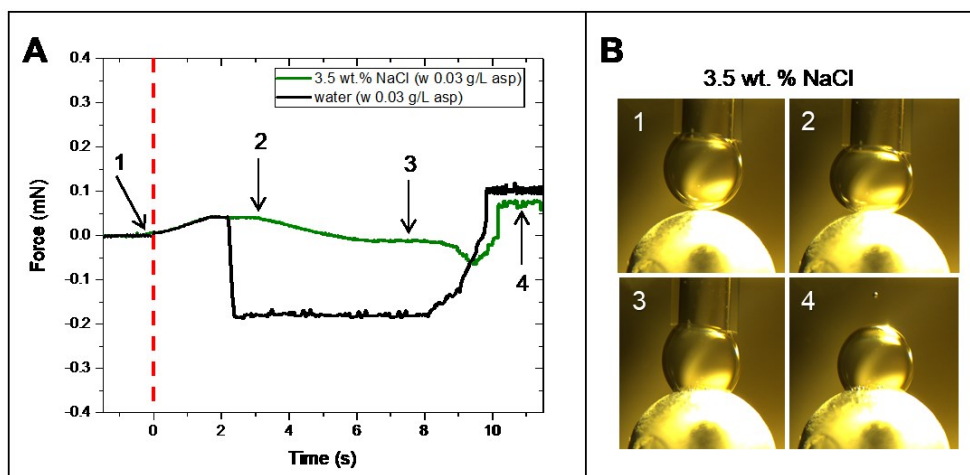


Figure 5-27: Effect of 3.5 wt. % NaCl on the interaction force between a water drop and a CP hydrate in the mixed oil phase at 2.0 ± 0.5 °C (A); Images captured at initial contact point (B-1), first point of droplet rupture (B-2), final point of solution spreading (B-3) and final point of detachment process (B-4).

On the other hand, the force curve obtained from the interactions between the 3.5 wt. % CaCl_2 solution drop with divalent ions, and the hydrate particle was slightly different from the 0.6 mol/L NaCl case (Figure 5-28 (A)). After applying the same preload force of 0.045 mN, the holding time started at 1.5 s and the rupture of the thin film was delayed by 2.1 seconds (point 2). Moreover, much lower attractive force was measured after droplet attachment because only a small amount of aqueous solution tended to spread on the surface at a slower propagation rate. The corresponding images captured from the side view are given in Figure 5-28 (B). In detail, four selected photographs are shown for better understanding of the force curves: contact point (1); first point of droplet attachment (2); final point of droplet spreading (3) and part of the aqueous solution left on the hydrate particle (4).

From Figures 3 to 5, when comparing between the three solutions, some interesting findings could be concluded: (1) Based on the observations of slower propagation rate and further delay of thin film rupture, the presence of salts enhanced the adsorption of asphaltenes along the interface maybe because of the salt-in effect, where the bonding forces were formed among the asphaltenes and then more asphaltenes were stable along the water/oil interface [82] [92]-[95]; (2) Salts with divalent ions could further encourage more asphaltenes adsorption along the interface because the cations with higher charge could enhance the ion-bridging effects [92]. Specifically, the movement of asphaltenes was accelerated by ions, resulting in more polar asphaltenes molecules forming bonds with cations in the aqueous phase [92]. Meanwhile, some

asphaltenes could attach to each other caused by the formation of chelation due to the presence of cations that acted as a bridge [92], in agreement with Demir et al. [96] who suggested that the tendency of agglomeration of asphaltenes was enhanced by the salts, especially by those with divalent ions. Furthermore, the reason for the larger contact angle measured for the bridge between brine solution and hydrate particle was probably because the surface charge of the hydrate changed from negative to positive caused by the presence of divalent cations [91] [97]. Mugele et al. [91] stated that the much stronger adsorption of higher concentration of CaCl_2 caused a layer of strongly adsorbed divalent ions on the surface hydrate particle, resulting in charge reversal of the hydrate surface. Consequently, the order of rigid layer formed by asphaltenes was given as following: no brine < NaCl < CaCl_2 .

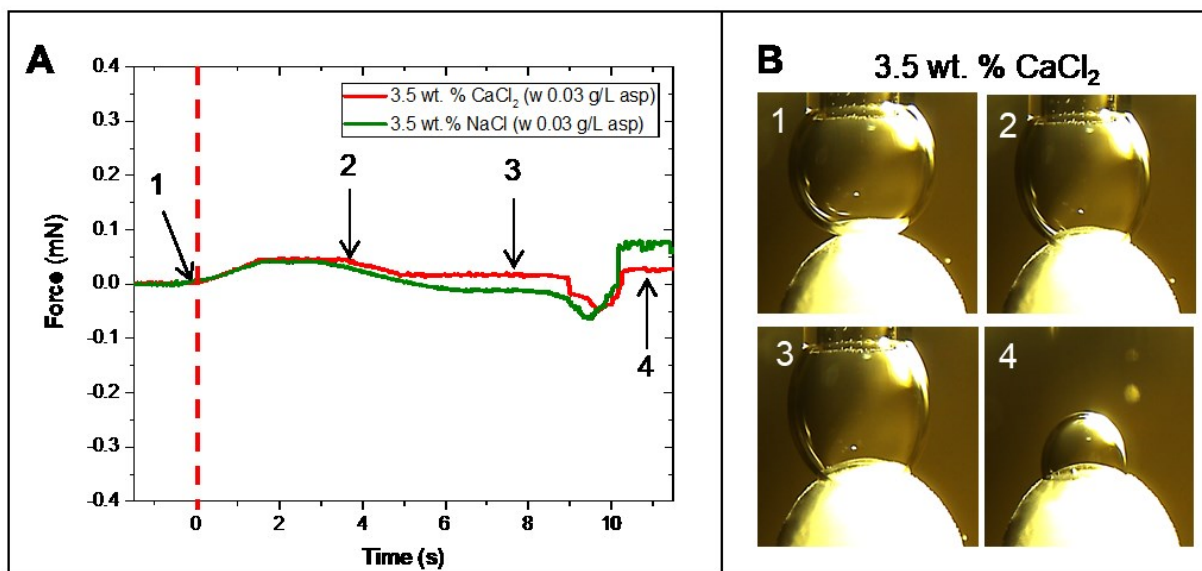


Figure 5-28: Effect of 3.5 wt. % CaCl_2 on the interaction force between a water drop and a CP hydrate in mixed oil phase (A) at 2.0 ± 0.5 °C; Images captured at initial contact point (B-1), first point of droplet rupture (B-2), final point of droplet spreading (B-3) and final point of detachment process (B-4).

5.8.4 Dynamic interfacial tension and crumpling ratio measurements

According to the literature [98], the dynamic interfacial tension was considered a reliable method to estimate the adsorption layer. Typically, the interfacial tension is reduced when surfactants stay along the interface. Figure 5-29 (A) presents the six dynamic interfacial tension curves obtained between the solution drop and mixed oil phase with addition of asphaltenes. The initial rapid decreasing of interfacial tension could be understood by the fast adsorption of surfactants on the interface, and both presence of salts and higher content of asphaltenes could enhance the adsorption of asphaltenes greatly. The equilibrium state was represented by the constant interfacial tension. The smaller interfacial tension suggested that more surfactants were adsorbed on the interface. Furthermore, a schematic diagram of asphaltenes adsorbed around the water drop is shown in Figure 5-29 (B).

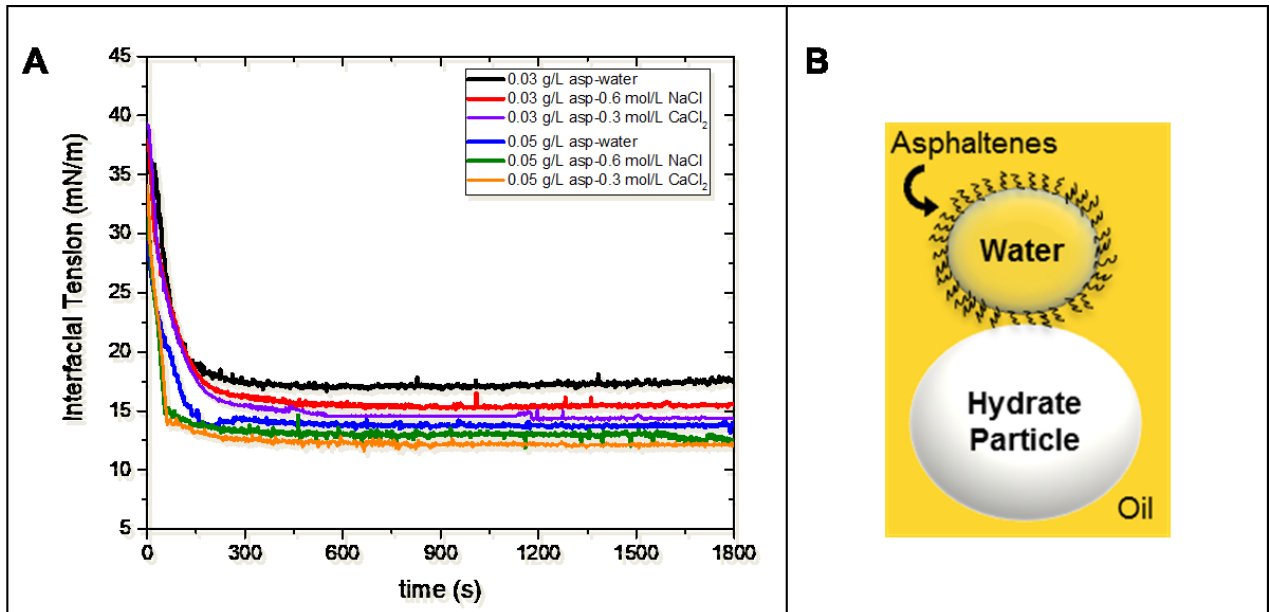


Figure 5-29: Dynamic interfacial tension between the aqueous droplet and oil phase with the addition of asphaltenes (A); Schematic diagram of adsorbed asphaltenes around the water drop (B).

Besides, after the adsorption layer reached equilibrium after 30 minutes aging time, the liquid inside the drop was retracted manually at a constant speed back into the capillary tube. Based on Equation 5, the crumpling ratio could be simplified as the ratio between the square of the radius of the water droplet right before crumpling, $(R_f)^2$, to the initial radius of the water droplet, $(R_i)^2$. Figure 5-30 (A) 1 to 3 shows the images of the water droplet, 3.5 wt. % NaCl and 3.5 wt. % CaCl₂ solution droplets captured at the crumpling point with the addition of 0.03 g/L asphaltenes, respectively, while images of the droplet given in Figure 5-30 (B) 4 to 6 represented the crumpling of the water droplet, 3.5 wt. % NaCl and 3.5 wt. % CaCl₂ solution droplet in 0.05 g/L asphaltenes systems, respectively. The indication of crumpling was the appearance of some vertical wrinkle-like lines. As expected, the crumpling ratio increased from 0.3214 to 0.5511 with concentrations of asphaltenes shown in Figure 5-30 (B), implying that a less compressible adsorption film caused by excess asphaltenes would enhance the strength of the water drop and then hinder water bridge formation. Furthermore, the higher crumpling ratio due to the presence of salts also agreed with our previous findings. Hydrate agglomeration inside pipelines causes significant issues on the flow assurance. Many researchers worked hard on solving this problem, suggesting the introduction of either thermodynamic inhibitors to prevent the formation of hydrates or some kinetic inhibitors to delay the growth of hydrate particles. However, these strategies were environmentally or economically unacceptable. Based on our study, asphaltenes, as one of the natural oil components, have been determined as an effective anti-agglomerant to prevent the attachment of water droplet on the pre-existing hydrates, and then inhibit the pipeline blockage.

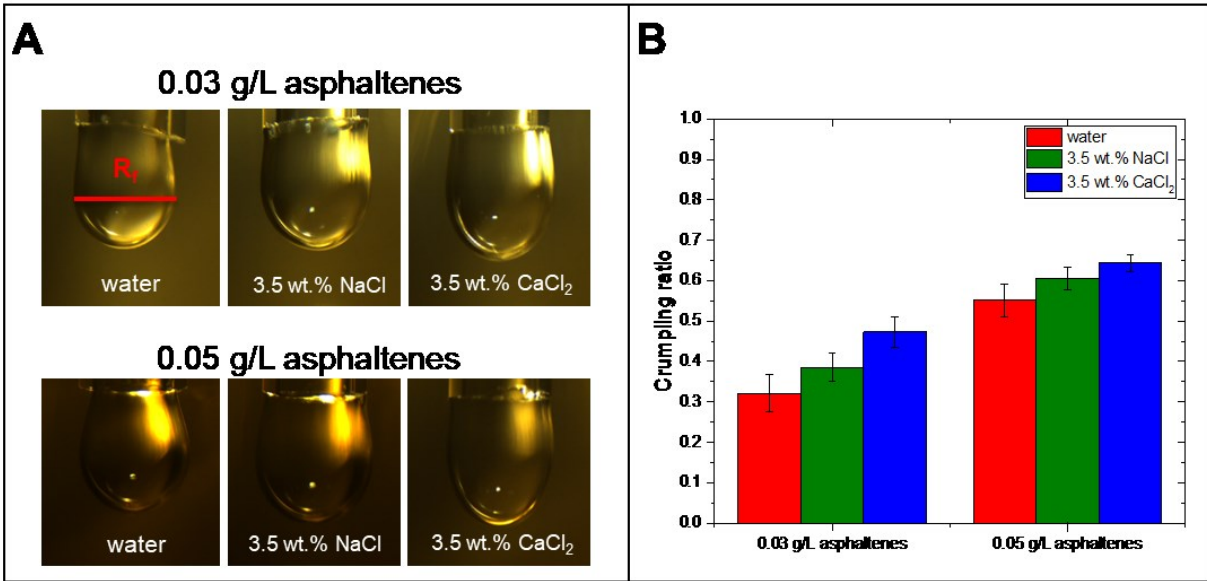


Figure 5-30: Images of water, 3.5 wt. % NaCl and CaCl₂ solution drops captured at crumpling point in mixed oil phase with addition of 0.03 g/L asphaltenes (A-1&2&3) and 0.05 g/L asphaltenes (A-4&5&6), respectively; Crumpling ratio measurements for the corresponding cases (B).

5.9 Effects of Span 80 on interactions between CP hydrate and electrolyte solution droplet in oil bulk phase

Span 80 is a common water-in-oil surfactant, and its impacts on interactions between water droplet and hydrate particle have been widely studied by both Liu et al. [14] and Li et al. [40]. In this study, the influence of Span 80 on interactions between solution droplet and CP hydrate particle was determined accompanying with salts effect. As mentioned above, even small amount of Span 80, as the kinetic hydrate inhibitor, could prevent the hydrate agglomeration based on the inhibition of capillary bridge formation without larger external force applied, while the salts, as the thermodynamic hydrate inhibitor, would slow down the hydrate growth based on shifting towards lower equilibrium temperature. In other words, only enough number of thermodynamic

inhibitors could avoid the hydrate formation totally.

5.9.1 Effects of contact time on adhesion force measurements

In this experiment, the adhesion forces were measured between water, 3.5 wt. % of NaCl, KCl and CaCl₂ solution droplets and CP hydrate particle after adding 1 wt.% Span 80 into oil phase at 2.0 ± 0.5 °C as a function of both contact time and preload force. In fact, Span 80 has hydrophilic head and hydrophobic tails, and the hydrophilic head can bind to the hydrate surface, while hydrophobic tails can extend into the continuous bulk phase (see Figure 5-31 (A)). Therefore, Span 80 as surfactants tended to adsorb on the water-oil interface, the hydrophilic head was in the water phase, while the hydrophobic tails stayed into the oil bulk phase, leading to a great reduction of interfacial tension (~ 1 mN/m at CMC) (see Figure 5-31 (B) for schematic diagram of adsorption mechanism). It was more likely that the adsorption layer caused by the hydrophobic tails was formed around hydrate particle and solution droplet. The comparisons of interaction mechanism between water droplet and CP hydrate in pure liquid cyclopentane bulk phase with and without Span 80 were illustrated in panel A and panel B of Figure 5-32, respectively. Even though the spontaneous spreading of water was not observed at the initial contact point, it took place with applying of external force (~ 0.05 mN) lasting for 10 seconds. When salts were added into the aqueous phase, the strength of adsorption layer caused by Span 80 around solution droplet was much stronger since the capillary bridge formation was prevented even applying larger external force. In general, the longer induction time was required to reduce the stability of solution droplet under employment of constant external force on the hydrate particle, agreed with our experimental results. More specific, the rupture of 3.5 wt. % NaCl/KCl solution droplets was observed when two surfaces being upon contact for lasting up to 16 seconds. However, no rupture of 3.5 wt. % CaCl₂ solution droplet occurred after more than 30 seconds holding time under same preload force. Therefore, the larger external force (i.e., 0.08

mN) was required to rupture the brine solution droplet after 15 seconds holding time. Once solution droplet ruptured, it tended to spread over the hydrate spontaneously, leading to rapid hydrate formation owing to the significant reduced interfacial tension between solution/hydrocarbon caused by addition of Span 80. Figure 5-33 presented the corresponding images to describe this interaction process between different solution droplets and CP hydrate probe with presence of Span 80.

The possible reason to explain the effects of salts on further inhibition of attachment between solution drop and CP hydrate particles was shown following: HLB (i.e., hydrophilic-lipophilic value) might be depressed by salts, resulting in surfactant becomes more oil soluble with presence of salts, and then thicker adsorption layers around drop and CP hydrate particle [99].

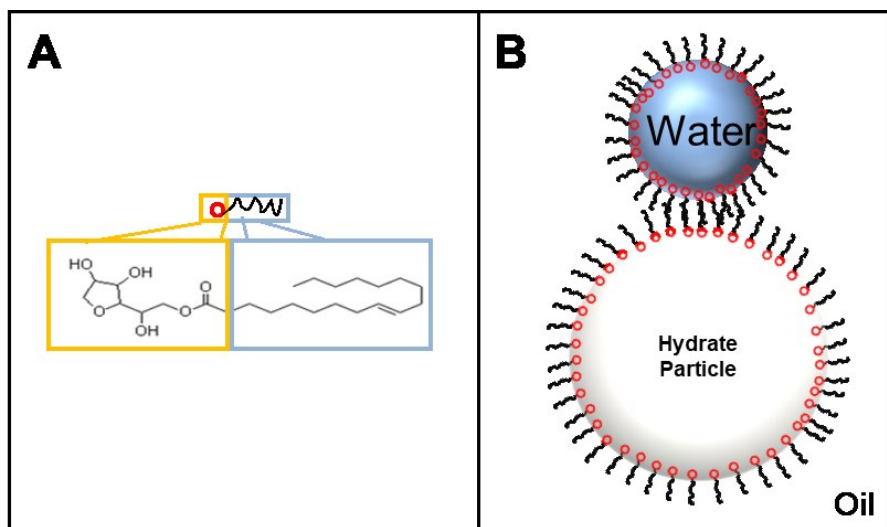


Figure 5-31: Structure of SPAN 80 (A); Schematic diagram of SPAN 80 adsorbed around droplet and CP hydrate particle (B).

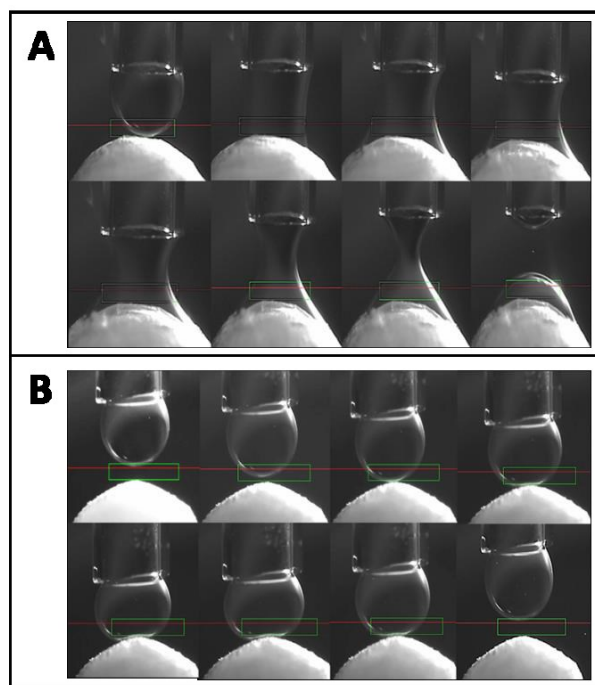


Figure 5-32: Comparison of interaction mechanisms between water droplet and CP hydrate in pure liquid cyclopentane bulk phase with and without Span 80, respectively at 2.0 ± 0.5 ° C.

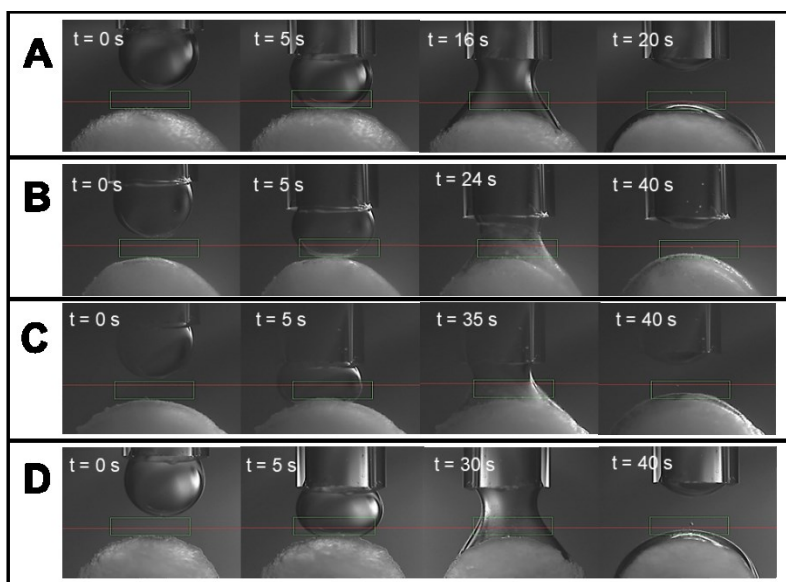


Figure 5-33: Photographic images captured from interactions between CP hydrate and water solution (A); 3.5 wt. % NaCl solution (B); 3.5 wt. % KCl solution (C); 3.5 wt. % CaCl_2 solutions (D) with respect to contact time.

5.9 Effects of subcooling on interactions between CP hydrate and electrolyte solution droplet

As suggested by Liu et al. [14], the lower subcooling could decrease the hydrate shell formation rate around the water solution. In our study, by reducing the subcooling from 5 K to 2 K, the impacts of subcooling on hydrate growth rate were investigated with the existence of salts. Compared to hydrate rate shown in Figure 5-13, the time required for hydrate conversion was increased by the lower subcooling no matter with or without the addition of salts. In other words, even though the slower conversion from any solution droplet to hydrate was expected due to the lower subcooling, the much longer time was measured once salts with divalent ions being employed into the system. The corresponding photographic images of hydrate morphology were presented in Figure 5-35. It was obvious that the amount of “new” hydrate growth was more than those in the higher subcooling, also concluded by Liu et al. [14]. Furthermore, from the observation found in the panel B of Figure 5-34, the final hydrate morphology in this case showed large variation from the other three morphologies. The regular hydrate shell formation was maintained to the final state of conversion because of the slow hydrate rate. As mentioned above, the fast hydrate formation would cause the collapse of original shape of hydrate shell coming along with the fast consumption of water [5]. As the salts introducing into the system, the amount of hydrate formation was decreasing, and the salts with divalent ions greatly rendered the hydrate formation. Therefore, the reasons for this phenomenon could be explained followings: (1) The salts with divalent ions could shift the equilibrium temperature towards even lower than the salts with monovalent ions do, causing delay of the hydrate growth rate owing to the lower subcooling; (2) Less amount of water was available to form hydrate cage created by hydrogen-bonding water molecules because the more polarized ions could bind the water molecules strongly.

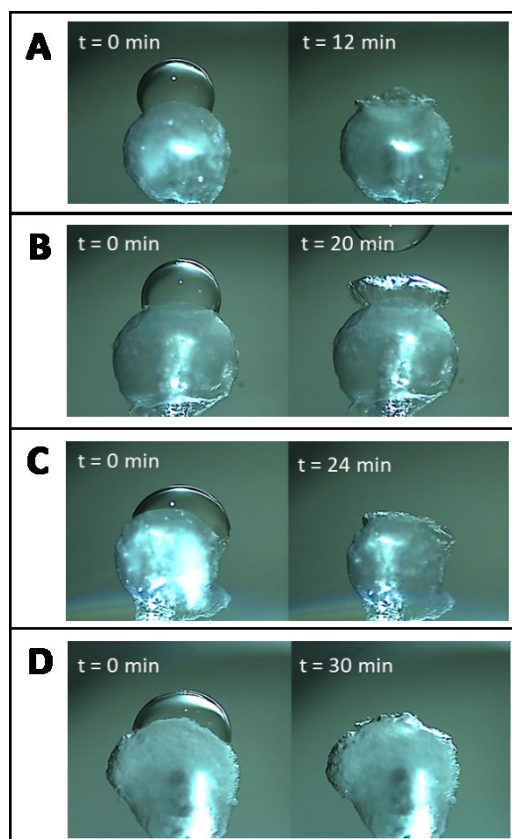


Figure 5-34: Corresponding images of hydrate morphologies obtained by the conversion from DI water (A); 2.5 wt. % NaCl (B); 2.5 wt. % CaCl₂ (C); 2.5 wt. % Na₂SO₄ (D) in the pure cyclopentane phase at 5 ± 0.5 °C.

Chapter 6 Conclusions and future work

6.1 Conclusions

As exploration of offshore reservoirs increases to meet the demand for energy, hydrates formation and agglomeration become the major flow assurance challenges in the oil and gas pipelines. In other words, in the conventional oil and gas transportation, such as deepwater-oil and gas flowlines, hydrates forming inside the pipeline may cause plugging. A low to moderate water fraction emulsified/dispersed in bulk oil phase being observed in early-to-mid-life oil system, hydrates formation at the oil-water interface is inevitable process under the moderate conditions because the hydrate component concentrations (i.e., mole ratio of water and guest molecules) greatly exceed the mutual fluid solubility. There is no doubt that the viscosity of the liquid bulk phase is dramatically increasing due to the dispersion of solid particles, and then the pressure drop is required. Hydrates aggregation caused by the strong inter-particles interactions would result in further viscosity increasing, and then complete pipeline blockage. Therefore, in order to prevent the pipeline blockage, it is essential to understand the interactions between water droplets and gas hydrates.

In order to understand the interactions including the capillary adhesion force and changing of hydrate morphology once water droplet attached to cyclopentane hydrate, the effects of a few variables, such as salts, solution droplet size, contact time, subcooling, addition of other hydrocarbon and surfactants, are investigated. Both gas and oil bulk phases are studied in the research. The cohesion or adhesion force between hydrate particles is dominated by capillary adhesion force which is relying on the surface tension and Laplace pressure. Specifically, not

only the contact angle between liquid bridge and hydrate particle but also the interfacial tension of water/oil interface plays important roles on capillary adhesion force. Cyclopentane hydrate is selected as the experimental sample because of its relative high equilibrium temperature and the same structure of hydrate formation as natural gas does. The experimental temperature is set as 2.0 ± 0.5 °C to maintain the stable CP hydrate probe.

Unlike previous research, the home designed integrated thin film drainage apparatus is used to measure the capillary adhesion force instead of micromechanical force apparatus, and this new instrument provides reliable data when compared with the results calculated from theoretical equation. The interaction force between CP hydrate particle and water droplet is defined as the largest capillary adhesion force during the experimental process.

In the oil phase, without the addition of salts, the interaction force measured between pure water droplet and CP hydrate particle is largest as 0.23 mN, mainly caused by the lowest wetting angle of bridge on the hydrate particle and formation of longest three-phase-contact line. As compared to brine solution drop, more amount of water sources is available to form the new hydrate along the interface where is the region of supersaturation of components of hydrate former when pure water drop attaches to CP hydrate particle. Moreover, once the water droplet separates from the hydrate particle, a larger amount of water tends to leave on the hydrate particle, resulting in the fast hydrate conversion from the hydrate shell formation around water droplet.

Even though the IFT is enhanced by the employment of salts since the ions are more likely to stay away from the interface, the lower interaction force measured between brine solution droplet and CP hydrate particle can be explained by the larger wetting angle. The hydrate nucleation is beginning from the formation of cage created by the hydrogen-bonding water molecules. Since

the stronger attractive force between ions and water molecules cause the competition between water molecules and ions molecules for water, the less amount of available water source could form capillary bridge with presence of salts, and then less new hydrate growth. Once the ions attract the water molecules strongly, it is less likely to generate enough number of hydrate cages, prohibiting the hydrate formation. Another reason for less hydrate growth may be because the salts could reduce the solubility of hydrocarbon in aqueous phase, which cannot meet the requirements for hydrate formation. More specific, the 5 wt. % of salt solutions with monovalent ions is considered as the critical concentration to delay the hydrate growth based on the almost unchanged of adhesion force measured between the electrolyte solution droplet and CP hydrate probe. Whereas the adhesion force is constant regardless of concentration of salts with divalent ions, implying the hydrate growth can be effectively delayed by the addition of 2.5 wt. % salts with divalent ions. Overall, the hydrate formation is greatly inhibited by the salts with divalent ions.

When CP hydrate particle is exposed into the gas phase, the hydrate surface shell is cracked into pieces so that the unconverted water from the hydrate core can easily diffuse towards the hydrate surface, and then hydrate probe is changing towards more wettable, leading to the thicker QLL on the hydrate surface. The wider capillary bridge is then formed coming along with the smaller contact angle, and the interaction force is almost twice higher than that measured in the oil phase due to the larger IFT and smaller contact angle. The impacts of salts, including of the delay of hydrate growth and lowered adhesion force, are also observed in gas bulk phase.

The interaction force between water droplet and CP hydrate probe also depends on solution droplet size and contact time. The larger contact area generated by larger droplet size corresponds to the longer TPC line, and then the higher interaction forces as expected. On the other hand, the

reactive hydrate growth mechanism is controlled by the contact time between two surfaces. Consequently, the interaction force is increasing with the droplet size, indicated by the wider capillary bridge formation. The longer contact time not only enhances the amount of hydrate growth due to the sintering mechanism but also increases the interaction force at the point of bridge rupture.

Two anti-agglomerants, asphaltenes and Span 80, are also added into the oil phase to investigate their impacts on interactions between CP hydrate probe and water droplet. After adding 0.03g/L asphaltenes into the oil phase, asphaltenes, as a natural oil component, tend to adsorb around the water droplet, resulting in an irreversible adsorption layer which increases the strength of water droplet. Therefore, the rupture of thin film is delayed by 0.7 seconds after initial contact point, which confirms the formation of adsorption layer around water droplet. Once the thin film ruptures, the water can spread on the hydrate particle spontaneous, which is similar as previous observation without presence of asphaltenes. Furthermore, the presence of salts make significantly negative contribution on the attachment between water droplet and pre-existing hydrate particles, indicated by the further delay of thin film rupture. Specifically, applying same external force, the rupture of thin film is observed after approximately 1.3 seconds holding time with addition of salts with monovalent ions. Rather than spontaneous spreading of solution on the hydrate surface, there is absence of dramatic attractive force when the salt solution droplet attaches to CP hydrate particle. This observation can be comprehended by the thicker adsorption layer formed around solution droplet. Once salts with divalent ions are added into the aqueous phase, the rupture of solution droplet is even delayed because the salts with the higher charge cations enhanced the ion-bridging effect. On the other hand, when the concentration of asphaltenes increased to 0.05 g/L, the thicker adsorption layer causes water to be stable versus

coalescence, thereby hindering the formation of liquid capillary bridge. As a consequence, the concentration of asphaltenes up to 0.05 g/L can effectively prevent the bridge formation and then inhibit the hydrate agglomeration inside pipeline. The strength of adsorption layer is studied by the crumpling ratio, and higher crumpling ratio represents the more stable adsorption layer, which is measured by the addition of salts with divalent ions because the more polarized solution could enhance the adsorption of asphaltenes.

1 wt. % Span 80, a common water-in-oil surfactant, is introduced into oil phase to evaluate its influences on interactions between hydrate particle and water droplet as well. Likely, once two surfaces are upon contact, the capillary bridge formation is rendered due to the presence of adsorption layers around water droplet and hydrate particle. For better understanding the impacts of SPAN 80, the contact time is increased, and the rupture of oil thin film is observed after 10 seconds holding time between water droplet and CP hydrate particle. Afterwards, the water spread over the hydrate particle, leading to rapid hydrate formation. With presence of salts with monovalent ions, the thin film ruptures when the external force is applied lasting up to 16 seconds. Nevertheless, the rupture of thin film is further delayed when water droplet is replaced by brine solution droplet with divalent ions.

Additionally, the hydrate growth is slowed down by the lower subcooling due to the lower driving force, while the lack of component to form hydrate (i.e., guest and host molecules) can reduce the hydrate formation owing to the lower mass transition limitations.

In our study, rather than the most common type of salts (i.e., NaCl) which has been discussed by other researchers, understanding the impacts of more types of salts and briefly comparing the effects of cations is one main unique contribution. Overall, the presence of salts hinders the

hydrate growth and decrease the interaction force measured between water droplet and CP hydrate probe. More specific, the salts with divalent ions are more effective on inhibiting the hydrate agglomeration because the more water tends to adsorb around ions, resulting in less amount of hydrate cage formed by hydrogen-bonding water molecules.

Besides, even though many different surfactants has been added into system to delay hydrate growth or prevent attachment between hydrates and water droplets, we believed it might be the first time to investigate the influence of dissolved asphaltenes on the interaction between water droplets and cyclopentane hydrates. Asphaltenes as a natural oil component is inevitable in offshore production and transportation, then the largest advantages of this surface-active surfactant is no need for external addition. Moreover, according to our study, 0.05 g/L asphaltenes has shown the positive contribution on the preventing attachment, resulting in much less amount of asphaltenes (i.e., 50 ppm) than that of other anti-agglomerants including Span 80 (i.e., 1 wt. %) required to hinder attachment. Therefore, it provides a more acceptable insight for economy and environment on the inhibition of hydrate agglomeration.

6.2 Future work

Many aspects related to this work are not fully covered due to applicability limitations. Further investigations are required to establish a more comprehensive understanding of the influences of salts on the interactions between the solution droplets and hydrate particle including the adhesion forces and hydrate growth rate.

1. In order to evaluate the specific effects of cations and anions on the interactions between

droplets and hydrate particle, more types of salts can be added into the system, such as NaI, MgCl₂ and CaSO₄. Moreover, the critical concentrations of each interesting types of salts to delay the hydrate formation are also useful for hydrate agglomeration inhibition. In general, fewer amounts of salts lead to less possibility of pipeline corrosion and further serious issues.

2. A better way for smoother hydrate particle preparation need to be developed, eliminating the impacts of roughness of hydrate particle on the interactions between it and other surfaces since the roughness can significantly lower the adhesion force, leading to inaccurate results.
3. For better understanding the morphology of hydrate, it is critical to observe the surface of the hydrate probe using Cryo-SEM.
4. A better way is required to eliminate the temperature loss during the experiment. Even though the experimental temperature is set above the ice point, it is more likely to form frost on the window of the aluminum experimental cell which is connected to the external water bath. Since the experiment is operated under the room temperature, the condensed water on the window is easily converted to ice if the experimental time lasts longer than 2 hours, resulting in the difficulty on recording video via side camera.
5. The study of other surfactants, such as sodium dodecylbenzenesulfonate (SDBS) and naphthenic acid, can provide better understanding of agglomeration of cyclopentane hydrate.
6. Pay more attention on the interactions between other surfaces and hydrate particle in the

gas phase, and to describe the proposed mechanisms of hydrate growth and hydrate agglomeration.

7. To valid the influences of various salts on thermodynamic mechanisms of hydrate particle, the change of equilibrium temperature is valuable to be determined.
8. A more accurate contact angle measurement between liquid bridge and hydrate particle is required for comprehending the impacts of salts on the hydrate growth and adhesive force.
9. Understanding the changes of hydrate surface charge when it contacts with cations, which is essential for explaining the larger contact angle with presences of salts with divalent ions.
10. Using Langmuir trough or other ways to quantity the number of surfactants on the water-oil interface, it could lead to more valuable insights on the prevention of attachment between water droplet and hydrate particle.

Bibliography

- [1] J. H. Song, A. Couzis and J. W. Lee, "Investigation of Macroscopic Interfacial Dynamics between Clathrate Hydrates and Surfactant Solutions", *Langmuir*, vol. 26, no.23, pp. 18119–18124, 2010.
- [2] Z. M. Aman, K. Olcott, K. Pfeiffer, E. D. Sloan, A. K. Sum and C. A. Koh, "Surfactant Adsorption and Interfacial Tension Investigations on Cyclopentane Hydrate", *Langmuir*, vol. 29, pp. 2676-2682, 2013.
- [3] PennState College of Earth and Mineral Sciences, "The Hydrate Problem", [Online]. Available: https://www.e-education.psu.edu/png520/m21_p3.html[Accessed: 07-May-2019].
- [4] C. Lo, J. S. Zhang, P. Somasundaran, S. Lu, A. Couzis and J. W. Lee, "Adsorption of Surfactants on Two Different Hydrates", *Langmuir*, vol. 24, no. 22, pp. 12723-12726, 2008.
- [5] E. D. Sloan and C. A. Koh. Clathrate hydrates of natural gases, 3rd ed., CRC Press: Boca, Raton, FL, 2008.
- [6] Z. M. Aman, E. P. Brown, E. D. Sloan, A. K. Sum and C. A. Koh, "Interfacial mechanisms governing cyclopentane clathrate hydrate adhesion/cohesion", *Phys. Chem. Chem. Phys.*, 13, pp. 19796-19806, 2011
- [7] A. K. Sum, R. C. Burruss and E. D. Sloan, "Measurement of Clathrate Hydrates via Raman Spectroscopy", *J. Phys. Chem. B*, vol. 101, pp. 7371-7377, 1997.
- [8] S. Takeya, K. A. Udachin, I. L. Moudrakovski, R. Susilo and J. A. Ripmeester, "Direct Space Methods for Powder X-ray Diffraction for Guest-Host Materials: Applications to Cage Occupancies and Guest Distributions in Clathrate Hydrates", *J. AM. CHEM. SOC.*, vol. 132, pp.

524-531, 2010.

[9] Z. M. Aman and C. A. Koh, "Interfacial phenomena in gas hydrate systems", *Chem. Soc. Rev.*, vol. 45, pp. 1678-1690, 2016.

[10] B. Liu, W. Pang, B. Peng, C. Sun and G. Chen (2012). Heat Transfer Related to Gas Hydrate Formation/Dissociation, *Developments in Heat Transfer*, Dr. Marco Aurelio Dos Santos Bernardes (Ed.), ISBN: 978-953-307-569-3, Available:

<https://www.intechopen.com/books/developments-in-heat-transfer/heat-transfer-related-to-gas-hydrate-formation-dissociation>.

[11] C. J. Taylor, K. T. Miller, C. A. Koh, and E. D. Sloan. "Macroscopic investigation of hydrate film growth at the hydrocarbon/water interface", *Chem. Eng. Sci.*, vol. 62, pp. 6524-6533, 2007.

[12] M. Kishimoto, S. Iijima and R. Ohmura, "Crystal Growth of Clathrate Hydrate at the Interface between Seawater and Hydrophobic-Guest Liquid: Effect of Elevated Salt Concentration", *Ind. Eng. Chem. Res.*, vol. 51, pp. 5224-5229, 2012.

[13] D. Corak, T. Barth, S. Hoiland, T. Slodvin, R. Larsen and T. Skjetne, "Effect of subcooling and amount of hydrate former on formation of cyclopentane hydrates in brine", *Desalination*, vol. 278, pp. 268-274, 2011.

[14] C. W. Liu, M. Z. Li, G. D. Zhang and C. A. Koh, "Direct measurements of the interactions between clathrate hydrate particles and water droplet", *Phys. Chem. Chem. Phys.*, vol.17, pp. 20021-20029, 2015.

[15] E. D. Sloan, "Fundamental principles and applications of natural gas hydrates", *Nature*, vol. 426, pp. 353-359, 2003.

[16] Z. R. Chong, S. H. Yang, P. Babu, P. Linga and X. S, Li, "Review of natural gas

hydrates as an energy resource: Prospects and challenges”. *Applied Energy*, vol. 162, pp. 1633-1652, 2016.

[17] “Unconventional Energy; Methane Hydrates.” [Online]. Available: <http://www.unoilgas.com/methane-hydrates.htm> [Accessed: 15-September-2015].

[18] D. Turner, K. Miller and E. Sloan, “Methane hydrate formation and an inward growing shell model in water-in-oil dispersions”, *Chem. Eng. Sci.*, vol. 64, pp. 3996-4004, 2009.

[19] G. Aspenes, L. E. Dieker, Z. M. Aman, S. HØiland, A. K., Sum, C. A. Koh and E. D. Sloan, “Adhesion force between cyclopentane hydrates and solids surface materials”, *J. Colloid Interface Sci.*, vol. 343, pp. 529-536, 2010.

[20] B. R. Lee, C. A. Koh and A. K. Sum, “Mechanism of Cohesive Forces of Cyclopentane Hydrates with and without Thermodynamic Inhibitors”, *Ind. Eng. Chem. Res.*, vol 53, pp. 18189-18193, 2014.

[21] W. Lee, S. Baek, J-D. Kim and J. W. Lee, “Effects of salt on the crystal growth and adhesion force of clathrate hydrates”, *Energy & fuels*, vol. 29, pp. 4245-4254, 2015.

[22] C. W. Liu, M. Z. Li, G. D. Zhang and C. A. Koh, “Direct measurements of the interactions between clathrate hydrate particles and water droplet”, *Phys. Chem. Chem. Phys.*, vol. 17, pp. 20021-20029, 2015.

[23] M. Li, J. Tian, C. Liu and K. Geng, “Effects of sorbitan monooleate on the interactions between cyclopentane hydrate particles and water droplets”, *J. Dispersion Sci. Tech.*, vol. 39, no. 3, pp. 360-366, 2018.

[24] L. E. Dieker, Z. M. Aman, N. C. George, A. K. Sum, E. D. Sloan and C. A. Koh, “Micromechanical Adhesion Force Measurements between Hydrate Particles in Hydrocarbon Oils and Their Modifications”, *Energy Fuels*, vol. 23, pp. 5955-5971, 2009.

- [25] J. Sjoblom, N. Aske, I. H. Auflem, O. Brandal, T. E. Havre, O. Saether, A. Westvik, E.E Johnsen and H. Kallevik, "Our current understanding of water-in-crude oil emulsions, Recent characterization techniques and high pressure performance", *Adv. Colloid Interface Sci.*, vol. 100-102, pp. 399-473, 2003.
- [26] J. S. Buckley, Y. Liu and S. Monsterieet, Mechanisms of wetting alteration by crude oils, SPE International Symposium on Oilfield Chemistry, Houston, TX, 1998.
- [27] G. Aspenes, S. Hoiland, T. Barth, K. M. Askvik, R. A. Kini and R. Larsen, Petroleum hydrate deposition mechanisms: The influence of pipeline wettability, Proceedings of the 6th Annual International Conference on Gas Hydrates, Vancouver, British Columbia, Canada, 2008.
- [28] A. E. Borgund, S. Hoiland, T. Barth, P. Rotland, R. A. Kini and R. Larsen, Critical descriptors for hydrate properties of oils: Compositional features, Proceedings of the 6th International Conference of Gas Hydrates, Vancouver, British Columbia, Canada, 2008.
- [29] S. A. Morrissy, V. W. Lim, E. F. May, M. L. Johns, A. M. Aman and B. F. Graham, "Micromechanical Cohesive Force Measurements between Precipitated Asphaltene Solids and Cyclopentane Hydrates", *Energy Fuels*, vol. 29, pp. 6277-6285, 2015.
- [30] J. H. Song, A. Couzis, and J. W. Lee, "Direct Measurements of Contact Force between Clathrate Hydrates and Water". *Langmuir*, vol. 26, no. 12, pp. 9187-9190, 2010.
- [31] London Dispersion Forces. [Online]. Available: <https://www.chem.purdue.edu/gchelp/liquids/disperse.html>
- [Accessed: 28-November-2016].
- [32] Z. M. Aman, E. D. Sloan, A. K. Sum, and C. A. Koh, "Adhesion force interactions between cyclopentane hydrate and physically and chemically modified surfaces", *Phys. Chem. Chem. Phys.*, vol. 16, pp. 25121-25128, 2014.

- [33] Z. M. Aman, K. Olcott, K. Pfeiffer, E. D. Sloan, A. K. Sum and C. A. Koh, “Surfactant Adsorption and Interfacial Tension Investigations on Cyclopentane Hydrate”, *Langmuir*, vol. 29, pp. 2676-2682, 2013.
- [34] Z. M. Aman, S. E. Joshi, E. D. Sloan, A. L. Sum and C. A. Koh, “Micromechanical Cohesion Force Measurements to Determine Cyclopentane Hydrate Interfacial Properties”, *J. Colloid Interface Sci.*, vol. 376, no.1, pp. 283-288, 2012.
- [35] J. Israelachvili, *Intermolecular & Surface Forces*, 2nd edn., Academic Press, Great Britain, 1991.
- [36] K. Erstad, S. Hoiland, T. Barth and P. Forland, Isolation and molecular identification of hydrate surface active components in petroleum acid fractions, Proceedings of the 6th International Conference of Gas Hydrates, Vancouver, British Columbia, Canada, 2008.
- [37] C. Lo, J. S. Zhang, A. Couzis, P. Somasundaran and J. W. Lee, “Adsorption of Cationic and Anionic Surfactants on Cyclopentane Hydrates”, *J. Phys. Chem. C*, vol. 114, pp. 13385-13389, 2010.
- [38] M. R. Anklam, J. D. York, L. Helmerich and A. Firoozabadi, “Effects of Antiagglomerants on the Interactions between Hydrate Particles”, *AIChE J.*, vol. 54, no. 2, pp. 565-574, 2008.
- [39] M. J. Cha, A. Couzis and J. W. Lee, “Macroscopic Investigation of Water Volume Effects on Interfacial Dynamic Behaviours between Clathrate Hydrate and Water”, *Langmuir*, vol. 29, pp. 5793-5800, 2013.
- [40] M. Li, J. Tian, C. Liu and K. Geng, “Effects of sorbitan monooleate on the interactions between cyclopentane hydrate particles and water droplets”, *J. Dispersion Sci. Tech.*, vol. 39, no. 3, pp. 360-366, 2017.

- [41] P. U. Karanjkar, J. W. Lee and J. F. Morris, "Surfactant Effects on Hydrate Crystallization at the Water-Oil Interface: Hollow-Conical Crystals", *Cryst. Growth Des.* vol. 12, pp. 3817-3824, 2012.
- [42] G. Aspenes, L. E. Dieker, Z. M. Aman, S. HØiland, A. K., Sum, C. A. Koh and E. D. Sloan, "Adhesion force between cyclopentane hydrates and solids surface materials", *J. Colloid Interface Sci.*, vol. 343, pp. 529-536, 2010.
- [43] J. W. Nicholas, L. E. Dieker, E. D. Sloan and C. A. Koh, "Assessing the feasibility of hydrate deposition on pipeline walls-Adhesion force measurements of clathrate hydrate particles on carbon steel", *J. Colloid Interface Sci.*, vol. 331, pp. 322-328, 2009.
- [44] Z. M. Aman, W. J. Leith, G. A. Grasso, E. D. Sloan, A. K. Sum and C. A. Koh, "Adhesion Force between Cyclopentane Hydrate and Mineral Surfaces", *Langmuir*, vol. 29, pp. 15551-15557, 2013.
- [45] D. Kashchiev and A. Firoozabadi, "Driving force for crystallization of gas hydrates", *J. Crystal Growth*, vol. 241, pp. 220-230, 2002.
- [46] Y. Ito, R. Kamakura, S. Obi and Y. H. Mori, "Microscopic observations of clathrate-hydrate films formed at liquid/liquid interfaces, II, Film thickness in steady-water flow", *Chem. Eng. Sci.*, vol. 58, pp. 107-114, 2003.
- [47] Y. Makogon, T. Makogon and S. Holditch, "Several aspects of the kinetics and morphology of gas hydrates", Proceedings of the Japan National Oil Conference, pp. 259-267, 1998.
- [48] K. Saito, A. K. Sum and R. Ohmura, "Correlation of Hydrate-Film Growth Rate at the Guest/Liquid-Water Interface to Mass Transfer Resistance", *Ind. Eng. Chem. Res.*, vol. 49, pp. 7102-7103, 2010.

- [49] E. P. Brown and C. A. Koh, “Micromechanical measurements of the effect of surfactants on cyclopentane hydrate shell properties”, *Phys. Chem. Chem. Phys.*, vol. 18, pp. 594-600, 2016.
- [50] P. U. Karanjkar, J. W. Lee and J. F. Morris, “Surfactant Effects on Hydrate Crystallization at the Water-Oil Interface: Hollow-Conical Crystals”, *Cryst. Growth Des.*, vol. 12, pp. 3817-3824, 2012.
- [51] M. J. Cha, S. Baek, J. Morris and J. W. Lee, “Hydrophobic Particle Effects on Hydrate Crystal Growth at the Water-Oil Interface”, *Chem. Asian J.*, vol. 9, pp. 261-267, 2014.
- [52] M. Nakajima, R. Ohmura and Y. H. Mori, “Clathrate Hydrate Formation from Cyclopentane-in-Water Emulsions”, *Ind. Eng. Chem. Res.*, vol. 47, no. 22, pp. 8933-8939, 2008.
- [53] Z. M. Aman, L. E. Dieker, G. Asoenes, A. K. Sum, E. D. Sloan and C. A. Koh, “Influence of Model Oil with Surfactants and Amphiphilic Polymers on Cyclopentane Hydrate Adhesion Forces”, *Energy Fuels*, vol. 24, no. 10, pp. 5441-5445, 2010.
- [54] C. J. Taylor, L. E. Dieker, K. T. Miller, C. A. Koh and E. D. Sloan, “Micromechanical adhesion force measurements between tetrahydrofuran hydrate particle”, *J. Colloid Interface Sci.*, vol. 306, pp. 255-261, 2007.
- [55] T. Uchida, I. Y. Ikeda, S. Takeya, T. Ebinuma, “CO₂ hydrate film formation at the boundary between CO₂ and water: effects of temperature, pressure and additives on the formation rate”, *J. Cryst. Growth*, vol. 237–239, pp. 383–387, 2002
- [56] R. Sakemoto, H. Sakamoto, K. Shiraiwa, R. Ohmura, T. Uchida, “Clathrate hydrate crystal growth at the seawater/hydrophobic-guest-liquid interface”, *Cryst. Growth Des.*, vol. 10, pp. 1296–1300, 2010.
- [57] G. Zylyftar, J. W. Lee and J. F. Morris, “Salt effects on thermodynamic and rheological

- properties of hydrate forming emulsions”, *Chem. Eng. Sci.*, vol. 95, pp. 148-160, 2013.
- [58] K. Maeda, Y. Katsura, Y. Asakuma and K. Fukui, “Concentration of sodium chloride in aqueous solution by chlorodifluoromethane gas hydrate”, *Chem. Eng. Process*, vol. 47, pp. 2281-2286, 2008.
- [59] T. Uchida, I. Y. Ikeda, S. Takeya, T. Ebinuma, J. Nagao and H. Narita, “CO₂ hydrate film formation at the boundary between CO₂ and water: effects of temperature, pressure and additives on the formation rate”, *J. Cryst. Growth*, vol. 237-239, pp. 383-387, 2002.
- [60] T. Uchida, T. Shiga, M. Nagayama and K. Gohara, “Observation of Sintering of Clathrate Hydrates”, *Energies*, vol. 3, pp. 1960-1971, 2010.
- [61] T. Uchida, D. Kishi, T. Shiga, M. Nagayama and K. Gohara, “Sintering Process Observations on Gas Hydrates under Hydrate-Stable and Self-Preservation Conditions”, *J. Chem. Eng. Data*, vol. 60, pp. 284-292, 2015.
- [62] S. Sjoblom, Structure and Thermodynamics of Water and Solutes Adsorbed on Solid Surfaces. PhD Thesis, 2015.
- [63] E. R. A. Lima, B. M. de Male, L. T. Baptista, M. Paredes and L. L., “Specific ion effects on the interfacial tension of water/hydrocarbon systems”, *Brazilian Journal of Chemical Engineering*, vol. 30, no. 01, pp. 55-62, 2013.
- [64] M. Firouzi, T. Howes and A. V. Nguyen, “A quantitative review of the transition salt concentration for inhibiting bubble coalescence”, *Advance in Colloid and Interface Sci.*, vol. 222, pp. 305-318, 2015.
- [65] G. Zylyftar, J. W. Lee and J. F. Morris, “Salt effects on thermodynamic and rheological properties of hydrate forming emulsions”, *Chem. Eng. Sci.*, vol. 95, pp. 148-160, 2013.
- [66] J. Zhang, M. K. Borg, K. Sefiane and J. M. Reese, “Wetting and evaporation of salt-

water nanodroplets: A molecular dynamics investigation”, *Phys. Review*, vol. E 92, 052403, 2015.

[67] M. Ramiasa, J. Ralston, R. Fetzer, R. Sedev, D. M. Fopp-Spori, C. Morhard, C. Pacholski and J. P. Spatz, “Contact Line Motion on Nanorough Surfaces: A Thermally Activated Process”, *J. Am. Chem. Soc.*, vol. 135, pp. 7159-7171, 2013.

[68] L. X. Wang, D. Sharp, J. Masliyah and Z. H. Xu, “Measurement of Interactions between Solid Particles, Liquid Droplets, and/or Gas Bubbles in a Liquid using an Integrated Thin Film Drainage Apparatus”, *Langmuir*, vol. 29, pp. 3594–3603, 2013.

[69] Skwarok, T.; Bi, J. B. and Tchoukov, P. Understanding interfacial properties of asphaltene model compound C5Pe using dynamic interfacial tension and crumpling ratio experiments, 2014.

[70] Woodward, R.P. Surface Tension Measurements Using the Drop Shape Method. [Online] Available: <http://www.firsttenangstroms.com/pdfdocs/STPaper.pdf> [Accessed: 03-October-2016].

[71] C. Tsamantakis, J. Masliyah, A. Yeung, A. and T. Gentzis, “Investigation of interfacial properties of water-in-diluted-bitumen emulsions using micropipette techniques”, *J. Colloid Interface Sci.*, vol. 284, pp. 176-183, 2005.

[72] S. Gao, S. K. Moran, Z. Xu and J. Masliyah, “Role of Bitumen Components in Stabilizing water-in-Diluted Oil Emulsions”, *Energy & Fuels*, vol. 23, pp. 2606-2612, 2009.

[73] K.C Hester, R. N. Dunk, S. N. White, P. G. Brewer, E. T. Peltzer and E. D. Sloan, “Gas Hydrate Measurements at Hydrate Ridge Using Raman Spectroscopy”, *GCA*, vol. 71 (12), pp. 2947-2959, 2007.

[74] J. Wang, J. Buckley, “Standard Procedure for Separating Asphaltenes from Crude Oils”, *New Mex. Tech, PRRC* 2002.

- [75] J. L. Parker, “A Novel Method for Measuring the Force between Two Surfaces in a Surface Force Apparatus”, *Langmuir*, vol. 8, pp. 551-556, 1992.
- [76] E.R.A. Lima, B. M. de Male, L. T. Baptista and M. L. L. Paredes, “Specific ion effects on the interfacial tension of water/hydrocarbon systems”, *Brazilian Journal of Chemical Engineering*, vol. 30, no. 01, pp.55-62, 2013.
- [77] S. Sjoblom, Structure and Thermodynamics of Water and Solutes Adsorbed on Solid Surfaces, PhD Thesis, 2015.
- [78] F. Mugele, B. Bera, A. Cacalli, I. Siretanu, A. Maestro, M. Duits, M. Cohen-Stuart, D. Ende, I. Stocker and I. Collins, “Ion adsorption – induced wetting transition in oil-water-mineral systems”, *Scientific Reports*, 5, 10519, 2015.
- [79] J. Á. Felipe, F. Abbas, “Hydrophobic Hydration and the Effect of NaCl Salt in the Adsorption of Hydrocarbons and Surfactants on Clathrate Hydrates”, *ACS Central Sci.*, vol. 4, no. 7, pp. 820-831, 2018.
- [80] S. Ho-Van, B. Bouillot, J. Douzet, S. Maghsoodloo Babakhani and J. M. Herri, “Experimental Measurement and Thermodynamic Modeling of Cyclopentane Hydrates with NaCl, KCl, CaCl₂, or NaCl-KCl Present”, *AIChE J.*, vol. 64, no. 6, pp. 2207-2218, 2018.
- [81] B. Liu, R. Manica, X. Zhang, A. Bussonnière, Z. Xu, G. Xie, Q. Liu, “Dynamic Interaction between a Millimeter-Sized Bubble and Surface Microbubbles in Water”, *Langmuir*, vol. 34, pp. 11667-11675, 2018
- [82] J. D. McLean and P. K. Kilpatrick, “Effects of asphaltene solvency on stability of water-in-crude-oil emulsions”, *J. Colloid Interface Sci.*, vol. 189, no. 2, pp. 242–253, 1997.
- [83] H. W. Yarranton, H. Hussein and J. H. Masliyah, “Water-in-hydrocarbon emulsions

stabilized by asphaltenes at low concentrations”, *Colloid Interface Sci.*, vol. 228, no. 1, pp. 52–63, 2000.

[84] J. Sjöblom, E. Mingyuan, A. A. Christy and T. Gu, “Water-in-crude-oil emulsions from the Norwegian continental shelf 7”, *Interfacial pressure and emulsion stability*, vol. 66, pp. 55–61, 1992.

[85] V. Pauchard, J. Sjö, S. Kokal, P. Bouriat, C. Dicharry and H. Mu, “Role of Naphthenic Acids in Emulsion Tightness for a Low-Total-Acid-Number (TAN)/ High-Asphaltenes Oil †”, pp. 1269–1279, 2009.

[86] P. Chaverot, A. Cagna, S. Glita and F. Rondelez, “Interfacial Tension of Bitumen - Water Interfaces. Part 1: Influence of Endogenous Surfactants at Acidic pH †”, vol. 9, pp. 790–798, 2008.

[87] J. P. Rane, D. Harbottle, V. Pauchard, A. Couzis and S. Banerjee, “Adsorption kinetics of asphaltenes at the oil-water interface and nanoaggregation in the bulk”, *Langmuir*, vol. 28, no. 26, pp. 9986–9995, 2012.

[88] L. Y. Zhang, Z. Xu and J. H. Masliyah, “Langmuir and Langmuir–Blodgett films of mixed asphaltene and a demulsifier”, vol. 19, no. 23, pp. 9730–9741, 2003.

[89] J. Sjöblom, N. Aske, I. H. Auflem, O. Brandal, T. E. Havre, O. Saether, A. Westvik, E. E. Johnsen, and H. Kallevik, “Our current understanding of water-in-crude oil emulsions.: Recent characterization techniques and high pressure performance”, *Adv. Colloid Interface Sci.*, vol. 100-102, pp. 399-473, 2003.

[90] N. Daraboina, S. Pachitsas and N. von Solms, “Natural gas hydrate formation and inhibition in gas/crude oil/aqueous systems”, *Fuel*, vol. 148, pp. 186-190, 2015.

[91] F. Mugele, B. Bera, A. Cavalli, I. Siretanu, A. Maestro, M. Duits, M. Cohen-Stuart, D.

Van Den Ende, I. Stocker, I. Collins, “Ion Adsorption-Induced Wetting Transition in Oil-Water-Mineral Systems”, *Sci. Rep.*, 10519, 2015.

[92] F. Shojaati, S. H. Mousavi, M. Riazi, F. Torabi, M. Osat, “Investigating the Effect of Salinity on the Behavior of Asphaltene Precipitation in the Presence of Emulsified Water”, *Ind. Eng. Chem. Res.*, vol. 56, pp. 14362-14368, 2017.

[93] C. Hu, N. C. Garcia, R. Xu, T. Cao, A. Yen, S. A. Garner, J. M. Macias, N. Joshi, R. L. Hartman, “Interfacial Properties of Asphaltenes at the Heptol–Brine Interface”, *Energy & Fuels*, vol. 30, pp. 80–87, 2015.

[94] P. Tchoukov, F. Yang, Z. Xu, T. Dabros, J. Czarnecki, J. Sjöblom, “Role of Asphaltenes in Stabilizing Thin Liquid Emulsion Films”, *Langmuir*, vol. 30, pp. 3024–3033, 2014.

[95] J.-M. Bai, W.-Y. Fan, G.-Z. Nan, S.-P. Li, B.-S. Yu, “Influence of Interaction between Heavy Oil Components and Petroleum Sulfonate on the Oil–Water Interfacial Tension”, *J. Dispers. Sci. Technol.*, vol. 31, pp. 551–556, 2010.

[96] A. B. Demir, H. I. Bilgesu, B. Hascakir, “The Effect of Clay and Salinity on Asphaltene Stability”, In *SPE Western Regional Meeting*; Society of Petroleum Engineers, 2016.

[97] H. Ganji, M. Manteghian, K. Sadaghiani zadeh, M. R. Omidkhah, H. Rahimi Mofrad, “Effect of Different Surfactants on Methane Hydrate Formation Rate, Stability and Storage Capacity”, *Fuel*, vol. 86, pp. 434-441, 2007.

[98] V. B. Fainerman, R. Miller, "Surface Tension Isotherms for Surfactant Adsorption Layers Including Surface Aggregation", *Langmuir*, vol. 12, pp. 6011–6014, 1996.

[99] K. Shinoda, H. Takeda, “The Effect of Added Salts in Water on the Hydrophile-Lipophile Balance of Nonionic Surfactants: The Effect of Added Salts on the Phase Inversion Temperature of Emulsions”, *J. Colloid Interface Sci.*, vol. 32, pp. 642–646, 1970.